DISSERTATIONES PHYSICAE UNIVERSITATIS TARTUENSIS
52

DISSERTATIONES PHYSICAE UNIVERSITATIS TARTUENSIS
52

CONDUCTION MECHANISMS IN THIN ATOMIC LAYER DEPOSITED FILMS CONTAINING TiO_2

INDREK JÕGI

TARTU UNIVERSITY
PRESS

The study was carried out in the Institute of Experimental Physics and Technology, University of Tartu.

The dissertation was admitted on June 27, 2007, in partial fulfillment of the requirements for the degree of Doctor of Philosophy in physics (optics and spectroscopy) and allowed for defence by the Council of the Department of Physics, University of Tartu.

Supervisors: Assoc. Prof. Matti Laan, Institute of Experimental Physics and Technology, University of Tartu, Estonia
Dr. Kaupo Kukli, Institute of Experimental Physics and Technology, University of Tartu, Tartu, Estonia

Opponents: Prof. Karol Fröhlich, Institute of Electrical Engineering, Slovak Academy of Sciences, Bratislava, Slovakia
Prof. Enn Mellikov, Department of Materials Science, Tallinn University of Technology, Tallinn, Estonia

Defence: September 26, 2007 at the University of Tartu, Estonia

ISSN 1406–0647
ISBN 978–9949–11–692–8 (trükis)
ISBN 978–9949–11–693–5 (PDF)

Tartu Ülikooli Kirjastus
www.tyk.ee
Tellimuse nr 317

CONTENTS

2

LIST OF PUBLICATIONS

List of original papers included to the thesis:

I. J. Aarik, V. Bichevin, I. Jõgi, H. Käämbre, M. Laan, V. Sammelselg, "Fowler-Nordheim tunnelling in Au-TiO_2-Ag film structures", Central Eur. J. Phys. 2 (2004) 147.

II. I. Jõgi, J. Aarik, K. Kukli, H. Käämbre, M. Laan, J. Lu, T. Sajavaara, T. Uustare,"The effect of precursors on the structure and conductivity of atomic layer deposited TiO_2 films", Proc. Electrochem. Soc. 2005–09 (2005) 575.

III. I. Jõgi, J. Aarik, M. Laan, J. Lu, K. Kukli, H. Käämbre, T. Sajavaara, T. Uustare, "Effect of preparation conditions on properties of atomic layer deposited TiO_2 films in Mo-TiO_2-Al stacks", Thin Solid Films 510 (2006) 39.

IV. I. Jõgi, K. Kukli, J. Aarik, A. Aidla, J. Lu, "Precursor-dependent structural and electrical characteristics of atomic layer deposited films: Case study on titanium oxide", Mater. Sci. Semicond. Process. 9 (2006) 1084.

List of other publications and conference presentations:

1. I. Jõgi, J. Aarik, V. Bichevin, H. Käämbre, M. Laan, V.Sammelselg, "Fowler-Nordheim tunnelling in TiO_2 films grown by atomic layer deposition", Proc. Eston. Acad. Sci., Phys., Math. 53, (2004) 226.
2. I. Jõgi, J. Aarik, K. Kukli, H. Käämbre, M. Laan, "Conduction mechanisms in metal-dielectric-metal structures", In; Book of abstracts; ALD2004: a joint American Vacuum Society ALD and Baltic ALD conference Celebrating 30 years of ALD, 16–18 August, 2004, Department of Chemistry, University of Helsinki, Finland, 2004, P84. (poster presentation)
3. I. Jõgi, J. Aarik, K. Kukli, H. Käämbre, M. Laan, J. Lu, T. Sajavaara, T. Uustare, "The effect of precursors on the structure and conductivity of atomic layer deposited TiO_2 films", EUROCVD-15, 4–9 Sept. 2005, Ruhr-Universität Bochum, Bochum, Germany. (oral presentation)
4. I. Jõgi, K. Kukli, J. Aarik, A. Aidla, J. Lu, "Precursor-dependent structural and electrical characteristics of atomic layer deposited films: Case study on titanium oxide", E-MRS IUMRS ICEM 2006 Spring Meeting, Symposium L: Characterization of High-K Dielectric Materials, 29. May – 2. June, 2006, Nice (French Riviera), France. (oral presentation)
5. I. Jõgi, K. Kukli, M. Laan, J. Aarik, A. Aidla, M. Pärs, J. Lu, "Effect of precursor chemistry on electrical and structural properties of TiO_2 films", In; Book of abstracts; Baltic Conference on Atomic Layer Deposition 2006,

19–20 June, 2006, Department of Chemistry, University of Oslo, Norway, 2006, 6. (oral presentation)

6. I. Jõgi, K. Kukli, M. Ritala, M. Leskelä, "Characterization of $Al_{1-x}Ti_xO_y$ Mixtures and Al_2O_3-TiO_2 Nanolaminates", In; Book of abstracts; American Vacuum Society 7th International Conference on Atomic Layer Deposition ALD2007, 24–27 June, 2007, Kona Kai Resort, San Diego, CA, USA, 2007, P20. (poster presentation)
7. I. Jõgi, M. Pärs, J. Aarik, A. Aidla, M. Laan, J. Sundqvist, L. Oberbeck, J. Heitmann, K. Kukli, "Conformity and structure of titanium oxide films grown by atomic layer deposition on silicon substrates", Thin Solid Films, Date of acceptance 28.08.2007.

Author's contribution

The author has made all electrical measurements, FTIR measurements and analysis of conduction mechanisms and wrote the articles II–IV.

3

ABBREVIATIONS

AFM	Atomic-Force Microscopy
ALD	Atomic Layer Deposition
ALE	Atomic Layer Epitaxy
BEES	Ballistic Electron Emission Spectroscopy
C-AFM	Conductive Atomic-Force Microscopy
CET	Capacitance Equivalent Thickness
CMOS	Complementary Metal-Oxide-Semiconductor
CVD	Chemical Vapor Deposition
DLOS	Deep-Level Optical Spectroscopy
DLTS	Deep-Level Transient Spectroscopy
DRAM	Dynamic Random Access Memory
DSSC	Dye Sensitized Solar Cell
EDS	Energy Dispersive Spectroscopy
ELD	Electron Luminescence Display
EOT	Equivalent Oxide Thickness
EPMA	Electron Probe Microanalysis
FED	Field Effect Display
FET	Field-Effect Transistor
FTIR	Fourier-Transform Infrared
GI-XRD	Grazing Incident X-Ray Diffraction
HR-TEM	High Resolution Transmission Electron Microscopy
IPE	Internal Photoemission
MEMS	Microelectromechanical Systems
MIGS	Metal-Induced Gap States
MIM	Metal-Insulator-Metal
MIS	Metal-Insulator-Semiconductor
MI(S)TT	Metal/Insulator (Semiconductor) Tunnel Transistor
MOSFET	Metal-Oxide-Semiconductor Field-Effect Transistor
Re-RAM	Resistive Random Access Memory
RBS	Rutheford Backscattering Spectroscopy
RCA	Radio Corporation of America
RHEED	Reflection High-Energy Electron Diffraction
SEM	Scanning Electron Microscopy
TCO	Transparent Conductive Oxide
TEM	Transmission Electron Microscopy
TFT	Thin Film Transistor
TMA	Tri-methyl Aluminum ($Al(CH_3)_3$)
TOF-ERDA	Time-of-Flight Elastic Recoil Detection Analysis
TTIP	Titanium Tetra-isopropoxide ($Ti(i\text{-}OC_3H_7)_4$)
VBET	Valence Band Electron Tunneling
WKB	Wentzel-Kramers-Brillouin

XPS	X-ray Photoelectron Spectroscopy
XRD	X-Ray Diffraction
XRR	X-Ray Reflection

1. INTRODUCTION

TiO_2 is abundant material which can potentially be used in numerous applications. Traditionally, TiO_2 has been used as a pigment in the paints and nowadays in plastic, paper and in sun creams [1–2]. At present, TiO_2 applications are widened and it is used as photocatalyst [1–3], solar cells [4], gas sensors [5–9] and in a smaller scale in ELDs [10–12]. Performance of TiO_2 has been studied in functional coatings [13–15], MEMS [16–18], photonics [19–20], spintronics [21–23], lithium ion batteries [24–26], TCOs [27–32], cold emitters [33–39] and microelectronics [40–62]. In electronics, TiO_2 has been considered as a candidate for insulator materials in conventional, silicon-based MOSFETs [40] as well as in DRAM capacitors [41–46]. However, TiO_2 will more likely find use in organic TFTs [47–48], MITTs [49–53], bioelectronics [54] and Re-RAMs [55–62].

In many of the aforementioned applications, the electrical properties of the TiO_2 play a crucial role. However, the demands for electrical properties can be contradicting in the case of different applications. In TCOs, MEMS and also in solar cells and photo-catalysts, the conductivity should be as high as possible, whereas in insulator applications the leakage currents should be minimized. In many cases the use of proper dopant atoms could drive the electrical properties to the desired direction, but the knowledge on the properties of undoped TiO_2 is still crucial. The knowledge on dominant conduction mechanism can assist in the optimization of deposition process of materials planned for use in different applications. If the conduction is controlled by the intrinsic properties of material, the optimization of deposition process is of lower significance. On the other hand, if the conduction is controlled by defects in the material, the growth process has to be optimized. Main difficulties in measuring the currents and consequent analysis of the conduction mechanisms in thin TiO_2 films stem from the intrinsically high leakage due to small band gap [63] and n type conduction [64]. In addition, the conductivity of pure TiO_2 is often screened by the variable quality of oxide/electrode interface [63,65–66] and residual impurities [67–69] caused by the chemical deposition process. These extrinsic effects have to be properly investigated and taken into consideration while analyzing the conduction mechanisms.

In many applications, the substrates for desired materials have rather complicated shape (catalyst, solar cells, MEMS, inverse opals, DRAM trenches, etc) [1–4,70–72,16–20,44]. In addition, the lateral dimensions of the substrate can be large (ELDs). Despite the substrate dimensions, the resulting film still has to be uniform and pinhole-free over the whole substrate area. The atomic layer deposition method is one of the few methods allowing to grow conformal and uniform films on large areas [19–20,70–75]. The maturing of the ALD process is confirmed by its use in the manufacture of integrated circuits which has very demanding requirements for deposition process [76]. In this

connection, the conduction mechanisms in mainstream high-k materials based on HfO_2, as well as ZrO_2, are thoroughly studied because of their popularity as prospective MOSFET gate insulators [63,78–79].

The present study was carried out to understand the conduction mechanisms in TiO_2 based materials grown by ALD. Considerable work has earlier been done to study the growth mechanisms, crystal growth and physical properties like band gap, refractive indices and permittivity of ALD grown metal oxide films including TiO_2 [80–97]. However, the conduction mechanisms in atomic layer deposited TiO_2 have not been studied thoroughly yet. In fact, there is almost no data concerning conduction mechanisms of ALD TiO_2 [55–56] Moreover, the data published to date about thin TiO_2 films synthesized by alternative methods is diverse [40,65–66,98–124], and may not be taken as relevant to ALD films. This work has been devoted to the clarification of the conduction mechanisms and, possibly, the improvement of insulating properties of TiO_2 based films. However, the conduction mechanisms in TiO_2 based thin film materials are relevant also for other applications.

The first chapter of this thesis will give the background needed for the analysis of the conduction mechanisms. At first, possible applications of TiO_2 will be described. The following section will describe the atomic layer deposition method and its features which can influence the properties of resulting films. Then, the material properties determining the electrical behaviour and conduction mechanism of materials will be described. After this, the overview of different conduction mechanisms will be given. The final part of this chapter will contain an overview of previous studies concerning conduction mechanisms in thin TiO_2 films.

The next chapter deals with the experimental methods describing the preparation of samples and the methods used to characterize the resulting films.

In the chapter “Results and Discussion” the results of various measurements and analysis on TiO_2 containing stacks will be brought out. At first, the electrical properties of TiO_2 in different stack configurations were studied in respect of deposition conditions. After this, the effect of inclusion of Al_2O_3 into the TiO_2 on the electrical properties of resulting film was examined. Finally, on the basis of the experimental work done, model calculations were used to predict the trends of different TiO_2 based insulators in future capacitor applications.

In the summary, the main results and conclusions will be highlighted.

2. BACKGROUND

This chapter casts insight into various concepts needed for the analysis of conduction mechanisms in thin films. Pure TiO_2 with its different phases is already thoroughly studied and has been considered as a model system in surface science [e. g. 125]. Contemporary studies are mostly focused on applications of TiO_2 films and therefore a lot of attention is paid to the dependence of TiO_2 properties on deposition methods. In this chapter the potential applications of thin TiO_2 films and the atomic layer deposition method are presented. Further, the material properties determining the conduction mechanisms and various conduction mechanisms recognized in thin films are described. Finally, earlier studies concerning conduction mechanisms in thin TiO_2 films are reviewed and on the basis the plan of present studies is proposed.

2.1. Thin film applications

2.1.1. Cold emitters

Main application of cold emitters is in FEDs as electron sources [33]. In addition, they are studied to obtain better knowledge on electron emission into corona discharge [37–38]. Historically, the metal electrodes have been used as emitting materials, but the use of thin insulating layers on the metal has enhanced the currents by several orders of magnitude [34–38]. One material used as insulator is atomic layer deposited TiO_2 and the electron emission from such systems is studied also in the University of Tartu in Gas Discharge Laboratory [37–38]. The exact mechanisms for increased currents are still under examination, although the model considered as the most successful to date is the two-step emission from the metal to insulator and from the insulator to the vacuum or gas [34–39]. In principle, the emission currents should depend on the barriers at metal/insulator and insulator/gas interfaces [37–38]. In addition, the band bending near electrode/insulator interface due to donor levels can affect the emission currents [34–36]. Thus, the knowledge on the barrier heights and shapes is necessary to model the emission, being one of the initial reasons to study the electrical properties of atomic layer deposited TiO_2.

2.1.2. Integrated circuits

The CMOS logic elements (e.g. CMOS inverter) consist of complementary n and p channel MOSFET's [see for example 126]. Main feature of CMOS elements has been effectively zero current flow during the off state. The switching speed of these transistors depends on the current between source and drain I_{DS}. Besides various other parameters, I_{DS} depends on gate insulator capacitance $C_{inv} = \varepsilon\varepsilon_0 A/t_{ox}$, where ε is the relative permittivity of gate oxide material, t_{ox} is the oxide thickness, ε_0 is vacuum permittivity and A the area of gate. The increase in drain currents has been achieved by decreasing the gate oxide thickness. Thermally or chemically grown SiO_2, traditionally used as gate oxide, is an exceptionally good insulator but has low permittivity (3.9). In order to increase the gate capacitance, the thickness of SiO_2 should be decreased below one nanometer, causing considerable increase in tunneling currents and limiting the scaling process. Because of this the use of materials with higher permittivity (high-k) is inevitable, allowing one to maintain or even increase the gate capacitance density at higher thickness values. The high-k materials which will replace the SiO_2 have to satisfy several requirements, including good thermodynamic stability on silicon, low amount of defects, high band offsets with silicon, high breakdown field and good temperature stability. Because of these reasons the possible candidates to replace the SiO_2 are limited. Several papers and overviews are devoted to the CMOS scaling problems [63,126–127].

DRAM consists of separately addressable capacitor cells (Fig. 1) which can storage charge for a certain time. MOSFET transistor is used as a switch for each cell. Similarly to ICs, there has been aggressive shrinking of cell dimensions to increase the memory density. Because of reliability problems, the charge stored in capacitor can not be decreased below certain values and thus, with the decrease in cell area, either the insulator thickness must be decreased or the dielectric material replaced by material of higher permittivity. An additional way to retain the capacitance value, while decreasing the cell area, is to increase the electrode area using complex three dimensional structures [128]. The constraints to DRAM capacitor insulators are not as stringent as for gate oxides, but high barriers at electrode interfaces and temperature stability are still desirable. In addition, the insulator considered should grow conformally with excellent step coverage.

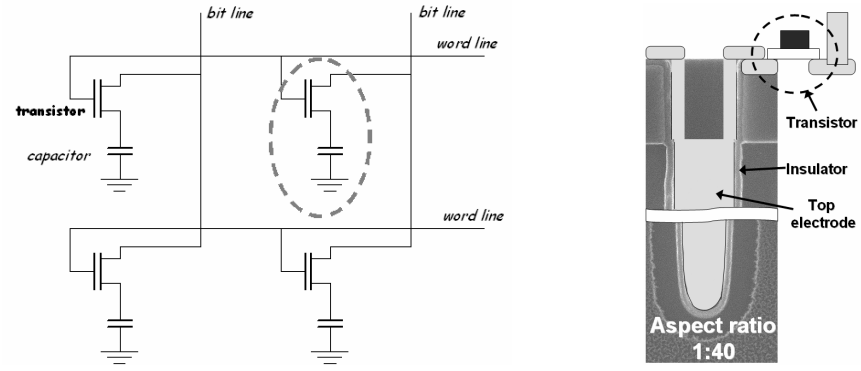

Figure 1. Scheme of DRAM memory (left) and a memory cell with high aspect ratio capacitor and transistor (right).

High-k materials as insulators may be used also in transistors not based on silicon technology [47–48,120–124,129–137]. The native oxides of alternative semiconducting materials (Ge, GaAs, organic substrates) may not be as good insulators as SiO_2 or are instable [129–133,135–137,47–48] whereas the deposition of SiO_2 on these substrates may be complicated [138]. Al_2O_3, for example, has received much attention as gate dielectric in such transistors [129–134]. Some high-k materials can be deposited at low temperatures allowing their use in thin film transistors grown on organic substrates (e.g. for flexible displays) [47–48,133].

2.1.3 Metal/insulator tunnel-transistors

Metal/insulator tunnel-transistor is a possible alternative candidate for future MOSFETs [49–53]. Herewith the proposed advantages are smaller dimensions, simpler fabrication process, high switching speed in the order of picosecond and higher tolerable fields [49–53]. Its working principle relies on the fact that tunneling currents through potential barrier depend strongly on the barrier thickness. After applying voltage between source and drain, the tunneling current will flow through the barrier with height ϕ_B and barrier thickness depending on the insulator thickness and applied bias (Fig. 2). The effective barrier thickness can be modulated by gate voltage (Fig. 2) and the currents may change by several orders of magnitude.

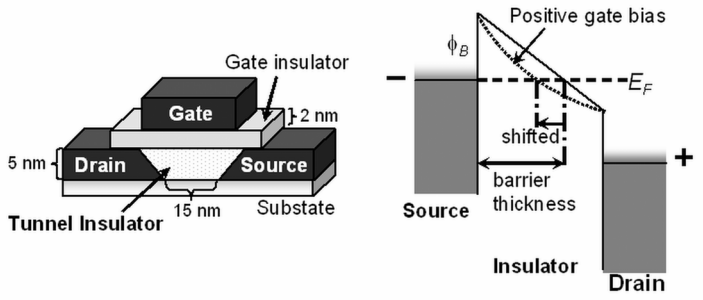

Figure 2. Schematic view of MITT structure (left) and band diagram illustrating working principle of MITT (right).

The barrier height ϕ_B must be lower than 1 eV for acceptable on/off ratio of source-drain currents. This makes TiO_2 suitable candidate for tunnel insulator material and there has been some success in fabricating MITTs based on Ti/TiO_2 barriers [49–53]. However, these transistors suffered from high thermionic currents at room temperatures [49–53] and, therefore, additional work has to be done to obtain more suitable barriers.

2.1.4. Resistive RAMs

Re-RAM is a new memory type where the resistivity of thin film can be repeatedly changed by several order of magnitudes with suitable voltage pulses [55–62,139–143]. TiO_2 (deposited also by ALD) has recently found much attention in respect with this application [55–62]. Usually, a high voltage pulse is applied at first to induce soft breakdown. After this, the conductivity will turn to high state due to the formation of highly conducting filaments. When the currents in high state will exceed some critical level, the conducting filaments will be destroyed and the conductivity will become low again. The exact mechanism for filament formation is not clear yet, but the movement of oxygen vacancies is probably contributing to the mechanism [55]. High switching speed, large on/off ratio and good stability has already been achieved with ALD grown TiO_2 films.

2.1.5. Other applications

The conductivity of TiO_2 films strongly depends on the amount of impurities on the surface and in the bulk of the film (oxygen vacancies, hydrogen etc.) [5–9]. Thus the conductivity is influenced by changes in environmental and deposition conditions. The dependence of conductivity on adsorbed impurities makes it a feasible material for solid state gas sensors [9]. Usually, porous films are used for sensor applications [6–8], but the use of thin, preferentially epitaxial, films

(~10 nm) can enhance the response time to the changes of environmental composition [144]. The n-type transparent conductors should have high electron affinity and band gap higher than 3 eV [32] which makes TiO_2 a good candidate for n-type TCO. With proper doping with metallic additives (e.g. Nb, V, Co, Pd), the conductivity can substantially improve [27–31]. Both the conductivity and transparency depend also on intrinsic impurities like oxygen vacancies and nonstoichiometry, as well as on structural defects [32], making the knowledge on properties of undoped films important. In MEMS, the TiO_2 coating can be used as protective layer [16–18], while the surface conductivity has to be as high as possible, in order to remove the static surface charge affecting the performance of micromechanical devices. TiO_2 is used also as a semiconductor material in DSSCs [4, 145–146] where high conductivity and small charge carrier trapping is desirable. Similar requirements are needed also in photocatalysts where generated carriers need to reach surface and react there [1–3].

2.2. Atomic layer deposition method

There are many methods suitable for the deposition of thin films which can be divided into physical and chemical deposition methods. In the case of physical deposition methods, the film deposition proceeds via evaporation, transport and (reactive) deposition of only the constituent elements or compounds. In the case of chemical methods, one applies chemical compounds as film precursors, whereby the ligands bound to cation are not supposed to remain in resulting films – they do not belong to the target composition of the film. ALD method belongs to the chemical methods, which involve surface exchange reactions as the dominant growth mechanism, whereby the surface reactions are self-limiting, allowing precise tuning of the thickness and growth largely independent of the shape of the substrate. The method will be described below together with potential applications, and finally the description of the deposition parameters for the films used in this study will be given.

2.2.1. Basics of ALD method

The ALD method is a gas phase deposition process, which uses alternating saturative surface reactions [147]. The principle of ALD method is described in the figure 3 exemplified by the deposition of TiO_2. The most important aspect of ALD is the self-limiting adsorption of precursors and layer-by-layer growth of the material (sub-monolayer deposited in one cycle) in the case of properly chosen thermal and pressure conditions (ALD window). Due to the self-limitation, the thickness increase remains mainly dependent on the number of applied cycles, rather than reactant flux or cycle time parameters. This allows

the growth of films with precise thickness control and uniformity even on most complex surfaces [14,19–20,73–75]. In addition, ALD method allows uniform deposition over large areas, when uniform growth conditions are provided over the whole area. Due to the surface reactions and chemically bound layers, the adhesion of deposited material is usually good and the deposition induced damage to substrate is low, provided that the precursors do not etch the substrate. The properties of resulting films should also not depend too strongly on the configuration of the used reactor if precursor pulses are long enough to achieve surface saturation (proper ALD).

The main drawback of ALD method is relatively low growth rate (200–500 nm in a day). Since the film deposition uses chemical exchange reactions on substrate surface, the ALD introduces also considerable amount of residuals, such as carbon or hydrogen, as initial constituents of precursor chemicals. Residual impurities are, at the same time, characteristic of any chemical deposition method. Especially in the case of non-optimized growth conditions, thermal decomposition of the precursors may occur. At too low temperatures, close to reaction threshold, the content of residues may even reach 10–15 at. %. The exact amount and nature of these residuals depends on substrate temperature, pulse times, vapor pressure and naturally on precursor composition.

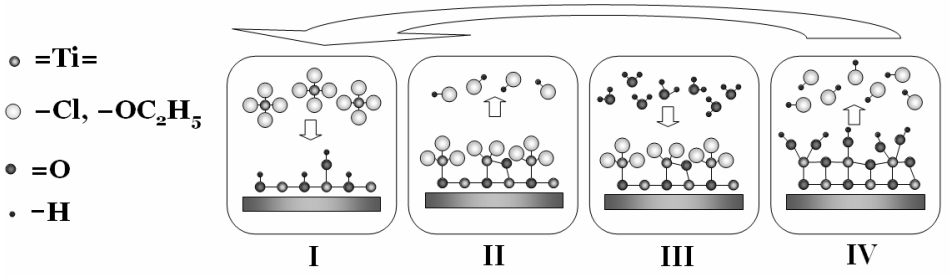

Figure 3. Principle of atomic layer deposition of TiO_2 from chloride or metoxide as Ti precursor and from water as oxygen precursor. Hydroxylated substrate surface is exposed to $TiCl_4$ or $Ti(OCH_3)_4$ fluxes (**I**). Ligand exchange reaction proceeds until the whole surface is terminated with $TiCl_m$ or $Ti(OCH_3)_m$ groups. During the purge period reaction products (HCl, $HOCH_3$) and excess precursor gas are removed (**II**). The surface is subsequently exposed to the H_2O which reacts with -Cl or –(OCH_3) until the surface is again hydroxylated i.e. covered with –OH groups (**III**). After removal of the reaction products and excess H_2O during the second purge time, the cycle becomes closed and next cycle can start (**IV**). Purified N_2 or Ar is usually used as both precursor carrier and purging gas.

To date, many different types of precursors (precursor classes) have been examined in ALD of different materials. The main properties characterizing an ideal ALD precursor include volatility, fast and reproducible vaporizing i.e. suitably high vapor pressure, resistance to thermal decomposition at the surface or in gas phase, high reactivity towards other precursors and volatile but not corrosive by-products (etching and tool corrosion) [148–149]. These features should result in fast growth, low amounts of residues, good reproducibility and long durability of tools. Available precursors seldom fulfill all the requirements but are good usually only at some aspects. Therefore the selection of precursors often depends on the objective and target substrate properties. In the case of simultaneous deposition of different constituent material layers, the precursors for these materials have to allow atomic layer deposition at the same temperature. The most common metal precursor classes are halides (chloride and iodide) and alkoxides (metoxide, ethoxide etc.) [80–96,148–149]. The oxide precursors have been water, hydrogen peroxide, oxygen, ozone, or radicals of these compounds [80–96,41–46,148–151]. Some of these are good for fast growth, some leave lower amount of residuals to the film (e.g. iodide and oxygen give the purest films due to the absence of hydrogen in the process) whereas some allow good conformity. Thus, practical applications and deposition of functional films are often trade-offs between precursor properties and eventual film quality considering the most crucial aspects described above.

2.2.2. ALD method for thin film applications

For industrial applications, large throughput has traditionally been more important than the purity or precise thickness control and ALD method may not be easily accepted as a viable method. On the other hand, ALD method is truly shining in the applications where the thickness of desired film is small and/or the film has to be uniform over large area or/with complex surface. The first application for ALD films was ELD even though the acronym ALE was used at that time [152]. In ELDs the need for precise thickness control on extremely large area (up to 17‘) outweighed the time consuming deposition (several days for one panel) while the functional thickness of deposited layer reached several hundreds of nanometers.

With the aggressive downscaling in electronics ALD method has become feasible also in the production of integrated circuit elements. The use of ALD as deposition method for Hf containing gate oxide in future “Intel” processors “Penryn” with 45 nm node length was reported recently [76]. The use of ALD for deposition of insulator layers in DRAM capacitor is under investigation as well [128]. In deep trenches with high aspect ratio (subsection 2.1.2) the ALD is likely the only viable technique allowing conformal growth, uniformity over large area and good adhesion of films. The resulting insulating films have to contain small amount of impurities for low leakage currents. The growth

temperature is not that important but crystalline films with leaky grain-boundaries should be avoided. In addition, the growth rate is not of crucial importance due to small thickness of layers. In the case of DRAM applications, conformal growth over large area is one of the main demands for precursor chemistry.

Along with the growing popularity of ALD method, it has found use in several other applications as well. ALD is probably the only usable technique in the production of inverse opals for photonic applications [19–20]. Because of low thermal budget, radical-enhanced ALD (RE–ALD) has been used in applications where high temperature could damage the substrate, e.g. ALD of Al_2O_3 has been studied for the use in flexible displays grown on organic substrates which do not survive temperatures higher than 200°C [153–155]. In addition, the RE-ALD method has been considered for functionalizing wool fibers [150–151]. ALD has been used for the preparation of thin film sensors [144], photocatalyst applications [156–159] and coating material for MEMS [16–18] etc. It has great potential in functionalizing highly porous substrates with new properties (new applications in photovoltaics, sensors, nanotubes, etc.) [158–161]. All these applications set limits to the precursor chemistry and other deposition parameters.

2.2.3. ALD of TiO_2 and Al_2O_3

The ALD processes of metal oxides used in this work are basically established and studied in terms of thermal behaviour of precursors, growth rate behaviour against substrate temperature, growth mechanisms, and basic temperature dependences of the crystalline structure of the resulting films [80–96,162–165]. In the present thesis, the dependence of electrical properties on precursor chemistry and deposition temperatures was examined, as described more thoroughly below.

Metal chlorides are probably the most studied metal precursors, such as $TiCl_4$ as an ALD precursor of TiO_2 [80–86]. Considering the ALD of Al_2O_3, probably the most feasible precursors are trimethylaluminum $Al(CH_3)_3$ (TMA) and H_2O [162–164], although the aluminum trichloride has also been often used [165–166]. The halides, especially chlorides, have high decomposition temperatures (up to 800°C) which allow probably the largest temperature range for ALD [167]. This in turn can be advantageous when intense crystal growth or achievement of phases with higher permittivity on arbitrary substrates are needed as it is in the case with TiO_2 [80–81,85,87–91]. $TiCl_4$ and TMA consist of rather small molecules, react aggressively with water and are highly volatile, which should be good for applications demanding good conformity. The main problem with chlorides is the reaction product HCl, which is corrosive. Besides, HCl contaminates films with chlorine and can block reactive surface sites by reacting with –OH groups [168–169]. Iodides, as compared to halides on the

basis of their smaller corrosivity, larger ionic radii of the ligands and weaker metal-ligand bond strength, may also perform as good precursors. As the iodides react even with pure oxygen, they allow ALD deposition of the purest TiO_2 films without detectable traces of contaminating residual impurities at relatively low substrate temperatures [89]. Unfortunately, the iodides are solid precursors with variable shelf-life and require high evaporation temperatures.

Alkoxides are popular thin film precursors especially because their importance in CVD. For ALD, well working alkoxide precursors exist for TiO_2, Ta_2O_5 and Nb_2O_5 [92]. The reaction products in the case of alkoxide precursors do not corrode the tools or etch the films. However, alkoxides have problems with the thermal decomposition [92–93] and with the increase of ligand molecules size (from titanium methoxide to butoxide), the decomposition temperature decreases [92–93]. Thus the films grown from alkoxides usually contain higher amount of residuals compared to halide processes [94,96–97].

The main oxygen precursor in ALD is water [80–86,91–96,162–165]. In addition, hydrogen peroxide [87–88,96], oxygen [89–90,41–42,56–57,164], ozone [43,55,164] and even metal alkoxides [170] with intrinsic oxygen have been used as oxygen sources. The water (as well as hydrogen peroxide) can be an additional source of hydrogen contamination in the case of alkoxide-based processes and the main hydrogen source in the case of halides. However, the handling of water is easy and it is reactive with most metal precursors. Hydrogen peroxide is usually more active but it has the tendency to decompose before reaching the surface [96]. The molecular oxygen itself is not active enough in reactions with the most of metal precursors (except iodides) but the oxygen radicals and ions produced by plasma have been found wide use especially in the case of low-temperature processes [150–151, 153–155].

The amount of impurities in resulting films depends on substrate temperature, often being smaller at higher temperatures. The substrate temperature is also the main factor controlling the phase composition. The onset temperature of crystallization to anatase depends on precursors, substrate material and film thickness and is usually between 130°C and 200°C. In the case of halide precursors, the crystallization starts at temperatures as low as 135–150°C [85,91] whereas in the case of alkoxide precursors the critical crystallization temperature is somewhat higher, 180°C [94,96]. With the use of halide precursors rutile starts to appear in TiO_2 grown on Si (1 0 0) at 300°C [87–88]. At the same time, thermal decomposition of alkoxide precursors starts also at around 300°C and probably complicates the formation of rutile [92–93]. In the case of substrates supporting epitaxial growth, such as sapphire, the rutile can be grown at temperatures lower than 300°C [85,87]. However, monocrystalline substrates enabling epitaxy are often insulating materials and thus hardly of interest when concerning the evaluation of capacitive properties. In the case of ALD TiO_2, probably the only exception has been RuO_2 formed on Ru electrode by ozone

treatment, where the growth of locally epitaxial rutile was achieved in a capacitor stack [45].

2.3. Properties of materials

The properties of stacks containing thin film insulator depend both on intrinsic properties of insulator and electrode material. The intrinsic properties of the material comprise the defects created during the preparation. Thus, in the first subsection, main parameters of films determining the electrical properties and conduction mechanisms will be described. The second subsection will describe the properties of materials used in this thesis.

2.3.1. Basic Concepts

The intrinsic characteristics defining an insulator or semiconductor comprise band gap, electron affinity and frequency dependent dielectric constant. These characteristics are related to each other via atomic interactions, determined by chemical and phase composition. The films can appear in crystalline or amorphous form. In crystalline form, there exists long-range periodicity in the spacing of atoms forming the material. Within the same nominal chemical composition, the phase depends mainly on conditions during synthesis of films (temperature, pressure etc). Often there exists only a short range order. This is usually the case for films deposited at relatively low substrate temperatures. Such amorphous films retain most properties of their crystalline counterparts which are defined by the interatomic forces. However, the structural disorder induces also differences in the characteristics. The films deposited at sufficiently high temperatures tend to form polycrystalline and contain crystals of variable size and/or phase composition. The properties of such films can vary considerably depending on exact phase composition.

Crystalline films have well defined band edges due to long-range periodicity of atoms forming the crystal (Fig. 4) [171–174]. The density of allowed states in the conduction and valence bands of crystalline solids is parabolic and the states induced by impurities have well defined energies in the band gap (Fig. 4). Even though the band gap width is retained in the amorphous films, the band edges become blurred. There is a gradual transition from quasi-continuous states where carriers are relatively free to move, to strictly localized states (density of states tail) or traps where carriers are immobile (Fig. 4) [171–175].

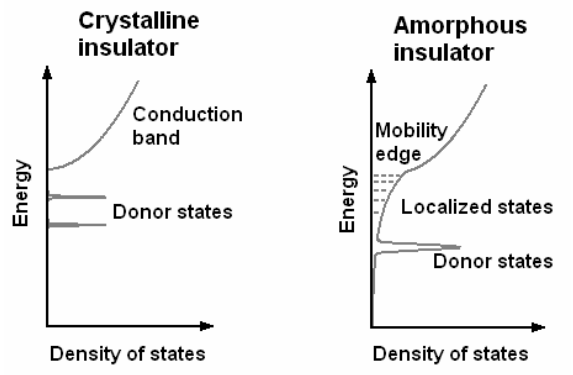

Figure 4. Band offset and defects in crystalline (left diagram) and amorphous (right diagram) insulator or semiconductor.

The electron affinity is another important parameter defining the insulating properties of films [63,77–79]. The electron affinity is the energy needed to move electron from the bottom of conduction band to the vacuum level. In the case of metal-oxides, the affinity is usually related to the band gap of the material and is larger if the band gap is smaller.

The dielectric constant of materials has several different contributions with different ability of dipoles and ions to response to the field and, therefore, the dielectric constant depends on frequency [63,77–78]. At CMOS working frequencies, the main contribution to the permittivity of high-k materials is caused by ionic polarizability. The ionicity of transition metal oxide bonds is one reason for large dielectric constant [63,77–78]. The measurements of low-frequency (static) dielectric constants are usually performed at the frequencies in the range of 10–10^6 Hz, where the orientational and dipolar contributions are also important. Thus these dielectric constant values are not entirely relevant to CMOS applications, although they characterize the same material. In the optical frequency range only the electron component of permittivity remains related to refractive index as $\varepsilon_\infty = n^2$ [78].

In addition to dielectric constant, the ionicity of oxide bonds is one factor determining both the band gap width and thermal stability which are decreased with larger ionicity [63]. On the other hand, the breakdown field is inversely dependent on dielectric constant [176]. Thus, benefits from increasing dielectric constant will be reduced by the decrease of band gap, thermal stability and breakdown field. The dielectric constant is also inversely related with unit cell volume of crystal [177]. Thus, in the case of crystal phases with smaller unit cell volumes (e.g. rutile), the dielectric constant is higher while band gap and breakdown fields are smaller.

2.3.1.1. Defects

In addition to the intrinsic parameters like band gap and dielectric constant, the properties of thin films depend on various chemical and structural defects, which often dominate over the intrinsic physical parameters. The defects can be divided to residual impurities and to disorder-induced defects which may as well be interrelated and can also be considered as intrinsic in terms of film growth technology, i.e. precursor chemistry. Another possibility is to divide the defects according to the charge state [171]. One type of defects is neutral in its electron-rich state and becomes positive after loosing the electron. The other is neutral in its electron-deficient state and becomes negatively charged after capturing an electron [171]. The first type is called donor. The impurity atoms with higher valence number, vacancies or interstitials can give rise to donor states when they can introduce their own electron(s) to the system. The other type is called traps. The trap states can be introduced due to the lack of long-range order and due to impurities with same valence as the lattice. Disorder induced traps have usually broad energy distribution while donor levels have still sharply defined energy in the band gap [171].

Impurities at one ppm level would result in the impurity concentration values in the order of magnitude 10^{17} cm^{-3}. The detection limit of most chemical analysis methods for solid films is 0.1 at % of impurities which would correspond to impurity concentrations in the order of 10^{19} cm^{-3}. The effect of different impurity atoms is not clarified yet and should strongly depend on the environment surrounding the impurity. In addition to the impurities due to point defects, the grain boundaries and amorphicity can induce high amount of traps. For crystallite sizes of 10 nm, grain boundary defects alone can result in trapping densities as high as 10^{18} cm^{-3} [173]. The trap concentrations in amorphous films which have gradual change of band states to localized states may reach the concentration of band states in the order $10^{21} – 10^{22}$ cm^{-3}.

2.3.1.2. Electrodes

The electrode material can strongly influence the electrical properties of insulating thin film stacks. The main parameters of electrodes affecting the electrical properties of the stacks are work function and thermodynamic stability. In the case of SiO_2 and metal oxides with high band gap, the barrier heights at electrode Fermi levels and oxide conduction/valence bands depend approximately linearly on the metal work function ϕ_m [178]. The exact values of barrier heights will vary due to Fermi level pinning $\phi_0 = S(\phi_m - \phi_{int}) + (\phi_{int} - \chi_i)$, where the ϕ_{int} is insulator work function at interface, χ_i is insulator affinity and S is Schottky pinning parameter [178–179]. The value of S can vary from 1 (Schottky limit of no pinning) to 0 (Bardeen limit of strong pinning) and is considered to be inversely proportional to high-frequency dielectric constant

[178–179]. Mechanisms behind the Fermi level pinning are not yet clarified, although MIGS, formation of surface dipole, oxygen vacancies or the diffusion of electrode and insulator atoms are usually used to explain the pinning [178–183]. The thermodynamic instability can result in thin interfacial layers between electrodes and insulators. For example, SiO_2 or Si-rich metal oxide layer often forms between silicon and metal-oxide films [63,77–79]. In addition, metals with low work function have usually large oxide formation enthalpy, and thus formation of interfacial layers is more probable [179–180,184]. These layers have usually smaller permittivity and higher amount of defects [184–185]. In addition, they can change the barrier heights [184]. The modifying effect of the interface defects on the barrier heights depends strongly on the manner in which the metal-insulator structure is prepared [180,184,186]. Therefore the barrier heights should be determined experimentally for any particular stack.

Apart from pinning effects which depend on the Fermi level at insulator interface and extend only to several ångstroms, there appear band distortions due to the differences in Fermi levels at interfaces and insulator bulk (Fig. 5). Resulting contacts between electrodes and insulating films can be divided into ohmic and non-ohmic [171,173]. The ohmic contacts are able to supply or remove charge carriers without giving rise to space-charge (Fig. 5a). Non-ohmic contacts can be divided to blocking or injecting contacts depending on differences of electrode and insulator Fermi levels (Fig. 5b and 5c) [171,173]. In the case of ohmic contacts, the currents should not depend on voltage polarity while in the case of non-ohmic contacts the dependences are asymmetric [171]. Rather large amount of charge is necessary for observable band bending (10^{19} cm^{-3} for a bending length of 10 nm if the difference between electrode and insulator Fermi levels is 1 V (Fig. 5b and 5c)). These effects are usually neglected in the case of ultrathin films. In addition, it is argued [171,173,187], that due to deep gap states in strongly disordered films the charge carriers are readily injected to insulator and the effect of electrode is effectively canceled.

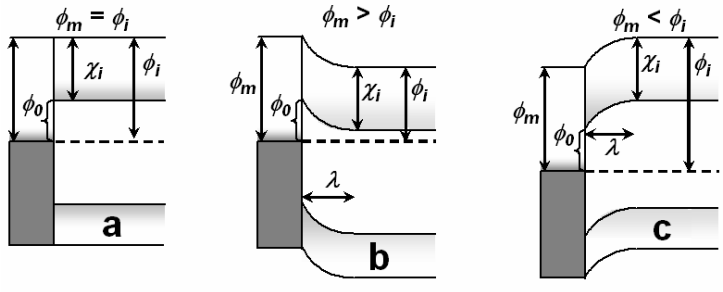

Figure 5. Schematic diagrams of (a) ohmic, (b) blocking and (c) injecting contacts at interfaces of electrodes and insulators [173].

Doped Si substrate has been and will likely remain for some time the main bottom electrode material in the MOSFETs, while poly-Si gate will be replaced by metal electrodes [78–79]. In similar way, metal electrodes will be used in DRAM capacitors [43–46]. The most promising electrode materials for MOSFETs are Ta based electrodes [78], Ru based electrodes [78,188] and metal-silicides (e.g. doped NiSi) [78–79]. Noble metal electrodes (Ir, Pt, Rh, Pd etc.) [189] and other metals, W, Mo, Ni and Al [190] are also studied especially for MIM capacitor applications. In the applications where ohmic contact is desirable, the metal electrodes with low work functions are used (e.g. Ti, Al) or, alternatively, indium-tin oxide (ITO) when the electrode has to be transparent [99].

2.3.2. Metal-oxides

The most common metal oxides used as insulators are Al_2O_3, HfO_2, ZrO_2, Ta_2O_5, TiO_2, but the oxides of rare-earth metals (lanthanides) are also intensely studied [63,77–78]. The metal oxides have ionic type of bonding and, due to strong ionic polarizability, they have higher permittivity compared to oxides and nitrides with more covalent bonds (SiO_2, Si_3N_4). The band gap is inversely related to permittivity, although in the case of metal oxides the relation is weaker [63]. The exact values of permittivity, band gap, band offsets and breakdown field of a certain oxide depend also strongly on phase composition. The metal-oxides studied in this thesis are TiO_2 and to a smaller extent Al_2O_3. These oxides will be described more thoroughly below.

2.3.2.1. TiO_2

TiO_2 has three well-known crystalline polymorphs: rutile, anatase and brookite (there exist also several exotic and different non-stoichiometric Magneli phases). Different physical properties of the anatase and rutile as the most abundant and widely used phases are listed in the table 1 [40,78,177,191–192].

Table 1. Physical properties of TiO_2. ε are static and ε_∞ high-frequency dielectric constants and m_e/m_{e0} is effective electron mass.

	unit cell Å^3	Density g/cm^3	ε	ε_∞	band gap eV	affinity eV	m_e/m_{e0}
anatase	136.25	3.895	31–50	6.3	3.2	3–4	1
Rutile	62.07	4.274	89–173	8.4	3.0	3–4	20

Anatase and brookite are metastable at normal conditions and transform exothermally and irreversibly to rutile at temperatures ranging from 750 to 1000°C [193–196]. Because of relatively low surface energy, the anatase is formed preferentially in the case of small size of crystallites [193–196]. In

addition to the crystalline polymorphs, amorphous phase is often found in films grown at low temperatures (< 200°C), while the contribution from disordered phase increases with the decrease in film thickness [95,167,197].

Among all of the TiO_2 phases, anatase has the highest photocatalytic activity and the best performance in sensor applications [167,196] whereas rutile has the highest permittivity [178,191]. The band gap of anatase is found to be larger than that of rutile [85, 192] whereas the data about electron affinities is varying [40,123 vs. 35,78,198–199]. Usually, TiO_2 has been considered as n type semiconductor because of oxygen vacancies or Ti interstitials (Ti donates electrons) [64], but there exist some works where the p type conductivity has been found [200]. In relation to the silicon based electronics, it has been found that the TiO_2 is not stable against Si and tends to form silicates [201]. The breakdown field of bulk TiO_2 is relatively low and usually between 0.5–3 MV/cm [65,176,202], although higher fields are also reported in thinner films where the interfacial layers play larger role [65,101]. DLOS studies on sputtered TiO_2 revealed a defect level at 0.86 eV from conduction band [68], while a DLTS study on MOCVD TiO_2 and hydrogen doped sputtered TiO_2 revealed defect levels at 0.52 eV and 0.85 eV from conduction band [69]. The state at 0.85–0.86 eV is attributable to O vacancy (capture cross-section $3.6\ 10^{-16}$ – $4.6\ 10^{-15}$ cm^2) [68, 203]. The state at 0.5 eV comes from residual hydrogen (capture cross section approximately 10^{-14} cm^2) [69]. The variation in exact energy values are possibly related with uncertainty in the detection of electric field values or due to the presence of several defect states.

2.3.2.2. Al_2O_3

Crystalline Al_2O_3 has also several different phases including γ-Al_2O_3 and α-Al_2O_3 but in most thin film applications, the films remain amorphous. Good stability against crystallization with high thermodynamic stability on Si is in fact one of the reasons why Al_2O_3 is popular in electronic applications. Amorphicity becomes technologically important in the cases where the grain boundary conduction has to be taken into account. In addition, Al_2O_3 has the highest band gap among metal oxides and high barriers at electrode/oxide interfaces which makes it good insulator [63,77–78]. The breakdown field of Al_2O_3 is also quite large (6–8 MV/cm) [176,204]. In the applications where thermal oxidation of Si is not possible due to different substrate material or low thermal budget, the Al_2O_3 is a good insulator candidate. The deposition of SiO_2 by ALD is complicated while the Al_2O_3 is one of the materials most conveniently grown by ALD. The main drawback of the Al_2O_3 is its relatively low permittivity (8–12), which limits its use as high-k material [63,204]. Al_2O_3 has also found use as coating and capping material in different applications [15,132,205–209].

2.3.2.3. Laminates and mixtures

In the case of mixtures and/or laminates of different binary metal oxides, there is possibility to vary the properties of the resulting films by changing the proportion of constituents. In the case of laminates, it can be expected that materials and their properties remain clearly defined. Thus, for high-k applications, the films with better insulating properties and thermodynamic stability could be used at interfaces while the films with higher permittivity could be used to increase the overall thickness of film. In the case of mixtures of materials with dissimilar properties (dielectric constant and electron affinity for example) the possibility to precisely adjust the material properties is desirable. In high-k materials it is hoped that the best properties of both materials are retained and effectively combined [210–214]. In practice, however, the resulting, real materials often behave worse than pure materials or model structures. The electron affinities of oxides of two metals are usually determined by the material of the higher affinity even at low concentrations [78,215–218]. At the same time, the dielectric constant is a linear function of the concentration of either constituent material in a good approximation. Therefore, the barrier heights at electrodes will be similar to the material with higher permittivity and smaller band gap whereas the permittivity of the mixture remains rather low. However, these trends are not too general and in some cases, the barrier heights are even higher in mixtures compared to constituent materials separately [219]. Thus the success in the use of mixture depends strongly on materials used [210–220].

2.4. Conduction mechanisms

The physical models for conduction mechanisms date back already to the first half of the 20th century. To derive quantitative formulas, many approximations have been used and often more or less ideal materials were assumed. The materials were supposed to be homogeneous, monocrystalline and trap-assisted models with well defined trap levels were exploited. Most of these models are verified and tested for materials whose fabrication is well established like Si, SiO_2, Si_3N_4, anodized Al_2O_3 etc. In addition, different mechanisms of conductivity can give similar functional dependencies and supplementary information is required to distinguish between the mechanisms.

The insulating films used in real applications can seldom considered ideal and, especially, electrical properties of TiO_2 are dependent on various defects. TiO_2 is a low band gap oxide and usually possesses n-type conductivity due to oxygen deficiency [64]. In addition, relatively high amount of residuals and variable phase composition is typical for films deposited by ALD in conditions where the method has advantage over other methods (e.g. low temperature

deposition and conformality). These defects will in turn affect the electrical properties of films. Because of the importance of defects, conduction mechanisms involving defects are described more thoroughly.

The conduction mechanisms can be divided into two subgroups: electrode limited and bulk limited [173]. The first group of conduction mechanisms deals with the charge carrier injection from cathode into the insulator while the second group deals with the transport of charge carriers in the insulator. The electrode limited conduction is more important in the case of thinner films and should depend strongly on the electrode materials. The bulk limited conduction is more important in thicker films and should not that significantly depend on electrodes. The mechanisms can also change from one type to other at some voltages depending on the material properties.

2.4.1 Electrode limited mechanisms

The ideal insulator itself has only a small amount of charge carriers thermally inserted from valence band to the conduction band. Thus, for observable currents, larger amount of carriers must be emitted from the cathode. The rate of carriers injected to the insulator is limited by the barrier between the electrode Fermi level and insulator conduction band minimum (valence band maximum) [171–174]. In the case of amorphous films the conduction band minimum is not clearly determined but there exists energy level above which the carge carriers are relatively free to move i.e. mobility band edge [174]. Fermi level pinning may also affect the barrier (subsection 2.3.1.2). Because of this, films with same nominal chemical composition can have different effective barriers depending on the preparation of film.

The charge carriers might overcome the barrier thermally or tunnel through the barrier (Fig. 6). When the film is sufficiently thin (< 5 nm), the probability of direct tunneling through the insulator layer to the anode is high enough to be seriously considered. If there are localized states due to the impurities in the forbidden gap near the cathode, the charge carriers can first tunnel to these states and, then, tunnel or become thermally activated to the conduction (valence) band or hop to the next state [171–174]. This type of tunneling is called trap-assisted tunneling which can be further divided and denoted as elastic and inelastic tunneling, one-step or multistep tunneling, etc.

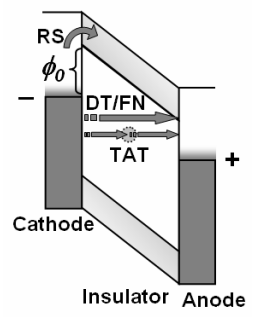

Figure 6. Band diagram of MIM structure showing barrier at interface ϕ_0 and different electron injection mechanisms; thermionic Richardson-Schottky (RS), direct tunneling or Fowler-Nordheim tunneling (DT/FN), or trap assisted tunnelling (TAT). Diagram is for electrons but is applicable for holes as well.

In general, the total amount of carriers surpassing the barriers is the integral of carriers over all energies passing the barrier

$$J = \int D(E)N(E)dE \qquad (1).$$

Here *N(E)* is the supply function and *D(E)* is the probability of emission at the energy *E*. The supply function *N(E)* is connected with the difference in Fermi distributions of electrodes $f(E) - f(E + eV)$ where $f(E) = [1 + exp(-(E - E_F)/k_BT]^{-1}$. The E_F in the formula is the Fermi energy of electrode, kT is the thermal energy, m_0 is the mass of carrier and h is the Planck's constant. For more accurate three-dimensional model, only the electrons with momentum in the barrier direction are taken into account and the supply function becomes

$$N(E_x, E_F) = \frac{4\pi m_0 kT}{h^3} ln\left\{\frac{1 + exp\left[-(E_x - E_F)/kT\right]}{1 + exp\left[-(E_x + eV - E_F)/kT\right]}\right\} \qquad [221].$$

Probability to surpass the barrier (transparency of barrier according to Hill [174]) is expressed by Wentzel-Kramers-Brillouin (WKB) approximation

$$D(E_x) = exp\left[-2\int\left|\sqrt{2m_{eff}m_0/\hbar^2\,(V(x) - E_x)}\right|dx\right] \qquad (2)$$

[222]. The *V(x)* is the potential energy of the barrier and the integral is taken over the range where potential energy of barrier is higher than E_x. It has been pointed out by Gundlach and Simmons [222] that the WKB approximation gives the same functional form when compared with exact methods when the $\Delta s\bar{\phi}^{1/2} > 4$. The Δs is the distance between turning points in angstroms and $\bar{\phi}$

is the mean barrier height above cathode Fermi level in electron volts. However, the pre-exponential factor in the probability calculations can vary in the case of WKB approximation from 1 to 10. The total current is an integral over currents over all energies in formula (1) but usually only a small energy range giving the major contribution to the currents has to be considered. The formulas describing the injection currents for more specific conditions are given below.

2.4.1.1 Richardson-Schottky effect.

At temperatures above 0 K, there is always certain amount of electrons with energy higher than the barrier height at electrode insulator interface. For such electrons, the probability to surpass the barrier is 1 ($(V(x) - E) \leq 0$ in formula (2)). Thus, the amount of these electrons is determined by the barrier height and the temperature-dependent energy distribution of electrons. When the barrier at cathode is higher than 3 kT (0.075 eV at room temperature), the amount of charge carriers having higher energy than the barrier can be approximated by the Bolzmann equation (the difference from Fermi distribution is less that 5 %).

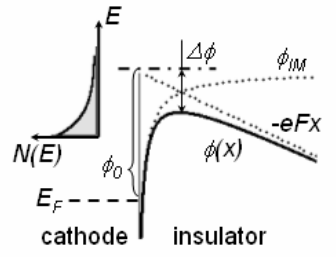

Figure 7. Diagram illustrating the Richardson-Schottky mechanism. The ϕ_0 is barrier height without image force effects. The decrease in maximum barrier height $\Delta\phi$ is determined by the potential lowering due to field E near the interface and by image force ϕ_{IM}. Bolzmann distribution of carriers is also shown to illustrate the strong effect of barrier lowering on the amount of carriers taking part in Richardson-Schottky currents.

Assuming triangular barrier at the interface and taking into the account the effect of image forces (Fig. 7) the Richardson-Schottky equation is achieved:

$$J = AT^2 \exp\left[-\left(\phi_0 - \beta_{RS} E^{1/2}\right)/kT\right]. \qquad (3)$$

Here $A = 4\pi m_{eff} m_0 k^2 / h^3$, $\beta_{RS} = \sqrt{e^3/4\pi\varepsilon\varepsilon_0}$, ϕ_0 is the barrier height at electrode at zero field and ε is the dynamic dielectric constant having value between low and high-frequency dielectric constant. It is argued that the dynamic dielectric constant is close to the high-frequency constant ($\varepsilon = n^2$ where n is the refractive indice) because the charge carrier spends only short

time at the electrode [223]. The temperature independent linear plot of *J-E* curves is $ln\left(J/T^2\right)\cdot exp\left(\phi_0/kT\right)\approx E^{1/2}/kT$ if Richardson-Schottky mechanism is dominating. The plot $ln\left(J/T^2\right)\approx 1000/kT$ is often used to obtain the value of barrier height, ϕ_0, but the decrease of barrier height by the value of $\beta_{RS}E^{1/2}$ must be taken into account.

2.4.1.2. Tunneling

To calculate the amount of tunneling electrons, the integral in formula (1) must be taken over all energies starting from the highest point of barrier to the lowest energies (can effectively be at infinity). The majority of charge carriers taking part from the tunneling currents lay in the energy range of $e\cdot V$ (V is applied voltage) between Fermi levels of cathode and anode [173,224] (Fig. 8). Using this presumption, following formula for tunneling through barrier with arbitrary shape has been derived [221]

$$J=\frac{e}{2\pi h}\frac{1}{\Delta s^2}\left\{\bar{\phi}\,exp\left[-\frac{4\pi\sqrt{2m}}{h}\Delta s\bar{\phi}^{1/2}\right]-\left(\bar{\phi}+eV\right)exp\left[-\frac{4\pi\sqrt{2m}}{h}\Delta s\left(\bar{\phi}+eV\right)^{1/2}\right]\right\}\cdot \quad (4)$$

Here Δs is the thickness of barrier at the Fermi level of cathode, $\bar{\phi}$ is the average height of the barrier higher than the Fermi level of cathode, V is the applied voltage, e is the electron charge, m is effective electron mass and h is the Planck constant (Fig. 8). Both Δs and $\bar{\phi}$ are functions of applied voltage V.

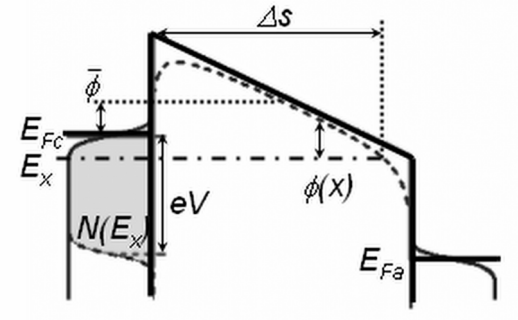

Figure 8. Band diagram including image force (dashed line) and supply function *N(E)* (shaded area) which depends on applied voltage $e\cdot V$. E_{Fc} and E_{Fa} are Fermi levels of cathode and anode respectively. E_x marks the energy level for which average barrier height $\bar{\phi}$ and barrier thickness Δs are calculated.

If the insulator is thin enough for the direct tunneling through the insulator, the energy limits considered for tunneling start approximately from the Fermi level of the cathode and end at the Fermi level of anode. At low voltage regime, Δs =

s and $\bar{\phi} = (\phi_c + \phi_a - eV)/2$ whereas at higher voltages ($eV > \phi_c$ where ϕ_c is the barrier height at cathode) the $\Delta s = s \cdot \phi_c / (\phi_c - \phi_c + eV)$ and $\bar{\phi} = \phi_c / 2$ in the formula (4) assuming trapezoidal barrier. The corresponding formulas have been shown by Simmons [173]. At voltages lower than smaller barrier height divided by electron charge, the current densities do not depend on voltage polarity. At higher voltages the *J-V* dependence can be approximated by the Fowler-Nordheim formula (5) discussed below.

The probability to tunnel through the trapezoidal barrier (Fig. 8) thicker than 5 nm is quickly approaching zero [173]. In the case of thicker films, the tunneling becomes dominant at voltages where the barrier is approximately triangular. Then the energy range used to calculate the currents is approximately *3kT* around the Fermi electrode of the cathode. The barrier lowering due to image forces is usually not taken into account as the important parameter is actually the average barrier height which is not changed considerably by the image forces. Assuming triangular barrier at cathode due to uniform field, the well known Fowler-Nordheim formula is derived:

$$J = aE^2 \exp(-b/E) \tag{5}$$

Here $a = e^3/8\pi h\phi_0$, $b = 4\sqrt{2m_{eff}m_0\phi_0^3}/3e\hbar$ and the constants in the formulas are same as in Richardson-Schottky currents.

Temperature dependence of tunneling currents is slightly quadratic:

$$J(V,T) = (V,0)\left[1 + 3 \cdot 10^{-11}(\Delta s \cdot T)^2 / \bar{\phi}\right],$$

where Δs is given in nanometers and $\bar{\phi}$ in electron volts [173]. Small temperature dependence of leakage currents, if established, would serve as a strong evidence of the dominance of tunneling currents. However, according to some models, the temperature dependence of tunneling currents can be stronger [225–226].

2.4.1.3. Trap assisted tunneling

In the films too thick for direct tunneling of charge carriers, the trap states enable an alternative path. As a first step, the charge carrier will tunnel to an empty trap state. In the case of elastic tunneling, the next step can be tunneling to the next trap of same energy (multistep tunneling or hopping), tunneling to conduction/valence band or to anode (two-step tunneling), or thermal injection to the conduction/valence band of insulator (Poole-Frenkel tunneling) (Fig. 9a–9c). A mechanism where the carrier energy is changed is called inelastic tunneling. In this case, the carriers will loose energy and occupy a neighbouring

trap with different energy (Fig. 9d). Multi-step tunneling and inelastic tunneling can be considered when the traps are distributed in a wide range of energy (Fig. 9a and 9d) whereas in the case of narrow trap distribution only the two-step tunneling and Poole-Frenkel tunneling may occur (Fig. 9b and 9c).

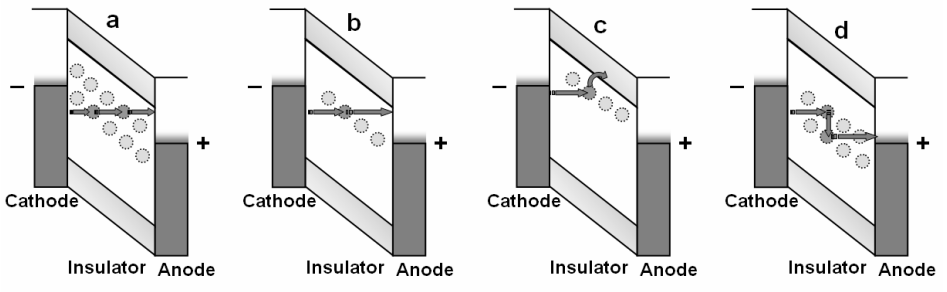

Figure 9. Schemes for trap assisted tunneling mechanisms: (a) multi-step tunneling, (b) two-step tunneling, (c) Poole-Frenkel tunneling and (d) inelastic tunneling.

In general, the probabilities for tunneling steps are calculated in the same way as in formula (2) whereas the integral is taken over the distance of one step to the next one. The total probability for carrier emission at certain energy is the inverse of sum over inverse probabilities for all steps: $D_{total}^{-1} = \sum_n D_n^{-1}$. In addition, the cross-sections σ_t and trap densities N_t have to be taken into account $J = \int N_t \sigma_t D_{total} dE$ [227–228]. If the last step is the thermal injection to the conduction band, the final probability is the probability for thermal ionization of the trap. Analytical formulas for trap-assisted tunneling currents are derived only for certain cases [229–223]. In the present work the analytical forms were not appropriate and numerical calculations were carried out to calculate the leakage currents. In these calculations, trap-assisted tunneling models with one discrete trap energy were applied.

2.4.2. Bulk limited mechanisms

When the electrodes do not limit the carrier flow into the film [171–174,234–235] and the film is thick enough, the transport of charge carriers is controlled by the bulk conductivity. In films with large amount of defects, the injection of charge carriers into insulator is easier because of the assistance of traps. Low barrier at electrode is another possible reason for small electrode resistance. At the same time, due to trapping and scattering of carriers, the transport through the defective bulk material becomes more difficult, if the film becomes thicker. Thus, the conductivity will be controlled by bulk limited mechanisms. The

independence of current densities on electrode materials and on voltage polarities should be one of the indicators of the bulk limited mechanism. However, if there are composition gradients in the film, such independence does not necessarily realize. For example, the conductivity of polycrystalline film is inhomogeneous and usually higher at grain boundaries due to higher amount of gap states. In such cases, the modeling of static *J-V* curves is complicated and it is suggested to avoid polycrystalline films [77].

2.4.2.1. Space charge limited currents

When the amount of excess charge carriers injected into the film is large, the charge starts to distort the applied electric field. The electric field due to space charge decreases the total field near the cathode and limits further injection of carriers from the electrode (Fig. 10d). Charge and field distribution in the film can be calculated by solving proper Poisson equation [234–235]. The exact solution depends on the film properties and trap distribution, but the distribution of charge, field and potential inside the film is similar with the one shown in figures 10a–c.

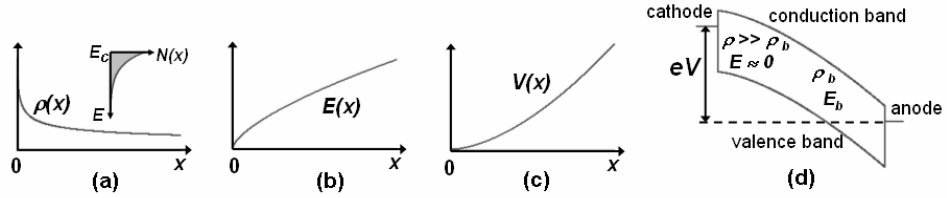

Figure 10. Distribution of (a) charge, (b) field, (c) potential and (d) resulting band bending in insulator with exponential distribution of traps (inset in a) in the case of space charge limited currents. Field at cathode is nearly zero due to large amount of excess charge (Q_B and F_B is free charge in the bulk and the field in the bulk).

The most common current density-voltage dependences describing the space charge limited currents are presented by Rose [234]

$$\text{for discrete trap distributions: } J \sim V^2/d^3 ,$$

$$\text{for uniform trap distributions: } J \sim V/d^2 \exp(\alpha V/d)$$

$$\text{and for exponential trap distributions: } J \sim V^{m+1}/d^{2m+1} .$$

Here *d* is the thickness of film, the factor α in second formula depends on the trap density and inversely in temperature and m in third formula depends inversely on temperature. The exact formulas and derivations are shown either in the works of Rose [234] or Mark and Helfrich [235]. In the case of discrete and exponential trap distribution, the *J-V* curves are expected to be linear in *log(J)-log(V)* plot with the slope 2 in the case of discrete trap distribution and higher than 2 in the case of exponential trap distribution. The discrete trap

levels correspond to certain impurities whereas uniform distribution of trap energies is expected in the case of structural disorder. The increase in trap densities or in average trap ionization energies decreases the currents because of decreasing free to trapped charge ratio. As a result, smaller amount of charge contributes to the currents whereas the field is altered by the total amount of excess charge in film. There is a substantial difference between donors and traps. The donors are neutral when filled with electrons and do not contribute to the space charge while they do increase the total amount of mobile charges. Thus, the increase in the amount of donor-like traps should increase the fields where the space charge starts to play a role.

2.4.2.2. Poole-Frenkel emission

Poole-Frenkel mechanism can be viewed as the bulk analogue of Richardson-Schottky effect whereas the transport of charge carriers is governed by trapping and de-trapping. At zero fields the amount of free carriers in film is determined by the trap ionization energy ϕ_{trap} and by the temperature (Fig. 11). When electric field is applied, the ionization energy of trapping centre decreases in direction of applied field by $\Delta\phi = \beta \cdot E^{1/2}$ (Fig. 11). Thus the increase in de-trapping probability and conductivity is $exp(\beta \cdot E^{1/2}/k_BT)$. The Poole-Frenkel constant depends on the dielectric constant, $\beta_{PF} = \sqrt{e^3/\pi\varepsilon_{dyn}\varepsilon_0}$, where ε_{dyn} is the dynamic dielectric constant standing between the static permittivity measured from capacitance methods and optical permittivity [236–237]. The pre-exponential factor which determines the currents at small fields depends mostly on trap distribution and densities.

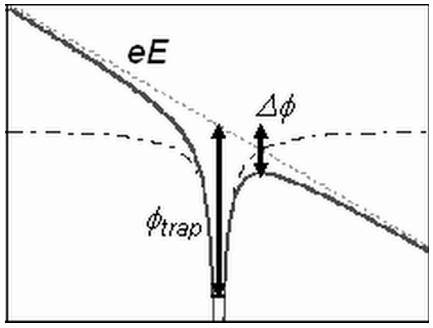

Figure 11. Field induced lowering of barrier in the direction of field.

In literature, the Poole-Frenkel emission is often used to explain experimental results when the *J-V* curves can be approximated by $J \sim exp(\beta \cdot E^{1/2}/k_BT)$ and the mechanism appears to be bulk limited. However, there appear frequently some inconsistencies with model and experiment. Thus, the simple Poole-Frenkel

model has different modifications to account for these inconsistencies. Some of these modifications are described below together with some limits to the model.

The Richardson-Schottky type of β (subsection 2.4.1.1.) can be obtained when there exist both deep donors and shallow traps [173]. This should happen quite often in real films with low degree of order and relatively high impurity content. The donors should lay in narrow and rather deep energy level while there is large amount of disorder induced shallow traps with energies near the conduction band offset.

The increase of trap ionization probability in classical Poole-Frenkel equation (similarly with Richardson-Schottky equation) is calculated assuming uniform barrier lowering for all directions of carrier motion (Fig. 11). More realistic ionization probability is achieved when the emission into the hemisphere centered in field direction is used. The resulting increase in the emission is $\alpha^2 [1 + (\alpha - 1) \cdot exp\ \alpha] + 1/2$, where $\alpha = \beta_{PF} \cdot E^{1/2} / k_B T$ [171]. In addition, there is a difference between semi-crystalline and completely amorphous materials (subsection 2.3.1). In the semi-crystalline material the carrier transport proceeds preferentially along the field whereas in the amorphous material the conduction should be treated as a random diffusion process [174]. In this connection, the pre-exponential factor describing the transport of charge carriers after de-trapping is μE in polycrystalline films and $\mu E^{1/2}$ in amorphous films [174]. In the case of semi-crystalline film, the *J-E* curves corresponding to Poole-Frenkel mechanism should be almost linear in $ln(J/E) = f(E^{1/2})$ plot which is usually called Poole-Frenkel plot and will further be referred to as normal Poole-Frenkel plot in this work (Fig. 12b). In the case of amorphous films, plotting the *J-E* curves in $ln(J/E^{1/2}) = f(E^{1/2})$ should give linear dependence (Fig. 12c). This plot will be referred to as Poole-Frenkel plot for amorphous films. Different *J-E* dependencies can be fairly linear in Richardson-Schottky plot and in both Poole-Frenkel plots, but there are usually deviations from the linearity at low fields (Fig. 12). In addition, the slopes will be somewhat different for poly-crystalline and for amorphous films, which could cause inconsistencies in dielectric constant values derived from the Poole-Frenkel plot.

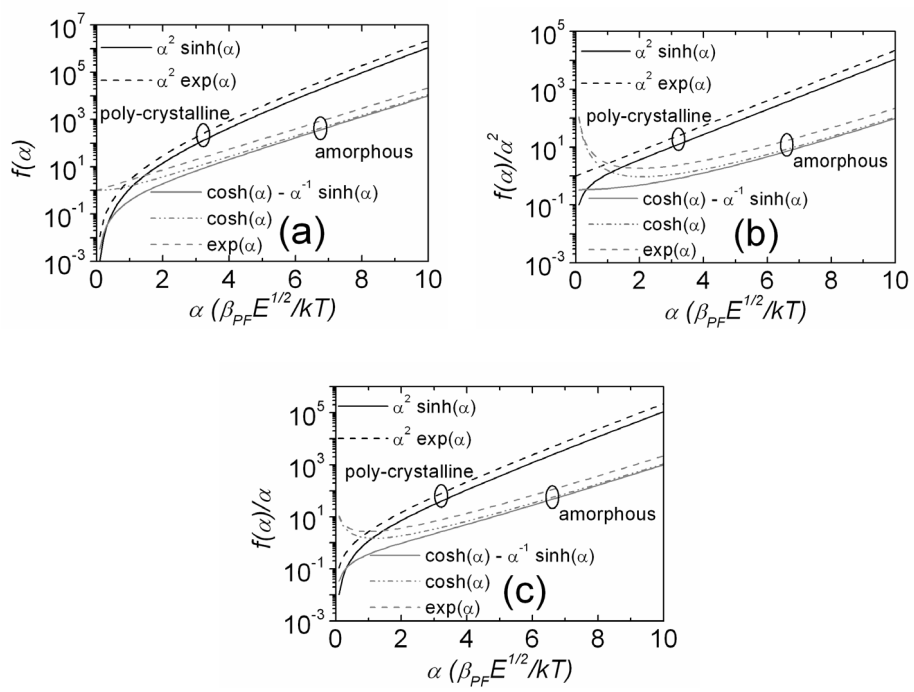

Figure 12. Different Hill formulas and similar formulas, when sinh or cosh are exchanged with exp; (a) in Richardson-Schottky plot ($ln(J) - E^{1/2}$), (b) in Poole-Frenkel plot ($ln(J/E) - E^{1/2}$) and (c) in modified Poole-Frenkel plot ($ln(J/E^{1/2}) - E^{1/2}$). One can see that the Hill formula for poly-crystalline films is linear in classical Poole-Frenkel plot whereas the Hill formula for amorphous films is linear in modified Poole-Frenkel plot.

The dependence of current density on electric field can be normalized between field and temperature with $E^{1/2}/T^{-1}$ and using normalized currents $\Im = JT^{-n} exp\,\phi_i / kT$ where n = 3 or 4 depending on the amorphicity of film [174]. The normalization between field and temperature, $E^{1/2}/T^{-1}$, is a strong proof to the Poole-Frenkel conduction [174].

In the Poole-Frenkel emission model, the trapping centre is usually assumed to be a single coulombic potential well e.g. hydrogen-like donor (Fig. 11). The neutral traps are usually assumed to have different shape of potential [238], with smaller cross-sections. Henceforth, the Poole-Frenkel effect is thought to be applicable only for donor-like traps. However, this presumption has been argued by Pulfrey and Shousa [223]. The Poole-Frenkel model sets constraints to the donor densities which may not exceed $(eE^{1/2}/\beta)^3$ because the coulombic potentials of donors start to overlap at higher densities [174]. If the overlapping appears, the decrease in potential well is a linear function of applied field and the resulting formula is called Poole's formula

$J \approx exp(-\phi_i / kT) exp(e_0 Es/2kT)$, where s is the distance between two overlapping traps [172,174].

In the case of thin films (< 10 nm), the distance between traps becomes comparable to the thickness of the films. Because of this the bulk limitation ceases to work as the trapping events will become rare at least for donor-like traps (distance of 5 nm corresponds to the spatial density of traps in the order of magnitude 10^{19} cm^{-3}). Nevertheless, linear dependence in Poole-Frenkel plot could still be observed in thinner films if Poole-Frenkel tunneling is dominating (subsection 2.4.1.3). In the latter case the electrons injected to the conduction band will not experience further trapping events and the pre-exponential factor in the formula descibing Poole-Frenkel effect should be field-independent. In addition, the conductivity itself should be considered as electrode-limited (injection-limited).

2.5. Present situation

The overview of conduction mechanisms in thin film stacks demonstrated, that the currents can be controlled by the barriers at the electrodes, by the impurities in the film and by the possible grain boundaries. Therefore, the determinations of structural and residual composition as well as the morphology of the films studied have a crucial importance, besides the knowledge of the intrinsic physical properties (band gap and affinity). In the following section, studies concerning electrical properties of different TiO_2-containing MIM and MIS stacks are compared to identify common traits and differences caused by deposition methods.

2.5.1. Conduction mechanisms in thin TiO_2 films

The studies on thin insulating films with high permittivity were intensified during 90s. The first studies concerning electrical properties of thin TiO_2 films in MIM [49–53,65,98–99] and MIS stacks [100–107,109] also probably originate from that time. Later, additional studies were devoted to the applications in MOSFET [66,110–119], DRAM [41–46], MI(S)TT [49–53,112] and ReRAMs [55–62]. For the preparation of films, various deposition methods were used including sputtering [65–66,98,104,113], pulsed laser deposition (PLD) [110], jet-vapor deposition [109], e-beam evaporation [107–108,112,117], MOCVD [40,100–102,114–116,119], PECVD [121–123], cold plasma torch (or PACVD) [105–106], spin-coating [103], sol-gel deposition [99,111] and ALD [41–46,55–57].

Early studies concerning the TiO_2 as gate dielectric were encouraging as the leakage currents were substantially decreased compared to pure SiO_2 with

similar EOTs [65,102–106]. Regarding the drawbacks, Matsuo et al. [104] pointed out the damaging effect of electrodes on the TiO_2 film when reactively sputtered TiN electrodes were used. The damage effect of solid electrode manifested itself in increased leakage currents compared to stacks where mercury probe was used as gate electrode. In addition, they observed unexpected decrease in leakage currents with the decrease in film thickness and this effect was connected with the decrease in grain sizes [104]. High interface trap density ($10^{11} - 10^{12}$ cm^{-2}) and low carrier mobility in channel were generally considered as the major problem of MOSFETs containing TiO_2 [65,101,103–104,107]. In addition, due to the unavoidable formation of SiO_x layer at TiO_2/Si interface, the EOT was usually thicker than 2 nm [40,65–66,104]. Lower EOT was sometimes achieved in as-deposited films [66,100,107], but substantial increase in EOT value was observed after the post deposition heat-treatment which was necessary to decrease leakage currents and interface traps. Therefore, the insulating properties of thin TiO_2 films are mostly studied for applications like DRAM capacitors [41–46], MITTs [49–53] and ReRAMs [55–62].

The proposed conduction mechanisms of stacks consisting TiO_2 films with thickness range of 10–50 nm are varying and sometimes conflicting in different studies. One of the most thorough early investigations was carried out by Campbell et al. [40,100–102] on p-Si/TiO_2/Pt stack. Because of large work function of Pt, they assumed hole emission from Si in the case of negative gate voltage and electron emission from Si in the case of positive gate voltage [40]. The proposed conduction mechanisms were hopping between traps at the lowest voltages, thermally activated emission over barrier (Richardson-Schottky) at medium voltages and Fowler-Norheim tunneling at the highest voltages [40]. The estimated barrier height for thermally activated emission was 0.5 eV for as-deposited and 1 eV for annealed films [100–101]. The increase in barrier height was proposed to be due to the crystallization of films or due to change the in band alignment. However, the change in activation energy could also be explained by differences in impurities. The activation energy of as-deposited films corresponded to that of hydrogen defects [69] whereas the activation energy after annealing corresponded rather to oxygen [68–69]. According to forward recoil spectrometry, the as-deposited films contained high amount of hydrogen which was considerably reduced after annealing [101]. In addition, the annealed film had approximately 3 nm thick SiO_2 interface layer, but its effect to the electrical properties was assumed to be neglible [100]. Lee et al. [65] linked the tunneling-like temperature dependence of leakage currents in their annealed Si/TiO_2/Pt structures to the 2.2 nm thick SiO_2 interface layer and concluded that this layer limits the currents. Similar conclusion was made by Kadoshima et al. [66], where the leakage currents in p-Si/TiO_2/Au stacks decreased with the increase of SiO_2 layer after annealing.

In the works concerning p-Si/TiO_2/Al stacks [103,107,109,112–117,119], the hopping was proposed to be dominant mechanism at the lowest voltages [107,112–113] similarly with p-Si/TiO_2/Pt [40]. At medium voltages, the Poole-Frenkel mechanism was proposed to be dominating according to some authors [103, 109, 119] whereas space-charge limited currents were found in other works [107, 113]. The dominating trap levels were 0.3 eV [113] and 0.5 eV [107] for as-deposited and 0.62 eV [107] for annealed films. Fukuda *et al*. [103] and Mikhelashvili *et al*. [107] did not vary the measurement temperature, but referred to the thermally activated emission behavior in films studied by Campbell et al. [100–101]. In their studies the electron emission from Al electrode should certainly dominate. The thickness of interfacial SiO_2 layer was 5 to 10 nm in the stacks used by Fukuda et al. [103], which made their analysis somewhat questionable. Mikhelashvili *et al*. [107] also ignored the effect of 2–3 nm thick SiO_2 in annealed films and did not account the work function difference between p-Si and Al/Ti [107]. At highest voltages, Mikhelasvili *et al*. [107] proposed Fowler-Nordheim currents through SiO_2 layer as the prevailing mechanism for annealed films. Richardson-Schottky mechanism for as-deposited films and films annealed at temperatures higher than 600ºC was proposed by Yang et al. [119]. For the films annealed at 600ºC, Yang *et al*. [119] and Luo *et al*. [109] assigned Poole-Frenkel effect at low voltages and Fowler-Nordheim emission at higher voltages. Chong *et a*l. [112] studied only as-deposited films and proposed Richardson-Schottky mechanism at 300 K and Fowler-Nordheim tunneling at 84 K as dominating mechanism. The calculated barriers at interfaces were 0.3–0.46 eV. In a study concerning sol-gel derived anatase TiO_2 in p-Si/TiO_2/Al stack [111], the leakage currents were modeled by MIS diode equation. Gritchenko *et al*. [117] proposed two-band conduction in their stacks using the band offsets derived by Campbell et al. [40]. Maiti *et al*. [120–122] has studied the TiO_2 on strained Si/Ge with top Al contact and evoked inelastic trap-assisted tunneling currents to explain the results [122].

The MIM stacks have been studied for DRAMs [41–46], MITTs [49–53] and ReRAMs [55–62]. In Pt/TiO_2/Ir stacks [65], the thermionic current with activation energy 0.78 eV for both voltage polarities was limiting the currents. Hopping at low voltages and space charge limited currents at higher voltages have been observed in ITO/TiO_2/Al stacks containing sol-gel TiO_2 [99]. In Ti/TiO_2/Ti MITT transistors, the Fowler-Nordheim emission was dominant at low temperatures (70 K), wheras Schottky emission dominated at room temperatures (300 K) [49–53]. The barrier at Ti/TiO_2 interface was estimated to be approximately 0.3 eV [49–53].

ALD has been used to grow TiO_2 for DRAM and ReRAM [41–46,55–57] applications. For the ReRAM applications the soft breakdown is evoked at first and, because of such kind of instabilities, the conduction mechanisms for as-deposited films has not been studied extensively. However, for a Pt/TiO_2/Pt system, Richardson-Schottky mechanism was proposed to be limiting the

currents at high resistant state (barrier height was 1.37 eV) [56]. For DRAM capacitors, Pt/TiO_2/Pt [41] and Ru(O_2)/TiO_2/Ru [43–46] stacks were used. Relatively small currents were observed, compared to films with low work function electrodes in as-deposited state, and decrease in the currents was achieved after annealing in O_2 [41] suggesting that the O_2 annealing decreases the significance of defect states. The conduction mechanisms have not been evaluated in these films, however.

As a conclusion, the mechanisms which were used to explain the conductivity in TiO_2 containing stacks varied considerably in these studies. In some cases, the bulk effects were dominating and sometimes the barriers at electrodes determined the currents. The use of high work-function electrodes usually decreased the leakage currents, but this decrease depended on deposition method and post-deposition treatment. Polycrystalline films with larger grains demonstrated increased leakage currents. In the case of MIS structures, the SiO_x interface layer had sometimes strong effect to the permittivity and currents. The properties of TiO_2 extracted from these measurements also varied. The affinity of TiO_2 was usually in the order of 4 eV [49–53,56,112] but in some works it was estimated to be 3 eV [40,117,119,122]. In the Schottky diode configuration (Pt or Pd electrode contact to porous anatase) the barrier at Pt/TiO_2 or Pd/TiO_2 interface has been found to be 1.5–1.7 eV derived from Fowler-Nordheim plots, which should correspond to the affinity of TiO_2 approximately 4 eV [198–199]. The first principles calculations by Robertson [78] have also given the barrier height of 4 eV. The estimated values of 3 eV could have resulted from the neglection of SiO_2 interface layer, but possible differences in TiO_2 phases or Fermi level pinning may also account for differences in barrier heights. The estimated defect level energies were between 0.3 eV to 0.78 eV below the conduction band, but often it was not possible to connect these defect levels to certain impurities. The neglection of interface layers could result in substantial error of the extracted properties because the low-permittivity interface layers influence the *J-V* characteristics considerably, especially for materials with higher permittivity [239].

2.5.2. Plan for the present study

Considering the outcome of the earlier studies described above, thorough characterization of the capacitor stacks containing ALD grown TiO_2 was necessary to determine the conduction mechanisms.

The TiO_2 properties which needed clarification were:

- phase and impurity composition and morphology of studied stacks, and
- dielectric constant and electron affinity of TiO_2.

These properties depend on deposition temperatures and on used precursors affecting the electrical properties and conduction mechanism. The relationship

between deposition conditions and electrical properties had to be clarified. The electrical properties and conduction mechanisms of stacks containing ALD TiO_2 had to be linked to

- precursors and substrate temperature during the growth of TiO_2,
- electrode materials,
- post-deposition annealing,
- interface layers expectedly forming between Si and TiO_2, but also between other electrodes reacting with TiO_2.

Expectedly, the effect of interfacial barriers to the leakage currents occurred smaller in films with low-work function electrodes and thus the $Mo/TiO_2/Al$ and $Si/TiO_2/Al$ stacks were used to study the effect of deposition parameters.

Noble metals with higher work function were used to evaluate the effect of electrodes.

The annealing often affected the electric properties of the films and, in the present study, the annealing in O_2 at temperatures permitting the formation of rutile was used. The annealing effect was studied for both MIM and MIS structures partially because in MIS structures, the increase of SiO_2 layer makes harder to distinguish the annealing effect to the TiO_2 layer.

At least six stack elements were tested in one sample to clarify the repeatability of results. Sometimes, different samples of films grown at identical conditions were compared to study the repeatability of the production of these stacks.

3. EXPERIMENTAL DETAILS

3.1. Film deposition

3.1.1. Reactors

Films were mainly deposited in a low-pressure flow-type hot-wall reactor with quartz reactor tubes. TiO_2 films were deposited in a in-house built reactor [240]. Mixtures and nanolaminates of Al_2O_3-TiO_2 were grown in a commercial F120 type reactor at the University of Helsinki. The latter device allowed the use of different metal precursors during the same growth experiment.

3.1.2. ALD routes

N_2 (99.999 % purity) was used as carrier and purge gas in all experiments. The pressure in the the in-house built reactor was 250 Pa [**II**] while in the F120, the pressure can be twice as high, reaching 500 Pa. Titanium precursors used to grow TiO_2 films were the representatives from halides ($TiCl_4$, TiI_4) and alkoxides ($Ti(OC_2H_5)_4$ and $Ti(OCH_2(CH_3)_2)_4$). Chloride was used because it is one of the most studied titanium precursor with quite well established growth parameters [80–86]. Similarly, ethoxide processes are also thoroughly studied in the in-house built reactor [94–95]. To obtain complementary information, iodide was chosen as another halide and isopropoxide belonging to alkoxides. The oxygen precursor was usually H_2O but, in the case of $Ti(OC_2H_5)_4$, also H_2O_2 was used. The pulse times for the chloride were usually 0.5 s whereas for other precursors and for purging 2 s were used. The substrate temperatures were between 125 and 500°C in the case of $TiCl_4$, between 125 and 350°C in the case of $Ti(OC_2H_5)_4$, and between 240 and 300°C in the case of TiI_4 and $Ti(OCH_2(CH_3)_2)_4$. The films submitted to structural and chemical analysis were usually thicker, 50–200 nm, whereas the films subjected to electrical characterization had thicknesses ranging between 5 and 50 nm (some films had also 80–180 nm thickness).

Al_2O_3 films and Al_2O_3-TiO_2 mixtures were grown in F120 reactor from $Al(CH_3)_3$ (TMA), $TiCl_4$ and H_2O. For these materials, the metal precursor pulse, purge, oxygen precursor pulse and subsequent purge times were 0.2-0.5-0.5-0.5 s (subsection 2.2.1). The temperatures were usually 300°C, but several thicker laminates were grown also at 400°C, in order to achieve higher purity in terms of residues in as-deposited state. For deposition of mixtures, alternating 5–10 deposition cycles for Al_2O_3 and 2–5 cycles for TiO_2 were applied whereas for laminates distinct Al_2O_3, TiO_2 and Al_2O_3 layers were grown using more cycles (40–400) for each constituent layer. The mixtures will be referred later in the text by the ratio of applied Al_2O_3 and TiO_2 cycles (10:2), (5:2) and (5:5). The

12

laminated Al_2O_3-TiO_2-Al_2O_3 films will be referred by using the rounded constituent layer thicknesses, such as 3-2-3 nm, 4-6-4 nm and 6-16-6 nm.

3.1.3. Post-deposition treatment

Post-deposition thermal treatment was carried out in N_2 or in O_2. The temperatures for N_2 treatment were 700–750°C and the duration of annealing was usually 1 minute. Temperatures in the range of 600–750°C were used in the case of O_2 annealing (99.999 % purity) and the annealing times were somewhat longer (5–10 minutes 1 atm pressure). 750°C was the highest temperature considered to be safe in the laboratory environment for oxygen annealing.

3.1.4. Electrodes

Si (1 0 0) substrates with native oxide or RCA cleaned substrates covered with 1.0–1.5 nm thick chemically grown SiO_2 were used when the films were grown for the determination of phase and chemical compositions. For MIS structures with TiO_2 and Al_2O_3 as insulator layers, HF etched Si (1 0 0), RCA cleaned Si (1 0 0) with 1–2 nm thick SiO_2 layer or Si (1 0 0) with native oxide were used as substrates. Both n-Si and p-Si have been used as semiconducting substrates with doping densities of approximately 10^{15} cm^{-3}. In the case of Al_2O_3-TiO_2 laminates, highly doped n-Si with donor densities 10^{19} cm^{-3} and with 0.6–1 nm thick SiN_x layer was additionally used. Al top electrodes were electron-beam evaporated through shadow mask. The thickness of Al electrodes was 100–200 nm and the resulting dot areas were 0.00204 and 0.00052 cm^2.

Bottom electrodes used in the case of MIM capacitors with TiO_2 films were Au, Mo, Al, Pt, Ir, Ru while Ag, Al and Pt were used as top electrodes. The Au electrodes with thickness of 300 nm were electron-beam evaporated on Si (1 0 0) substrate which was HF-etched and rinsed in deionized water before the evaporation. The silver suspension with dot areas between 2–5 mm^2 was used as top electrode only in the case of Au bottom electrode. Mo electrodes with 300 nm thickness were deposited using cathode sputtering method on Si (1 0 0) substrate covered with thermally grown SiO_2 layer (Fig. 1 in [**II**]). Al as an alternative bottom electrode was grown by electron-beam evaporation method. The Pt, Ir and Ru bottom electrode layers were grown using ALD with growth details published by Aaltonen *et al.* [241–242]. The Al and also Pt top electrodes for MIM structures were deposited in the same way as for MIS structures.

3.2. Characterization methods

3.2.1. Structural characterization

Bruker D8 Advance X-ray diffractometer was used for XRD measurements mainly in grazing incidence mode (incidence angle 1°) but some reference measurements were made in Bragg-Brentano mode. The GI-XRD mode was preferred because it allows one to collect data from large area and thus can be used on ultrathin (2–20 nm) films. The same apparatus was used also for XRR measurements to evaluate the thickness of the thinnest films grown. Film thicknesses exceeding 50 nm as well as refractive indices of these films were determined from reflection spectra taken with Hitachi U2000 spectrophotometer, evaluated by the method developed by Ylilammi and Ranta-aho [243].

RHEED measurements allowed to obtain information about crystalline structure and texture from a relatively thin surface layer (10–20 nm). In addition, the method permits the estimation of the degree of crystallization in the case of incomplete crystallization. The patterns were recorded photographically with electronograph EMR-100 and processed by computer. The energy of incident electrons was 25–75 keV and the current of primary beam 10–15 μA. The detectable minimal average thickness of crystalline phase is less than 5 nm and the accuracy in the determination of lattice parameters is up to 0.3 %.

Raman spectra were measured using an in-house built Raman spectrometer. The spectrometer was based on a standard Olympus microscope, equipped with a single-grating spectrometer and thermoelectrically cooled Andor CCD camera. Raman shifts were recorded in the range of 100–900 cm^{-1} with the grating-determined spectral resolution of 1.5 cm^{-1}. An objective of 50 times magnification was used, providing the sampling spot with approximately 2 μm in diameter. The intensity of Nd-YAG 532 nm laser excitation focused onto this area was about 2mW.

FTIR spectra were measured with Interspec 2000 spectrometer. The spectrometer allowed one to determine the adsorption of infrared beam with diameter of approximately 10 mm in the range of 4000–400 cm^{-1}. Spectra of specimen were collected from 25 consecutive runs. The transmission spectra of films were determined as the ratio of the intensity of covered Si substrate to the intensity of bare Si substrate. The measurements were made in laboratory environment and the bands corresponding to CO_2 and H_2O absorbed on the surfaces were also detected. The intensities of these bands varied noticeably from test to test. To reduce the influence of CO_2 and H_2O bands on the spectrum, the spectra from film and reference Si substrate were alternately collected 10 times and the resulting transmission spectra were averaged. In this way, the bands due to absorbed specimens were effectively eliminated.

3.2.2. Morphology

AFM was used to study the morphology of TiO_2 films. The measurements were made with a multimode scanning probe microscope AutoProbe CP, PSI/ThermoMicroscopes/Veeco in intermittent contact atomic force mode. The samples were exposed to air. Silicon cantilevers (Ultralevers^{TM}, PSI) with conical probes and tip radii < 10 nm were used in these studies. Image-processing package IP2 from PSI was used to filter the low frequency noise from raw images of the microscope and to calculate root mean square (RMS) roughness of the film surface.

HR-TEM was used to determine the film and interface layer thickness, as well as to recognize the crystallinity on ultrathin layers. The electron microscope was equipped with a field-emission gun TECNAI F30 ST operating at 300 kV. The specimens for cross-sectional TEM pictures were prepared by bonding two pieces of films face to face with epoxy. The resulting sandwich structure was cut into slice with thickness of about 0.5 mm. The slice was ground and polished to 0.1 mm thick from both sides and then dimpled ground to 0.01 mm at the center of the cross-sectional specimen. After that the specimen was ion-milled to achieve electron transparency. EDS in HR-TEM apparatus was used to determine the composition gradients.

SEM was used to estimate the step coverage in conformity tests. Before the SEM measurements, the samples were gently etched in diluted or buffered HF containing solution (for example 1% of HF in water) to enhance the interface contrast between film and silicon hole wall.

3.2.3. Chemical composition

Some data about chemical composition of films grown at conditions similar to those in the present study was collected with EPMA and RBS. Details about these measurements can be found in [97].

TOF-ERDA was performed in IMEC, Leuven, Belgium. The projectile beam of $^{63}Cu^{7+}$ ions with 16 MeV energy was used to bomb the film (thicker films 70–100 nm on Si substrates). The advantage of TOF-ERDA is the ability to detect light residuals like H which can not be detected by EPMA or RBS. In addition, depending on residual mass, the detection limit can be as low as 0.1 at. %.

3.2.4. Electrical characterization

In the course of current density – voltage (*J-V)* measurements, different measurement equipments were used. *J-V* characteristics of thicker films grown on Au were measured with multi-range galvanometer M 193 (maximal sensitivity $4 \cdot 10^{-8}$ A per division) and digital voltmeter ИЦ 4300 [**I**]. The applied

voltage was increased stepwise and, after the stabilization of current, the mean current value was fixed (approximately 10 sec per step).

Temperature dependence of *J-V* curves and current transients were measured with Digital multifunctional oscilloscope PCS 500 and function generator PCG 10/8016 in a mode using resistors for current measurement (Fig. 13). The rising voltage ramps had rise times of 1s with the maximum voltage of 1–2 V. These fast ramp rise times were chosen in the case of apparently long-term current transients. In order to check, whether the currents remain constant during the 1 s ramp time, 1 s rectangular pulses were also used. In the films where the long-term current transients were not observed, the voltage ramps with 0.1 V/s were used. In the case of the measurement setup with function generator and oscilloscope, the voltage steps were not determined as the function generator divided the voltage amplitude by 256. Thus, the exact step voltage magnitude and step durations depended on the voltage and ramp times. The temperature during temperature dependent *J-V* measurements was varied between –5°C to 65°C. The current transients were measured by applying constant voltage to the film and measuring current with the oscilloscope in transient recorder mode.

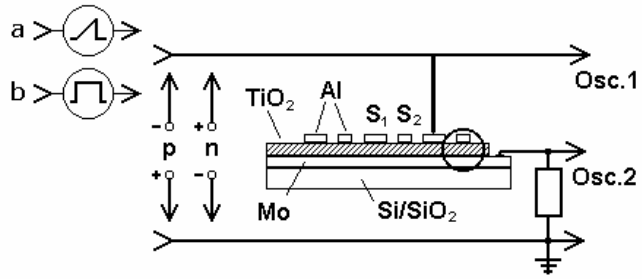

Figure 13. Experimental setup for measurements with multifunctional oscilloscope PCS 500 and function generator PCG 10/8016.

J-V curves of more resistive films and zero-breakdown characteristics were measured with Keithley 2400 Sourcemeter. The 0.1 V steps with duration of 1 s were used for voltage ramps. Smaller steps with longer step durations (0.05 V/ 5 s) were used to verify that the *J-V* curves with 0.1 V/s were stationary.

Capacitance – voltage *(C-V)* curves were measured with Hewlett Packard 4284A Precision LCR Meter. The same apparatus was also used to measure frequency dependence of capacitance and dissipation. To measure the *C-V* curves, the voltage was swept from inversion to accumulation and back to inversion with 0.05 V/s. The amplitude of a.c. voltage was 5 mV, trigger delay was 1 s and the presented *C-V* curves were usually measured both in Cp-D (parallel capacitance) and Cs-D (series capacitance) mode at frequencies 100 kHz, 500 kHz and 1 MHz. Several sweeps from inversion to accumulation and

13

back were made before the measurement of the actual *C-V* curves. To determine EOT and flatband voltage shifts from *C-V* curves, 1D Poisson/Schrödinger solver by G. Snider was used. The details about the used algorithms are given in [244–245].

4. RESULTS AND DISCUSSION

4.1. Stacks consisting of ALD TiO_2

The crystalline phase composition and impurity content in TiO_2 films grown by ALD at different temperatures and from different precursors has extensively studied earlier [80–97]. Nevertheless, some additional measurements were carried out during the studies relevant to this thesis work to obtain more detailed information about the chemical composition and bonding using TOF-ERDA and FTIR methods. In addition to the electrical measurements, the morphology of stacks fabricated was studied whenever possible. These results are presented below because they assist in the understanding of the appearance of different conduction mechanisms.

4.1.1. Phase composition

In earlier studies two different methods, RHEED and XRD, were mainly used for the determination of the phase composition of TiO_2 prepared by ALD [80–85,87–91,94–96]. The studies were separately carried out for different precursor systems with variable thicknesses, substrate temperatures, vapor pressures etc. (preferably at 300°C and above). However, the effect of precursors on the phase transformation was not yet completely clarified. Because of this, complementary investigations were devoted to study the phase composition of films grown at similar temperatures and thicknesses, but using different precursors: $TiCl_4$ – H_2O, $Ti(OC_2H_5)_4$ – H_2O and $Ti(OC_2H_5)_4$ – H_2O_2. These studies were preferably carried out on TiO_2 films which were grown under similar conditions as the films used in electrical measurements. In addition to abovementioned methods, complementary characterization methods – GIXRD, Raman and FTIR – were applied. Several samples were annealed in oxygen at 750°C for 10 minutes to examine the effect of heat treatment to the phase content.

The trends in the spectra of as-deposited films generally matched with earlier results. The films grown at 125 and 175°C were amorphous except the film grown at 175°C from chlorine which has considerable amount of anatase (Fig. 14a). Films grown at 350°C from ethoxide and at 500°C from chlorine possessed strong anatase bands in the spectra (Fig. 14a). The latter film had also a band from rutile in FTIR spectra (Fig. 15a).

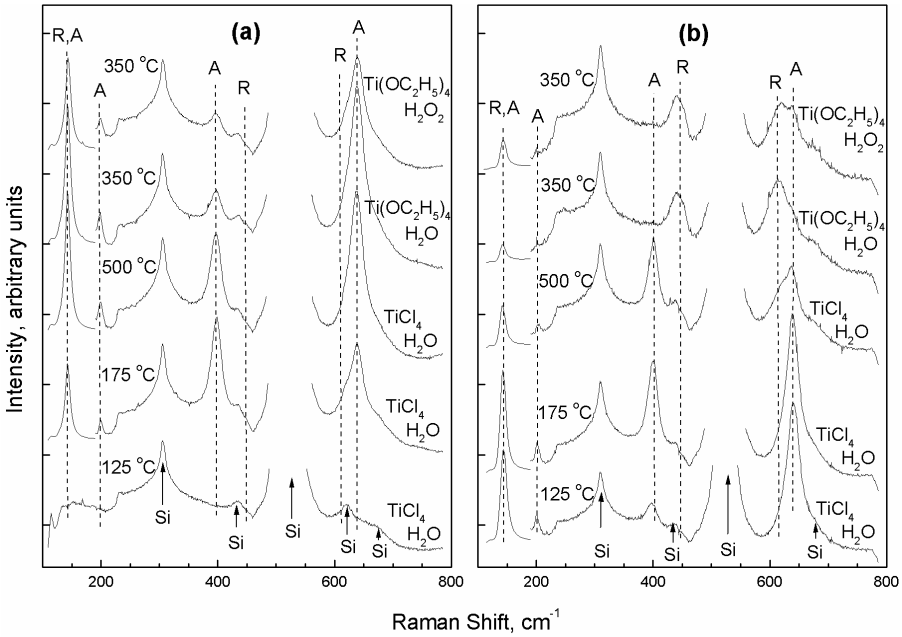

Figure 14. Raman spectra of (a) as-deposited and (b) annealed TiO_2 films grown from different precursors at different temperatures. Annealing was carried out in O_2 at 750°C for 10 minutes.

After annealing, (re)crystallization became apparent in all films in a certain extent (Fig. 14b). The amorphous films grown at the lowest temperatures (below 200°C) crystallized in the form of anatase. The amount of the anatase phase increased also in the films which contained already some amount of anatase in as-deposited state, such as that grown at 175°C from chloride. The films which were grown at higher temperatures and contained anatase in as-deposited state (e.g. at 350°C in the case of ethoxide and 500°C in the case of chloride) possessed some amount of rutile after annealing and the content of rutile depended on the precursors used. In the films grown from chloride, the amount of anatase phase remained dominant after annealing, whereas in the case of ethoxide the transformation to rutile was stronger. This is likely due to different residuals i.e. chlorine or carbon. It is argued that the transformation to rutile is accelerated in the presence of O vacancies whereas the transformation is inhibited by Ti interstitials [193]. The chlorine has been found to prohibit the phase transformation [167,193] probably because of interaction with O vacancies [246]. The carbon on the other hand can occupy the position of Ti and create Ti interstitials [247].

One interesting finding was strong dependence of apparent amount of different crystalline phases on the characterization methods. These particular films were almost X-ray amorphous whereas Raman and FTIR clearly indicated

both anatase and rutile phases, possibly due to the small size of crystallites. The possible reasons for the appearance of different anatase/rutile ratios were the variable (small) size of crystallites, the sensitivity of characterization methods in respect of crystalline orientation (texture) and structural profile throughout the film thickness.

4.1.2. Chemical composition

Data about chemical composition of films grown from chloride, iodide, ethoxide and isopropoxide precursors are published already in earlier works [84,87,89–91,94,96–97]. During the present study, additional data was collected by TOF-ERDA [**II**], enabling lower detection limits and better accuracy in the case of light elements. Importantly, TOF-ERDA has been, in practice, the only method at our disposal enabling calibrated profiling of residual hydrogen. The results are presented for precursor sets of $TiCl_4 – H_2O$, $Ti(OC_2H_5)_4 – H_2O$ and $Ti(OC_2H_5)_4 – H_2O_2$ (Table 2). As a comparison, the iodine concentration in films grown from TiI_4 and O_2 has been below detection limit of XRFS (0.1 at. %) in the films grown at temperatures between 200 and 445°C [90]. The carbon content in films grown from isopropoxide did not exceed 0.2–0.5 at % according to EPMA [96]. Usually the films were stoichiometric TiO_2 in the measurement error of methods but at low temperatures there appeared some deviations [96–97].

Table 2. Impurity content of TiO_2 films grown at different temperatures from chloride or ethoxide. The data is based on several studies with different methods [97,**II**]. The measurement errors are shown for the samples used in **II**. TOF-ERDA was preferred when multiple measurement methods were used [97].

Precursors	Growth temp., °C	Concentration, at %		
		H	C	Cl
$TiCl_4 – H_2O$	100	1.7	–	2.4
	125	0.8±0.2	–	1.1±0.2
	150	0.5	–	0.7
	200	0.3±0.1	–	0.3±0.1
	300	–	–	–
$Ti(OC_2H_5)_4 – H_2O$	100	12.5	2.8	–
	200	1.3±0.3	0.6±0.2	–
	350	0.1	0.4	–
$Ti(OC_2H_5)_4 – H_2O_2$	125	20±3	3.8±0.8	–
	175	7±1	3.5±0.4	–
	200	1.0±0.3	1.2±0.2	–

14

In addition to the above mentioned analysis methods, FTIR measurements were carried out to examine the presence of different chemical groups and, possibly, bonding of different impurity atoms in the film. Surprisingly, it was found that in spite of relatively high concentration of residual hydrogen, –OH bands were not observed in FTIR spectra (not shown). At the same time, in the films grown from ethoxides at 125°C, bands corresponding to carbon containing groups appeared in FTIR spectra (Fig. 15a). The band attributable to $-C_2H_5$ vibrations were detected in the case of H_2O and to carbon oxide in the case of H_2O_2 as the oxygen precursors. This indicates different oxidation ability of the oxygen precursors. The above mentioned bands in the FTIR spectra disappeared upon annealing, but a new band attributable to the residual CO_2 appeared (inset in Fig. 15b). These bands were present also in the films grown from ethoxide at 175°C, still being weaker probably due to lower amount of carbon in these films.

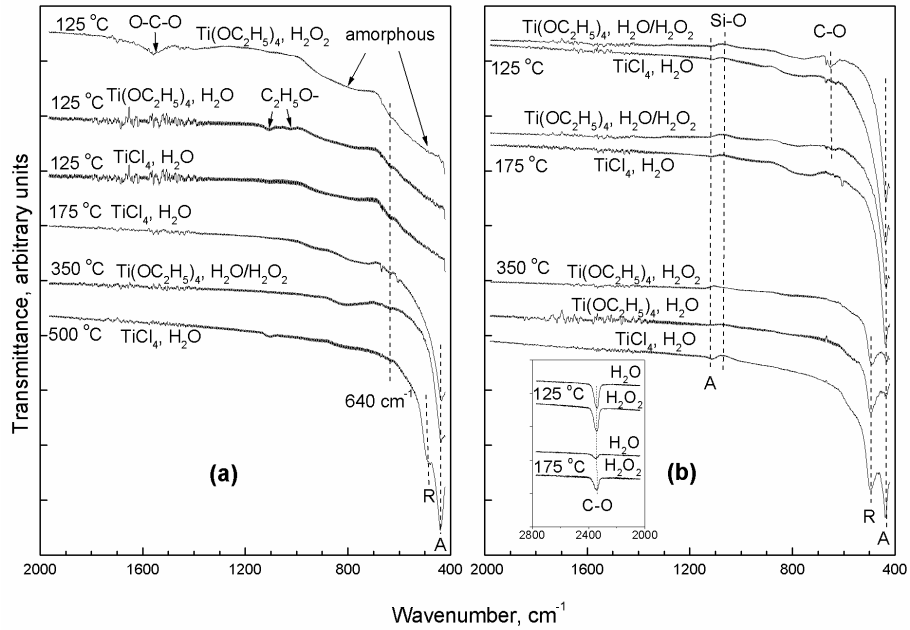

Figure 15. FTIR spectra of (a) as-deposited and (b) annealed TiO_2 films grown from different precursors at different temperatures. Annealing was carried out in O_2 at 750 ˚C for 10 minutes.

4.1.3. Morphology

The thicknesses of films used in the studies were usually obtained by XRR, measured on films grown on smooth silicon substrates. In order to get reference thickness values from films grown on relatively rough metal substrates and to investigate the quality of interfaces between electrodes and dielectric films, TEM images were taken from selected stacks (Fig. 16–18). The images revealed the formation of several nanometers thick interface layers between dielectric films and both bottom and top electrodes (Fig. 16). Since the TEM measurements were carried out on samples actually evaluated by electrical measurements, the values of thickness obtained by TEM were preferably used in the analysis of conduction mechanisms (Table 3). In addition, TEM imaging revealed that the thin TiO_2 layers were truly uniform following the morphology of rather rough metal substrates (Fig. 16 and 17). Besides, TEM analysis gave some additional information about the crystallinity of films. It became possible to visualize different large crystallites (Fig. 18b) or small crystallites (Fig. 18c). At the same time, there was a discrepancy concerning phase content detected by other methods. In the case of 20 nm thick TiO_2 film grown from $TiCl_4$ and H_2O at 175°C where RHEED showed small amount of anatase phase [**II**], the TEM image (Fig. 17a) showed that bulk of the film was still amorphous.

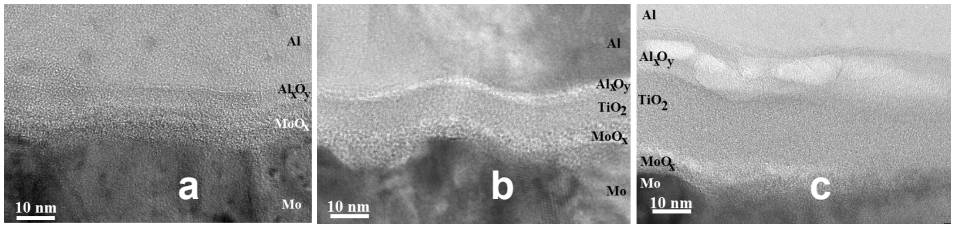

Figure 16. TEM pictures of films grown on Mo at 125°C with (a) 80, (b) 150 and (c) 330 cycles of $TiCl_4$ and H_2O applied to grow the films.

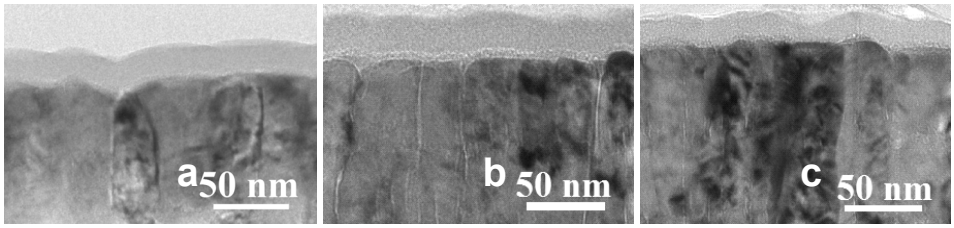

Figure 17. TEM pictures of films grown on Mo at 175°C with 400 cycles of (a) $TiCl_4$ and H_2O, (b) $Ti(OC_2H_5)_4$ and H_2O, (c) $Ti(OC_2H_5)_4$ and H_2O_2 applied to grow the films.

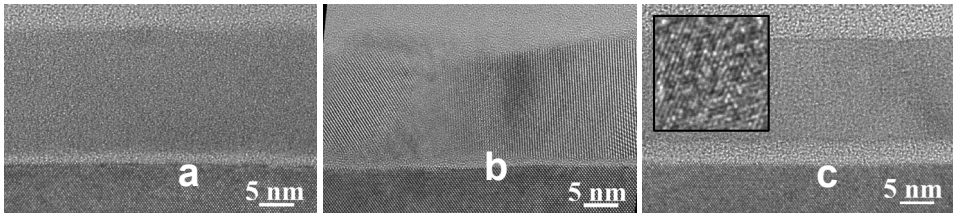

Figure 18. TEM pictures of films grown on Si (a) at 125°C from $TiCl_4$ and H_2O, (b) at 275°C from $Ti(OC_2H_5)_4$ and H_2O and (c) at 175°C from $Ti(OC_2H_5)_4$ and H_2O after annealing in O_2.

Table 3. TiO_2 and interface layer (IL) thicknesses from TEM pictures.

Precursors and deposition temperature	Applied cycles	Bulk TiO_2, nm	IL at Mo, nm	IL at Al, nm
$TiCl_4 – H_2O$, 125 °C	80	4.4±0.5	4	4
$TiCl_4 – H_2O$, 125 °C	150	8.6±0.4	3	3
$TiCl_4 – H_2O$, 125 °C	330	19.5±0.8	4	4
$TiCl_4 – H_2O$, 175 °C	400	16.8±0.4	4	<1
$Ti(OC_2H_5)_4 – H_2O$, 175 °C	400	21.0±1.8	5	4
$Ti(OC_2H_5)_4 – H_2O_2$, 175 °C	400	12.7±1.1	4	2

4.1.4. Conclusions

The studies concerning phase composition showed that the films were dominantly amorphous when grown below 200ºC, even when there appeared some amount of anatase in thicker films grown at these temperatures. At higher temperatures up to 300ºC, anatase crystals were formed. Formation of the high-permittivity phase – rutile – was quite complicated in ALD TiO_2 films. Post-deposition heat-treatment was not sufficient for the complete anatase-to-rutile phase transformation, leaving considerable amount of anatase present in all the films studied. In further electrical characterization, coexistence of highly disordered TiO_2 phases (amorphicity) and anatase had to be considered.

Considerable amounts of residual elements (chlorine, carbon, hydrogen) were detected in TiO_2 films. The amount and effect of residues diminished with increasing deposition temperature. The nature of chemical groups containing these residues was not completely clarified. The lack of hydroxyl groups indicated that hydrogen is relatively free in most films whereas it is tied to carbon in films grown from ethoxide and water. In all cases, one has to consider the formation of band gap states due to the chemical defects and their influence to the electronic quality of the dielectric films evaluated by current-voltage and capacitance measurements.

Studies on the cross sections of TiO_2 films showed that uniform TiO_2 films grow conformally also on relatively rough substrates. One can thus rely on the uniform thickness of TiO_2 films fabricated between electrodes. On the other hand, during the interpretation of electrical characteristics, one has to consider the formation of interface oxide layers between electrodes and TiO_2. These interface layers probably possess lower dielectric permittivity compared to TiO_2. Especially in the case of upper aluminum electrodes, the thickness of interfacial layers varied considerably within the distance probed. This increases the experimental uncertainty during the electrical measurements, giving rise to the interface defect profile and reducing the control over leakage properties.

4.2. Electrical properties of MIM stacks based on ALD TiO_2

4.2.1. Mo/TiO_2/Al stacks

4.2.1.1. J-V characteristics

To study the dependence of electrical properties on deposition parameters, ultrathin TiO_2 films were grown on Mo from different precursors at temperature range 125 to 325°C [**II**,**III**]. The precursors used in these studies were $TiCl_4$ – H_2O, $Ti(OC_2H_5)_4$ – H_2O and $Ti(OC_2H_5)_4$ – H_2O_2 and the targeted thickness was usually 20 nm or smaller (see Table 3 for the number of applied cycles). Films with different thicknesses were grown from $TiCl_4$ and H_2O at the lowest temperature, 125°C, to estimate the dependence of electric properties on the thickness. Films grown at temperatures below 200°C had non-linear *J-V* dependence and for different films the current density was in the range of 1–10 A/cm^2 at 1 V. When higher growth temperatures were used, the current densities became much higher (~10 A/cm^2 already at 0.02 V), depending linearly on voltage. The leakage currents were almost always too high for the reliable capacitance measurements and thus the permittivity of these films remained unknown. The *J-V* curves of films grown at low temperatures (<200°C) demonstrated dependence on film thickness, substrate temperature and precursors (Fig. 19). Films grown from $TiCl_4$ and H_2O possessed the same absolute values of current densities for both voltage polarities (Fig. 19a and 19b) whereas in the case of $Ti(OC_2H_5)_4$ the current densities were higher for the positive voltage polarity of Mo electrode (Fig. 19b).

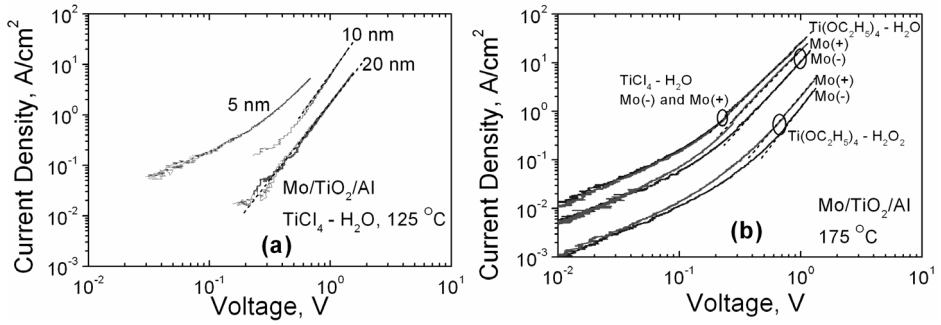

Figure 19. *J-V* characteristics of Mo/TiO_2/Al stacks when the films were grown from (a) $TiCl_4$ and H_2O at 125°C with different applied cycles (Fig. 16) and (b) $TiCl_4$ and H_2O, $Ti(OC_2H_5)_4$ and H_2O and $Ti(OC_2H_5)_4$ and H_2O_2 at 175°C with 400 applied cycles (Fig. 17).

4.2.1.2. Dielectric breakdown

The breakdown voltages depended on film thickness reaching approximately 0.8 V for 5 nm thick films and up to 4.6 V for 20 nm thick films. Thus, we can say that the breakdown appeared in bulk TiO_2 and the corresponding breakdown field increased from 1.6 to 2.4 MV/cm with the increase in film thickness. The maximum current densities before breakdown were 45 A/cm^2. In comparison, in more than a micrometer thick TiO_2 films and/or in the MIM stacks where the influence on interface layers to electrical properties can be neglected [65,176,202], the breakdown field was between 0.5–3 MV/cm. The fact that the breakdown field is higher in thicker films indicates that the effect of Al-rich interface oxide layer (Fig. 16 and 17) to breakdown field is weak and the breakdown field is likely increasing due to the densification of the films upon growing thickness.

4.2.1.3. Conduction mechanism

Polycrystalline films grown at higher temperatures (> 200°C) possessed several orders of magnitudes higher currents supposedly due to the grain boundary conduction [**II**] and these films were neglected in further analysis. For the films grown below 200°C, more comprehensive analysis of conduction mechanism was carried out. As described earlier (section 2.4.), for different conduction mechanisms there are different plots where *J-V* dependence is a linear function. Apparently, the experimental *J-V* dependence had linear sections in all plots but the best results were obtained for the *log(J) – log(V)* plot (Fig. 19) corresponding to the space charge limited currents. The slope of the dependence was higher than 2, consistent with the exponential distribution of traps

$N(E) = N_t / k_B T_C \cdot exp(-E / k_B T_C)$ typical for amorphous films (Fig. 19). The exact formula describing these currents is [235]:

$$J_{SC} = q\mu N_C \left(\frac{\varepsilon\varepsilon_0}{qN_{t0}} \frac{m}{m+1} \right)^m \left(\frac{2m+1}{m+1} \right)^{m+1} \frac{V^{m+1}}{d^{2m+1}} \qquad (6).$$

Here μ is the mobility of electrons and N_C is the effective density of states in the conduction band, ε is the low frequency dielectric constant, ε_0 is the vacuum permittivity, $m = k_B T_C / k_B T$, k is the Boltzmann's constant, T is the temperature during measurements and d is the thickness of oxide. The space charge limited currents as dominant conduction mechanism was consistent with the other experimental results which are described in the next subsections.

The finding that space-charge limits the currents actually means that, in these films, the barriers at Mo and Al electrode-insulator interfaces do not limit the injection of charge carriers. However, at the same time it does not mean that the barriers do not exist at all. As discussed earlier (subsection 2.4.2.), disorder induced trap states allow easier pass into the film for charge carriers (Fig. 20). However, the barrier at the electrode-insulator interface cannot be too high as the density of defect states diminishes exponentially inside the band gap. Trap density at 1 eV below the conduction band edge is only in the order of magnitude 10^{13} cm^{-3} provided that the trap distribution characteristic T_C is 50 meV and the total trap density is 10^{21} cm^{-3}. Because the work function of Mo is 4.6 eV, the electron affinity in TiO_2 films should be rather close to 4 eV.

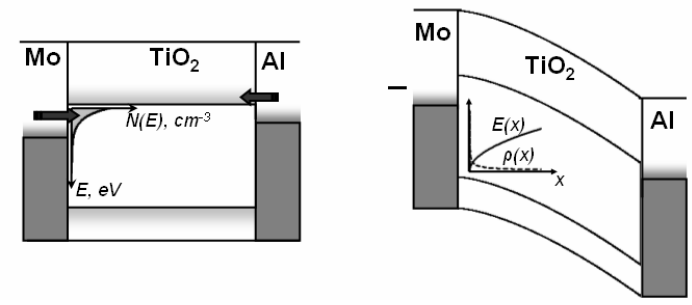

Figure 20. Band diagram illustrating injection of electrons into the films. When barrier at interface is small (Al/TiO_2 interface in this diagram), there will be a plenty of electrons with energy higher than the barrier height. When the barrier at interface is higher (Mo/TiO_2 interface in this diagram) and there is a considerable amount of traps in the band gap of TiO_2, the electrons enter the film through the trap states. Diagram in right illustrates the band bending near the injecting electrode due to injected and trapped space charge $\rho(x)$, with x denoting the distance from the interface. As a result, the electric field $E(x)$ is diminished at the electrode and further injection of carriers is blocked.

4.2.1.3. Temperature dependence of J-V curves

To verify the space-charge limited currents proposed for the prevailing conduction mechanism, the temperature dependence of leakage currents was measured for the films grown from $Ti(OC_2H_5)_4$. The temperature dependence of the *J-V* curves allowed also the estimation of the trap densities (Table 4) [**II**]. Calculated trap densities had very high values, up to $4{\cdot}10^{22}$ cm^{-3}. These values could be overestimated because of simplifications made in the calculations [**II**]. In any case, high amount of disorder induced states are expected to exist in amorphous films [173]. It seems plausible that a large proportion of TiO_2 unit cells (10% or even more) can possess these states due to lattice dislocations and strained structure. Besides, in the derivation of the formula (6) by the Mark and Helfrich [235], it was assumed that the Fermi energy is far below the conduction band edge and the Bolzmann statistics apply for trapped and free carriers. The calculated total space charge at 1 V was $5{\cdot}10^{20}$ cm^{-3} when the permittivity value was assumptionally 50 and the thickness of dielectric layer was 20 nm. The total trap density must be somewhat higher to preserve Bolzmann statistics and to observe the power law dependence at these voltages.

Table 4. Slopes of linear parts of *J-V* curves in *log(J) – log(V)* plots corresponding to space-charge limited currents and calculated values of kT_C, μN_C and N_{t0}/ε in the case of films grown at different temperatures and precursor sets.

films		slope	kT_C, meV	μN_C, $(V{\cdot}s{\cdot}m)^{-1}$	N_{t0}/ε, Cm^{-3}
$TiCl_4 – H_2O$, 125°C, 10 nm		3.3	58 ± 1	–	–
$TiCl_4 – H_2O$, 125°C, 20 nm		3.0	50 ± 1	–	–
$TiCl_4 – H_2O$, 175°C, 20 nm		2.4	35 ± 1	–	–
$Ti(OC_2H_5)_4 – H_2O$, 175°C,	Mo(–)	2.55	39 ± 1	$8.2{\cdot}10^{18}$	$1.9{\cdot}10^{20}$
20 nm	Mo(+)	2.60	40 ± 1	$4.6{\cdot}10^{19}$	$4.7{\cdot}10^{20}$
$Ti(OC_2H_5)_4 – H_2O_2$, 175°C,	Mo(–)	3.15	55 ± 3	$1.8{\cdot}10^{18}$	$1.4{\cdot}10^{20}$
20 nm	Mo(+)	3.05	52 ± 1	$9.5{\cdot}10^{18}$	$1.1{\cdot}10^{20}$

4.2.1.5. Correlation with phase content

There was no clear correlation between the leakage currents and the thickness of interface layers at electrodes (Fig. 16–17 and Fig. 19). Thus, the differences in current density values should be caused by differences in trap densities and distributions (subsection 2.4.2.1.). The clearest correlation can be drawn between the leakage currents and structural disorder. Compared to films grown at 175°C, the films grown at 125°C had both higher slope and lower intercepts in *log(J) – log(V)* plot (Table 4). This indicates the existence of deeper traps with higher density and/or lower mobility in these films (formula (6)) and coincides with the experimental trends in structural disorder (Fig. 14 and 15).

Similar correlation characterizes also the films grown at different precursors at 175°C.

4.2.1.6. Correlation with impurity content

Regarding the chemical composition of our films, the hydrogen content was somewhat higher in the films with lower leakage currents (Table 4). In addition, the analysis of FTIR spectra demonstrated that the hydrogen was bound to carbon when H_2O was used as oxygen precursor but hydrogen was, possibly, rather free when H_2O_2 was used (Fig. 15). Thus, the decrease in leakage currents might be correlated to film structure containing relatively high content of hydrogen, still not attached to carbon or oxygen. The polarity dependence in the case of ethoxide-processed films is more likely related to carbon residuals.

The analytical formula (6) assumes exponential distribution of traps which is usually attributed to structural disorder rather than to impurities which are thought to give rather narrow distribution of (donor) states (see subsection 2.3.1.). To account for differences in impurity content, discrete donor level was added to the exponential distribution of traps and numerical calculations were carried out. The model used to calculate the currents was somewhat different than usually used in the calculation of space-charge limited currents [248]. At first, the voltage dependence of allowed space charge was calculated according to the treatment proposed by Rose [234]. Then the change in the position of Fermi level due to the injected space charge was numerically calculated. Using the derived Fermi level, the proportion of free and trapped charges and, finally, the current values were calculated. Such approach allowed one to achieve power law dependence at high voltages and linear dependence at low voltages where the space charge was not important (Fig. 21a).

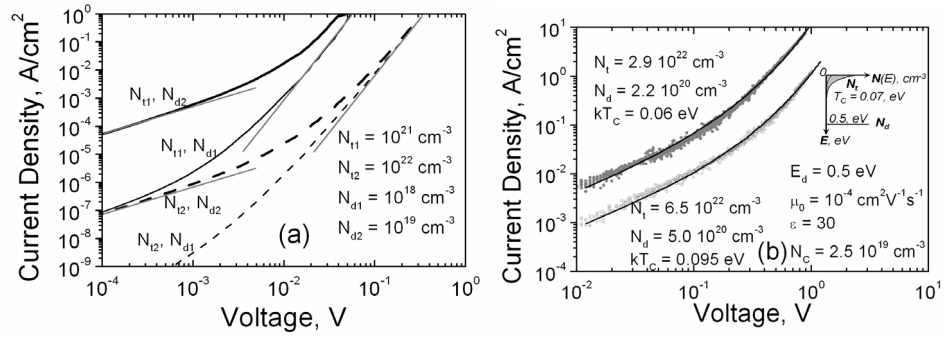

Figure 21. Modeled space charge limited currents in the case of different donor and neutral trap densities (a) and activation energies (b), compared to the experimental curves of films grown from $Ti(OC_2H_5)_4$ and H_2O/H_2O_2. Inset in panel b shows the donor states laying 0.5 eV below the conduction band offset with the characteristic energy of traps 0.07 eV. N_{t1} and N_{t2} are the total densities of neutral traps, whereas N_{d1} and N_{d2} are the donor densities.

The calculated power law dependence at high voltages converged with the analytical dependence for discrete or exponential distribution of traps and did not depend on donor states as long as the density of traps was much higher than the density of donors (Fig. 21a). This seems reasonable as the carriers from donors do not contribute remarkably to the currents when the amount of space charge is much larger. At low voltages the linear dependence was the same as proposed by Simmons for discrete trap states [173]:

$$J = e_0 \mu N_C \left(\frac{N_d}{N_t} \right)^{1/2} \frac{V}{d} \cdot exp\left(-\frac{E_d + E_t}{2kT} \right).$$

Increase in donor and trap densities increased and decreased the currents, respectively. Increasing depth of trap and/or donor levels decreased the currents. For exponential distribution of traps, the tendencies were similar. The donor energy was arbitrarily set to 0.5 eV because energy levels close to this value are often found in works concerning TiO_2 and should be related to the hydrogen impurities [69,107].

Calculated curves fit fairly well to the experimental ones, but the values of trap and donor densities consistent with the fitted curves were quite high (Fig. 21b). In addition, characteristic energies, kT_C, used in numerical calculations had higher values compared to the ones determined from simple fitting of experimental *log(J) – log(V)* plots. Probably there were even deeper trap levels present in the films, which were not taken into account in in the model. Nevertheless, assuming similar trap and donor levels in all the films grown from $Ti(OC_2H_5)_4$, the modeling suggests higher trap and donor densities in the film where H_2O_2 was used as oxygen precursor consistently with experimental findings.

4.2.1.7. Reliability: current transients

After applying constant voltage to the stack, current transients appeared in most of the films. When the voltage was raised and lowered stepwise with step durations longer than several seconds, the transients manifested themselves as remarkable hysteresis of *J-V* curves. These transients were more thoroughly studied in the films grown at 175°C from three different precursor combinations [**III**]. At a fixed voltage, the time dependence of currents had the shape of stretched exponentials or hyperbola with characteristic time constants in the order of 10^4 seconds. The currents increased in the case when the Mo bottom electrode had positive voltage polarity and decreased when Mo had negative voltage polarity.

In the case of hydrogenated amorphous or polycrystalline silicon [249], similar transients were observed and the generation of traps due to hydrogen diffusion was thought to be the reason of these transients. The thermalization

energy concept was successfully applied to explain the transient behaviour at different temperatures and the concept allowed one to estimate the distribution of trap generation energies [249]. In our case, the hydrogen was present as residual impurity and the films were amorphous. Thus, similar mechanisms could also account for the transients in our films. When the transients were measured at different temperatures the thermalization energy concept was also applicable. Using this model, we were able to estimate the energy distribution and other parameters but the reliability of these parameters was poor due to the logarithmic dependence of currents on the fitting characteristic ν_c [**III**].

4.2.1.8. Reliability: long term changes

The films were stored in ambient air. Changes in the *J-V* curves appeared after the storage with duration of several months. The leakage currents of the films grown from $TiCl_4$ became polarity dependent in a way similar to the films grown from $Ti(OC_2H_5)_4$. In addition, the current densities were somewhat reduced in all films. One possible explanation would be an additional hydrogen or carbon contamination arising from adsorbed H_2O or carbon containing molecules – hydrocarbons. The carbon contamination could explain the appearance in polarity dependence in chloride-processed films containing no residual carbon. However, the annealing experiments indicated that the diffusion of carbon is small even at high temperatures. In addition to impurity contamination, slow solid state reactions at interface layers, e.g. formation and growth of aluminum oxide or aluminum-rich titanium oxide between Al electrode and TiO_2, could also account for changes in *J-V* characteristics.

4.2.1.9. Reliability: electrodes

Measurements carried out with Mo/TiO_2/Al stacks showed that in spite of the same preparation procedure the insulating properties of interface layer between Al top electrode and TiO_2 varied in some cases [**IV**]. Compared to the films where space charge limited currents were dominating, in some stacks the currents were several orders of magnitudes smaller and there was no correlation with TiO_2 layer thickness [**IV**]. When these films were grown at temperatures higher than 200°C, the current densities depended non-linearly on applied voltage and had no clear dependence on precursor chemistry or substrate temperature [**IV**]. In the films grown at temperatures lower than 200°C the currents were smaller whereas in the case of films grown at 125°C, there appeared also a dependence on precursors. In addition, the currents in these stacks had voltage polarity dependence with all precursor sets. Contrarily to the results where the space charge limited currents were observed, the currents were smaller in the case of positive Mo polarity. The dependence on the measurement temperature was weak and even weaker in the case of negative Mo polarity [**IV**]. The changes in current values in the case of constant applied

voltage were also smaller compared to the films where the space charge limited currents prevailed.

The results described above indicated that the leakage currents were controlled by interfaces rather than by bulk TiO_2. Weak temperature dependence of currents in the case of electron injection from Mo was indicative of tunneling as possibly dominant conduction mechanism. However, the calculated barrier heights were too low (0.1–0.4 eV) when Fowler-Nordheim tunneling through barrier at Mo-TiO_2 interface (formula (5) in subsection 2.4.1.2) was assumed to be the current limiting factor. In the case of these low barriers, thermal emission over the barrier should dominate. The considerations described above led to the recognition that, instead of Mo-TiO_2 interface, thin Al_xO_y interface layer between TiO_2 and Al (Fig. 16–17) controlled the current. In the case of negative voltage polarity on Mo, the electrons were transported freely to the Al_xO_y interface layer and then the tunneling through this thin layer started to contribute to the current limiting mechanism (Fig. 22a). The experimental *J-V* curves coincided well with the calculated direct tunneling currents (formula (4) in 2.4.1.2). When the thickness of Al_xO_y layer was fixed at 0.8 nm in the calculations, one obtained the barrier heights at Al-Al_xO_y and Al_xO_y-TiO_2 interfaces 1.5 and 0.95 eV, respectively. With interface layer thickness 1.2 nm, the suitable barrier heights were decreased to 0.9 and 0.55 eV, respectively [**IV**]. These results supported the role of insulating Al_xO_y interface layer. The actual values of barrier heights and thickness could differ from the presented ones as the image force effects were not taken into account and the WKB approximation could not give quantitatively exact results. When positive voltage polarity was applied to Mo, the barrier became somewhat higher at lower voltages and some thermal assistance was needed to surpass the barrier (Fig. 22b). In the films grown at lower substrate temperature, the lower conductivity of TiO_2 observed also in earlier measurements affected also the currents.

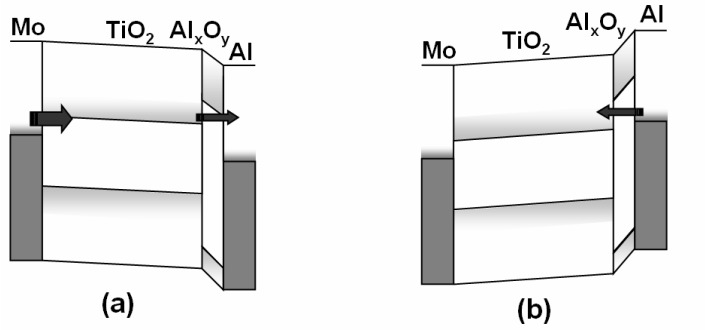

Figure 22. Band diagram illustrating conduction mechanism in the case of insulating interfacial layer between Al and TiO_2. Barrier at Mo interface is transparent and thin Al_xO_y layer is blocking the electron flow injected from Mo electrode (a). Barrier at Al/Al_xO_y interface is higher than barrier between TiO_2 and Al_xO_y layers, decreasing leakage in the case of negative Al electrode polarity (b).

The stacks with insulating Al_xO_y layer were also characterized by higher breakdown fields (up to 5 MV/cm), allowing one to measure the capacitance especially when the films were amorphous and less leaky. The effective permittivity values were between 14–43 and were inversely proportional with the leakage currents [**IV**]. This observation can be explained by the effect of interfacial insulating Al_xO_y layer being probably thicker in less conductive stacks, also decreasing the permittivity of the whole stack. Finally, if the Al bottom electrode was used instead of Mo, the currents became much smaller when the bottom electrode had negative polarity, referring again to thicker and more insulating interfacial Al_2O_3 layer formed at the bottom contact.

4.2.2. Stacks with noble metal electrodes

4.2.2.1. Au/TiO₂/Ag stacks

The TiO_2 films were grown on Au from $TiCl_4$ and H_2O at 225 and 275 °C and the thicknesses of these films were approximately 180 and 30 nm. Due to crystal growth during the deposition, the films had rather rough surface. XRD and RHEED studies showed the anatase phase [**I**]. In these films, the *J-V* curves depended only slightly on the film thickness (Fig. 23a), most likely due to the formation of blocking Au-TiO_2 Schottky diode junction which controlled the currents (subsection 2.3.1.2) and [**I**]. The areas of top Ag electrodes were not determined accurately and because of this, the uncertainty in current density determination could be up to 10 %. In the case of positive voltage applied to Au, the uncertainty in the current density estimation could be even higher as the surface of the top electrodes was rough.

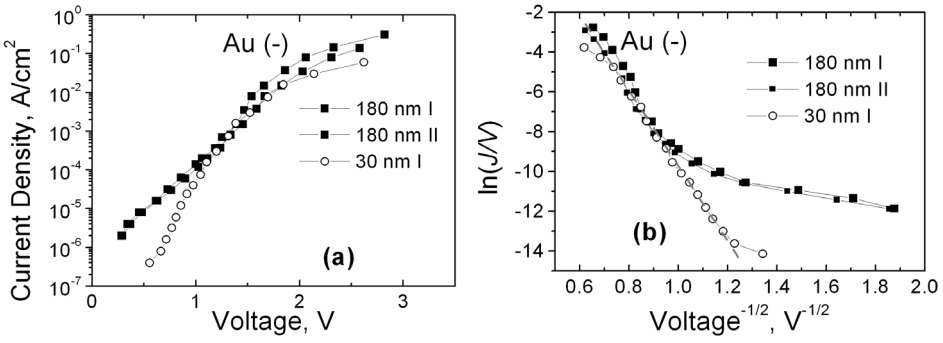

Figure 23. *J-V* curves of TiO_2 films grown on Au with (a) negative voltage polarity on Au and (b) same curves in Fowler-Nordheim plot.

Assuming Fowler-Nordheim tunneling through the blocking Schottky contact at Au-TiO_2 interface (Fig. 24), the barrier heights were calculated from the linear part of *J-V* curves in Fowler-Nordheim plot (Fig. 23b) [**I**]. In these calculations, the electron effective mass, m_{eff}, and dielectric constant, ε, were set to 1 and 50, respectively, and the value of donor density was varied from 10^{19} to 10^{21} cm^{-3} (ionized donor densities from 0.01 to 1 at. %). The barrier height of 1.2 eV, which is the difference between Au work function 5.2 eV and TiO_2 electron affinity 4 eV, corresponds to the donor density $3 \cdot 10^{20}$ cm^{-3} (Table 5). At these densities, the donor potential barriers will overlap (subsection 2.4.2.) and the effective conduction band offset should be somewhat lower. Thus, shallow donor densities around 10^{20} cm^{-3} and barrier heights around 0.9 eV should be quite realistic.

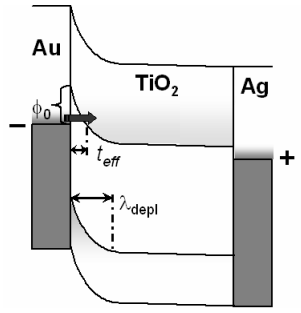

Figure 24. Band diagrams illustrating the band bending at Au/TiO_2 interface with barrier height ϕ_0 and tunneling through the barrier with effective thickness at electrode Fermi level t_{eff}. The voltage dependent thickness of depletion layer is λ_{depl}.

For all donor densities and barrier heights, the width of blocking contact at zero voltage is considerably smaller than 30 nm (Table 5) and thus the model is realistic. In the case of 30 nm thick film, deviation from the linear dependence in Fowler-Nordheim plot occurs at voltages above 2 V (Fig. 23b). The deviation is understandable assuming that, starting from this voltage (2 V), the width of the blocking contact becomes larger than 30 nm. Surprisingly, at lower voltages (<1 V) the currents increased with film thickness. Thicker film was grown at lower temperatures and may contain higher amount of deep traps which can allow an alternative electron conduction path to the film. According to Gupta *et al*. [233], the *J-V* curves should be also linear in Fowler-Nordheim plot (Fig. 24b) in the case of trap assisted tunneling through blocking contact.

Table 5. The donor densities, barrier heights and blocking contact length at zero voltage calculated from the slope of linear part of *J-V* curves in Fowler-Nordheim plot (Fig. 23b). The electron effective mass, m_{eff}, was assumed to be 1 and the dielectric constant, ε, was 50.

Donor density	10^{19} cm^{-3}	10^{20} cm^{-3}	$3{\cdot}10^{20}$ cm^{-3}	10^{21} cm^{-3}
Barrier height	0.39 eV	0.84 eV	1.2 eV	1.8 eV
Length of blocking contact	14.7 nm	6.8 nm	4.7 nm	3.2 nm

4.2.2.2. Mo/TiO_2/Pt stacks

To clarify the influence of the top electrode material, some stacks were prepared by evaporating both aluminum and platinum top electrodes on the same Mo/TiO_2 films (Fig. 25). The work function of Pt is approximately 1.5 eV higher than the work function of Al. Nonetheless, the actual barrier heights at interfaces might differ due to the Fermi level pinning (subsection 2.3.1).

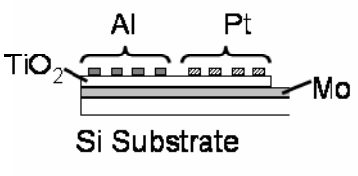

Figure 25. Scheme of Mo/TiO_2 film with aluminum and platinum electrodes.

The representative *J-E* curves for Mo/TiO_2/Pt stacks are shown in figure 26a. The leakage currents of the Mo/TiO_2/Pt stacks were always several orders of magnitude smaller compared to Mo/TiO_2/Al stacks (Fig. 26b). This is consistent with expectedly larger barrier values at electrode-insulator interfaces when Pt was used. However, compared to the stack elements with Al electrodes, the scattering of *J-V* curves was much higher in the case of Pt top electrode (Fig. 26b) making reliable analysis of results more complicated. The scattering here means the deviations in current density values at a certain voltage for different elements on same stack. The most likely reason for the scattering of *J-V* curves was high amount of defects induced during the evaporation of Pt electrode. The CET values evaluated from *C-V* curves of 10 nm and 30 nm thick amorphous films were 3 nm and 5.6 nm giving the effective dielectric constant values 13 and 21, respectively. Lower permittivity values in the case of thinner films can serve as an evidence for the formation of depletion area near the Pt electrode [250–251].

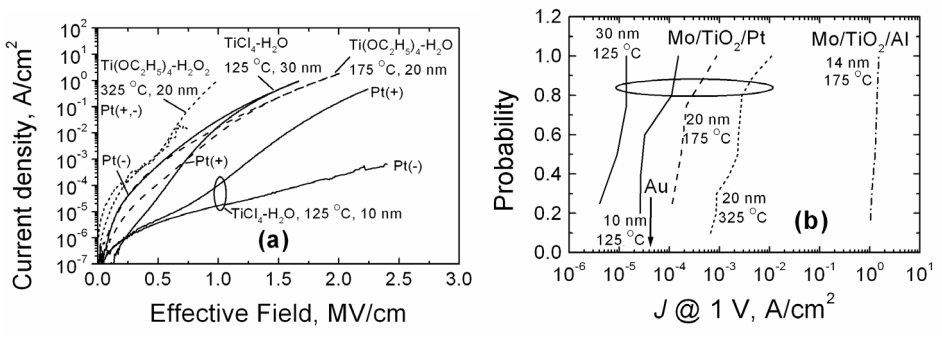

Figure 26. Current density dependence on effective electric field for Mo/TiO_2/Pt stacks (a). Right panel (b) shows the distribution of current densities at 1 V for different stack elements.

There was an abrupt increase in *J-E* curve at fields between 0.5 and 1 MV/cm, when the Pt electrode had positive voltage polarity, probably due to work function difference of Mo and Pt electrode. In the case of thinner amorphous and polycrystalline films, the best results were obtained when the work function difference between electrodes was assumed to be 0.9 eV. Further, the *J-V* curves were linear in Poole-Frenkel plot at higher positive voltages where the abrupt rise in *J-E* curves appeared (Fig. 26a). The evaluated refractive indice values were 2.6 for amorphous film and 2.7 for polycrystalline film. At lower voltages, leakage was probably due to multi-step tunneling for both voltage polarities (subsection 2.4.1.3.). In the case of thicker amorphous films the leakage currents did not depend on voltage polarity at fields exceeding 1.2 MV/cm. At these fields, the *J-E* curves were linear both in Poole-Frenkel and Richardson-Schottky plot with negative voltage polarity on Pt. The dynamic permittivity, ε_{dyn}, calculated from Poole-Frenkel plot, was between 7 and 8 consistently with refractive indice values of 2.3 for amorphous TiO_2 films. At low (<1V) and high (>2 V) voltages with positive voltage polarity on Pt, the *J-E* curve was also linear in Poole-Frenkel plot with similar slopes (ε_{dyn} values between 6 and 8). At intermediate voltages the currents increased much faster. The reason for such behavior remained unclear.

The observation of Poole-Frenkel emission as the bulk mechanism in the case of films with Pt electrode indicates poor interface quality near Pt electrode consistently with strong scatter of *J-V* curves measured. The currents remained considerably smaller in Au/TiO_2/Ag stack compared to similar stacks with Pt electrodes. Thus, in the case of Au/TiO_2/Ag stacks, the currents were apparently limited by the Au/TiO_2 interface with smaller amount of defects. The evaporation of Pt electrode can damage the underlying TiO_2 film and induce higher amount of defect levels [104,252]. The Au/TiO_2 interface forms during atomic layer deposition of TiO_2 on the Au electrode and has expectedly better

quality. Similarly, films with comparable thicknesses grown by Kim *et al*. [43] on sputtered Pt, Ru and RuO_2, possessed much smaller leakage currents, indicating better quality of TiO_2 and substrate interface.

4.2.2.3. Stacks with ALD Ir, Ru and Pt electrodes

In several stacks, ALD was used to deposit bottom electrodes of Ir, Ru and Pt, to avoid the effect of evaporation to the interface of high work-function electrode and TiO_2. In addition, the use of ALD for the deposition of both the bottom electrode and insulating layer is of great interest for technological applications. Unfortunately, some of these films did not give any measurable currents whereas in most cases the current densities were extremely high and the dependence on voltage was linear (resistivity only 10^2 Ω·cm). One probable reason was poor quality of electrodes with high surface roughness. Many metal films were even visually rough or had areas with different colors – the deposition process of metals was not yet optimized. Only two films grown on Ir at 175°C from $Ti(OC_2H_5)_4$ and H_2O had somewhat smaller currents which depended non-linearly on voltage. These films were 20 and 40 nm thick and the number of capacitors which were not highly conducting was much higher in thicker film. A film grown to thickness 10 nm under similar conditions possessed too high leakage for all capacitors. The scatter of *J-V* curves was much larger in the films grown on Ir compared to films grown on Mo or Si at similar conditions. The increase of leakage currents due to rough substrate has been observed also in other works [46].

In the case of 40 nm thick as-deposited film grown from $Ti(OC_2H_5)_4$ and H_2O at 175°C (X-ray amorphous), the best results concerning the reliability and determination of conduction mechanisms were obtained using modified Poole-Frenkel plot ($ln(J/E^{1/2}) - E^{1/2}$) for amorphous films (subsection 2.4.2.2). The dynamic dielectric constant, ε_{dyn}, calculated from the slope of the linear part in Poole-Frenkel plot, of different capacitors was in the range of 5–10. These values were compatible with typical values of refractive indices, n, of 2.3–2.6 of amorphous films [82,85]. There was no clear dependence of absolute values of leakage currents on voltage polarity: sometimes negative, sometimes positive polarity on Ir resulted in higher currents. Such behavior was also consistent with Poole-Frenkel emission as bulk mechanism controlling the currents. The leakage currents flew probably through a small amount of highly conducting filaments as indicated by the large variation in *J-V* curves and by relatively large amount of strongly leaking capacitors in the case of thinner films. The carriers are expected to enter the film through these filaments despite the high work function of Ir [55–56]. Apparent absence of space charge effects can be due to the presence of both electrons and holes in the film.

18

4.2.3. Annealing of Mo/TiO_2/Al stacks

Regardless of deposition conditions of TiO_2 films grown on Mo, the scattering of *J-V* curves (Fig. 27 for example) increased after annealing in O_2 ambient at 600°C or 750°C for 10 minutes. The currents in different capacitors on the same film, taken at the same voltage, varied within almost three orders of magnitude. Still, the leakage remained usually lower than in the case of non-annealed samples and allowed one to measure the permittivity. The calculated CET values of different samples did not depend on the thickness of TiO_2 films and were between 4 and 6 nm. This indicates the increase of thickness of low permittivity interface layers. In spite of large scattering, the leakage currents were generally lower in the films grown at lower temperatures and in thicker films. The overall shape of *J-V* curves and their independence of voltage polarity suggested Poole-Frenkel type of conduction mechanism. For thicker films, the dielectric constant values between 8–16 were obtained when the compensation effect was taken into account. Thinner films did not give clearly linear dependences in any plot.

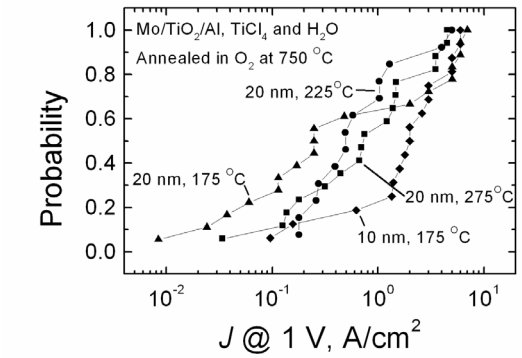

Figure 27. Distribution of current density values at 1 V for films grown from $TiCl_4$ and H_2O at different temperatures.

The overall behavior of *J-V* curves of the annealed films was rather similar with the films grown on atomic layer deposited Ir. The figure 27 shows that the majority of the capacitors formed on the thinner films tended to be highly conductive. Thus, the formation of highly conducting channels seems to be more probable in thinner films. The large scatter in *J-V* curves could be due to the presence of areas of different conductivity. More comprehensive understanding of the boundary effects could be achieved with conductive atomic force microscopy studies.

4.2.4. Conclusions

In $Mo/TiO_2/Al$ stacks, the currents were usually controlled by the space charge, demonstrating the formation of injecting contacts at interfaces. The currents were tunable by deposition parameters and were lower in films with higher degree of disorder and amount of residuals. Even though the amount and nature of residual impurities affected the behavior of *J-V* characteristics, it was not possible to relate certain impurities unambiguously to these effects. However, the polarity dependence of curves was correlated to carbon content and the long time transients were correlated to hydrogen. The increased amount of defects decreased both the short and long term stabilities of *J-V* curves in these stacks. Thin AlO_x layers, forming between TiO_2 and Al electrode, were sometimes insulating and complicated the comparison of electrical properties in different films (Fig. 28a). The electrical properties and conduction mechanisms were clearly different if the interface layer was insulating, though. This allowed discrimination between films where the injecting contacts formed from the films where the interface layer dominated the currents.

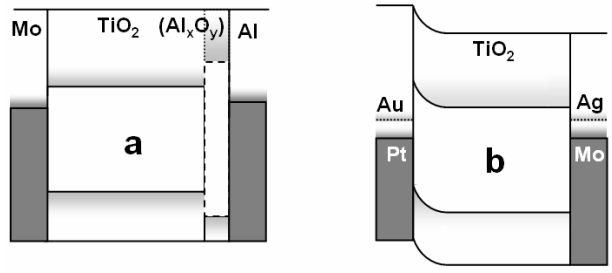

Figure 28. Band diagram of (a) $Mo/TiO_2/Al$ structure and (b) $Au/TiO_2/Ag$ and $Pt/TiO_2/Mo$ structures.

When one electrode was a noble metal with high work function, the barrier between electrode and TiO_2 was also high and the influence of electrode on the currents was stronger (Fig. 28b). In polycrystalline films grown on Au, Schottky contact formed at Au/TiO_2 interface apparently controlled the currents (Fig. 28b). In films with Pt top electrode the quality of electrode-insulator interfaces was poor i.e. concentration of defects was high. Thus, the Poole-Frenkel effect as a bulk mechanism remained dominant, with larger barrier at interfaces suppressing space charge effects. In the case of TiO_2 films grown on atomic layer deposited noble metals Pt, Ru and Ir, the analysis of *J-V* curves was not possible.

From the viewpoint of reliability of *J-V* curves, the best results were achieved with amorphous films and with low work function electrodes (Fig. 29). On the other hand, the leakage currents were remarkably smaller in the capacitors with high work function electrodes.

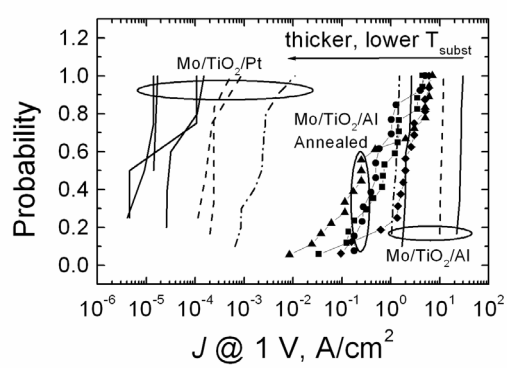

Figure 29. Distribution of current density values at 1 V of different TiO_2 containing stacks.

The annealing of Mo/TiO_2/Al structures decreased somewhat the leakage currents, but resulted also in a much higher scatter in *J-V* curves. Besides, the annealing did not lead to the increase of effective dielectric constant. Thus, the optimization of annealing process of these films needs an optimization before the annealing can be used to improve the electrical properties of the MIM stacks with ALD grown TiO_2 films.

4.3. Electrical properties of MIS stacks based on ALD TiO_2

4.3.1. As-deposited TiO_2 films

Some of the electrical properties of MIS stacks consisting of atomic layer deposited TiO_2 were described in the work [**IV**], but the analysis of conduction mechanisms was not carried out. The films were grown both on HF etched Si and on Si substrate covered with chemically grown SiO_2, but after the deposition of TiO_2, interfacial layer was visible for both substrates (Fig. 18). Films which were grown at higher temperatures possessed also higher leakage currents similarly with MIM stacks (Fig. 30). At voltages higher than 0.5 V, the currents were controlled by the conductivity of silicon substrate of 0.5 mm thickness in most films (thicker lines in Fig. 30). The shape of *J-V* curves was somewhat different when the films were grown at 175°C or 125°C allowing the distinction between two characteristic regions (Fig. 30). The change from one region to other took place between 0.4 and 0.5 V on HF-etched substrates. Similar trends were observed in the case of films grown on SiO_2/Si but the leakage was usually somewhat smaller in the latter case (Fig. 30b). This indicated that the interface layer between Si and TiO_2 was more insulating with chemically grown SiO_2. The dependence of leakage currents on TiO_2 layer thickness was weak and did not exceed the variation in *J-V* curves of different

capacitors on the same film. *J-V* curves of films grown at 175°C depended somewhat on the measurement temperatures varied in the range of 0–60°C, and the dependence was stronger in the low voltage range below 0.5 V.

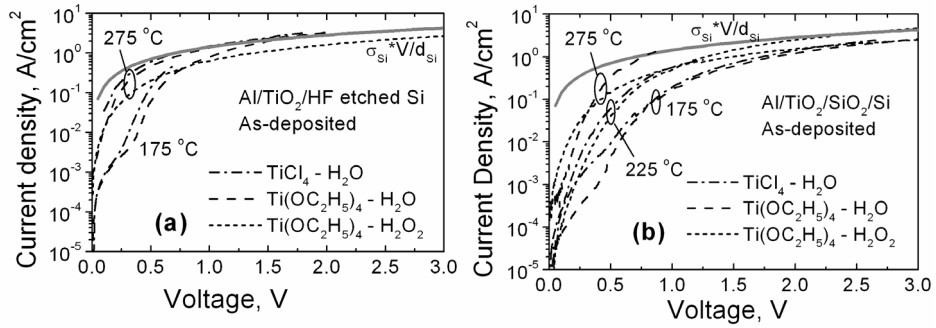

Figure 30. *J-V* characteristics of TiO_2 films grown at different temperatures and from different precursors (a) on HF Si and (b) on chemically grown SiO_2. The *J-V* curves of films grown at the temperature 325°C coincided with the curves of films grown at 275°C.

Thicker films grown from $TI_4 – O_2$ and Ti(i-OC_3H_7)$_4$ – H_2O demonstrated still high leakage currents with no clear dependence on film thickness (Fig. 31). However, films processed from both iodide and isopropoxide possessed somewhat lower leakage when lower growth temperature (240°C) was used.

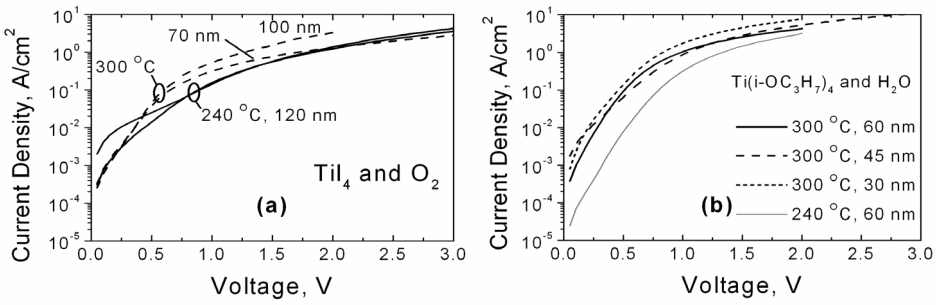

Figure 31. *J-V* characteristics of relatively thick TiO_2 films grown (a) from TiI_4 and O_2 and (b) from Ti(i-OC_3H_7)$_4$ and H_2O at different temperatures indicated by labels. Film thicknesses are also indicated by labels.

The use of films thicker than 20 nm allowed to measure the *C-V* curves (Fig. 32). The accumulation capacitance depended both on substrate temperature and film thickness. In a film grown from iodide, the increase of substrate temperature resulted in lower accumulation capacitance and thus in lower permittivity (Fig. 32). The CET values calculated from accumulation capacitance were

3.4 nm and 8.8 nm for films grown from iodide at 240°C and 300°C, respectively. The effective dielectric permittivities were 137 and 44, respectively. Similar decreasing trend has been observed in the case of refractive indices [89–90] and was explained by the larger porosity in the films grown at higher temperatures. In films grown from TTIP, higher substrate temperatures applied in the growth process resulted in higher accumulation capacitance (Fig. 32). The accumulation capacitance was, expectedly, higher in thinner films, depending also on the substrate. The capacitors fabricated on SiO_2/Si instead of HF-etched Si possessed smaller accumulation capacitance even with thin TiO_2 layer. For 45 nm and 60 nm thick films grown from TTIP on HF etched Si, the CET values were 2.4 nm and 1.8 nm respectively, whereas the value of 2 nm was calculated for film grown on SiO_2/Si. Thus, the low-permittivity SiO_2 layer at the interface affects the permittivity of the capacitor dielectric considerably even in the case of rather thick TiO_2. The effective dielectric permittivities were 99 for both films grown on HF etched Si whereas for film grown on SiO_2, the permittivity was 60.

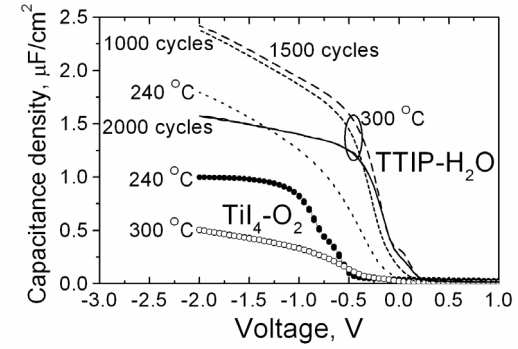

Figure 32. *C-V* characteristics of relatively thick TiO_2 films grown from $TiI_4 – O_2$ and $Ti(i\text{-}OC_3H_7)_4 – H_2O$. Series capacitance model (Cs-D) was used during the measurements at frequency 1 MHz.

Raman spectra obtained from the films grown from TTIP and H_2O at 240°C and 300°C demonstrated only anatase being stronger in the film grown at 240°C (not shown). The bands were, expectedly, weaker in the XRD and Raman spectra obtained from thinner films (not shown). The films grown at lower temperatures (240°C) may contain larger crystals [44], due to the lower degree of the thermal decomposition of the alkoxide precursor at lower deposition temperatures, and smaller surface roughness [44,253] which could explain somewhat lower leakage currents in these films.

4.3.2. Annealed TiO_2 films

After annealing the films in O_2 ambient at 750°C for 10 minutes, the leakage decreased considerably (Fig. 33). The *J-V* curves of most films grown on HF etched Si, became similar after annealing regardless of the deposition temperature or precursors (Fig. 33). In the films grown on SiO_2/Si, the leakage decrease was not as significant as in the films grown on HF-etched (Fig. 33). The most plausible reason seems to be the smaller change in the thickness and quality of chemically grown SiO_2 layer between Si and TiO_2 compared to the possible effect of annealing to the HF-etched substrates, where the Si-rich interface oxides have to form upon annealing. The exact composition of such an interface layer is not known. Unfortunately it was not possible to obtain TEM pictures with EELS analysis and/or capacitances from all of these films to prove the effect of SiO_2 layer.

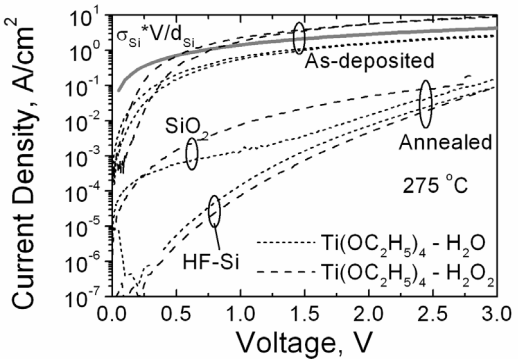

Figure 33. Current density-voltage curves of as-deposited and annealed films grown from $Ti(OC_2H_5)_4$ and H_2O or H_2O_2 at 275 °C on HF etched Si and on chemically grown SiO_2. For as-deposited films grown on SiO_2, the current densities are somewhat lower compared to films grown on HF-etched Si.

Films which were grown on HF-etched Si had CET values between 2.4 and 3 nm. These values are higher than the CET values of thicker as-deposited films grown from TTIP. Such an increase in CET is caused by remarkable increase of interface layer thickness, as seen in TEM images (Fig. 18c).

4.3.3. Conduction mechanisms in MIS structures

It was apparently possible to measure *J-V* curves only for positive voltage on Al (n-Si as substrate) in most of the films, complicating the discrimination of bulk and interface mechanisms. In the structures where TiO_2 was grown at temperatures 225°C and higher, the currents were determined by the conductivity of Si substrate as can be seen from the figure 30. In the case of films grown at

temperatures 125°C and 175°C, the *J-V* curves were linear in Richardson-Schottky and Poole-Frenkel plots up to 0.5 V where the change of conduction mechanism took place. At higher voltages, the curves were linear in Fowler-Nordheim plot, up to the point where the conductivity of substrate started to limit the currents. Assuming Poole-Frenkel effect as the dominating mechanism, the calculated activation energy was less than 0.1 eV whereas the refractive indice changed with measurement temperature from 6 to 13. Thus, the Poole-Frenkel mechanism as the dominant one can be ruled out. Considering thermal emission over the barrier, the activation energies calculated from the measurements carried out at variable temperature occurred between 0.2–0.25 eV and refractive indice was between 1.5–1.6. The relatively low refractive index could correspond to Si-rich titania layer, but the activation energy seemed to be too low for such layer. In these calculations, the effect of SiO_2 layer was not taken into account.

Apparently, these inconsistencies were based on a simple $Si/TiO_2/Al$ structure used in these calculations. Further calculations were performed for more realistic $Si/SiO_2/TiO_2/Al$ stack with a discrete donor level in TiO_2 layer (Fig. 34). Richardson-Schottky, tunneling, and trap-assisted tunneling mechanisms were considered in the model. The general formulas for injection currents (treated in section 2.4.) were used in the numerical calculation. At low voltages, the model assumed electrons tunneling to the traps during the first step and, then, the thermal activation to the conduction band by Poole-Frenkel effect (Fig. 34b). At higher voltages, tunneling through thin SiO_2 layer became dominating (Fig. 34c). As a note, Poole-Frenkel assisted tunneling (see subsection 2.4.1.3) could not be observed at low voltages if the work functions of electrodes are different. Remarkable electric field should act in the direction opposite to the currents. Because of this, the work function values of Si and Al were considered as being effectively the same (4.18 eV) to get zero flat-band voltage. Approximately zero flat-band voltage was found also in the *C-V* characteristic even though the capacitance did not accumulate.

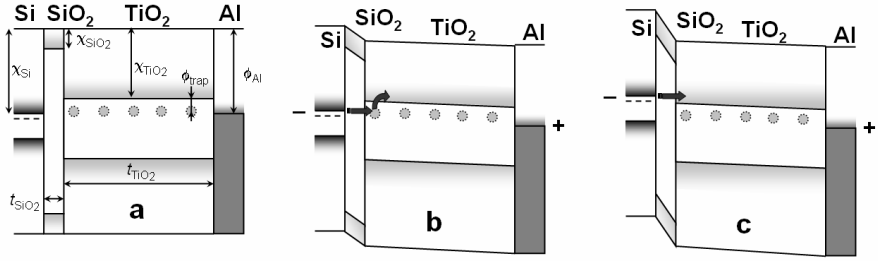

Figure 34. Band diagrams of $Si/SiO_2/TiO_2/Al$ structure (a) with work function of Al, electron affinities of Si, SiO_2 and TiO_2, trap ionization energy and thicknesses of SiO_2 and TiO_2; (b) under low positive gate voltage where the trap assisted tunneling is dominating; (c) under high positive gate voltage, where the tunneling through the band gap of SiO_2 to TiO_2 conduction band is dominating.

The electron affinity of SiO_2 was fixed at 0.8 eV whereas the affinity of TiO_2 was varied between 3.5 eV to 4 eV to achieve the best fit with experimental curve. The low-frequency dielectric constant was 3.9, taken for SiO_2 and 40 for TiO_2. The thickness of SiO_2 was varied from 1 to 2 nm whereas the thickness of TiO_2 was varied from 10 to 30 nm. The image forces were also accounted at Si/SiO_2 and TiO_2/Al interfaces. The high-frequency dielectric constant was fixed at 2 for SiO_2 and 5.3 for TiO_2 (n = 2.3). The dynamic dielectric constant was varied between 6 and 40 (high-frequency and low-frequency dielectric constants of TiO_2) to fit the calculations with the experimental data. The electron effective mass $0.5m_{e0}$ was used for SiO_2 [78] whereas the value m_{e0} was used for TiO_2 according to several works concerning anatase [98,192,199]. The voltage drop at Si was not taken into account and the electron distribution in Si was assumed to be similar as in metals.

At first the tunneling currents without trap assistance were calculated for different TiO_2 affinities if the SiO_2 thickness was fixed to 1.2 nm and TiO_2 thickness to 20 nm. Richardson-Schottky effect was assumed to be negligible with high Si/SiO_2 barrier (Fig. 35a). At higher voltages, the currents did not depend on TiO_2 affinity (Fig. 35c). At lower voltages, where an abrupt increase of the currents occurred, the currents depended strongly on the affinity of TiO_2. At a fixed TiO_2 affinity, the increase in the interfacial SiO_2 layer thickness shifted the *J-V* dependences to smaller current densities in the whole voltage range (Fig. 35b). With the SiO_2 thickness of 2 nm, the tunneling component was already below 10^{-7} A/cm^2 in the voltage range of 0–2 V. The dependence of *J-V* curves on TiO_2 thickness was much smaller as it is shown in figure 35c. Thus, the variation in the SiO_2 thickness by several tenths of nanometers can effectively screen the dependence of currents on TiO_2 thickness. The modeling result is also consistent with the experimental results. Some of these effects have been modeled for other high-k materials, and the trends were essentially the same [254].

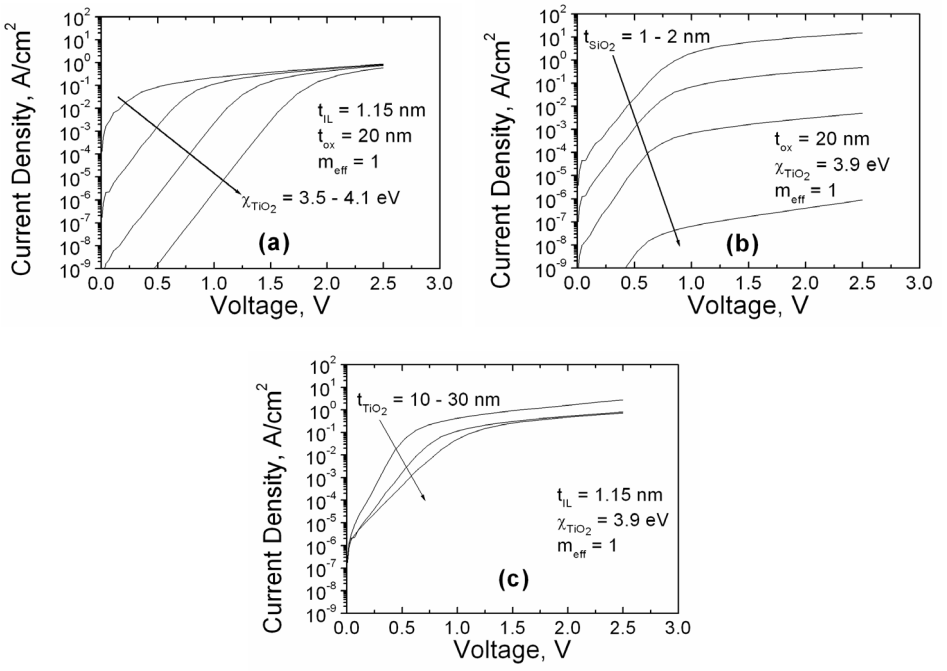

Figure 35. Numerically calculated *J-V* curves of $Si/SiO_2/TiO_2/Al$ stack without defects when (a) the affinity values of TiO_2 were 3.5, 3.7, 3.9 and 4.1 eV; (b) the thickness of SiO_2 layer was 1, 1.2, 1.5 and 2 nm and (c) the thickness of TiO_2 layer was 10, 20 and 30 nm. Other variables were fixed and are shown in figures.

When the injection of electrons through the trap assisted tunneling was added to the model, change in the shape of *J-V* curves takes place at low voltage region (Fig. 36). The rate of the current increase at low voltages depended on the product of donor density and donor capture cross-section $N_d \cdot \sigma_d$. In the calculations, the electron capture cross-section by donors was set to 10^{-14} cm^2 and the donor density was varied from 10^{17} cm^{-3} to 10^{20} cm^{-3}. The product $d_{ox} \cdot N_d \cdot \sigma_d$, which indicates the ratio of total trap states to electrode states, changed from 0.002 to 2 (it has no effect to the currents at values higher than 1). At the lowest concentration, 10^{17} cm^{-3}, the traps did not contribute to the currents whereas at the highest concentration, 10^{20} cm^{-3}, their contribution to currents was comparable to the tunneling currents even at highest voltages (Fig. 36a). It is important to note, that the donor-induced coulomb fields will have significant overlap at concentrations exceeding $5 \cdot 10^{18}$ cm^{-3} and thus the Poole-Frenkel effect is not applicable at higher concentrations. The variation of trap ionization energy (0.5–0.65 eV) affected the currents strongly, but it was not possible to separate the influence of trap ionization energy from the effect of donor concentration (Fig. 36b). The ε_{dyn} changed the currents only slightly (Fig.

36c). Finally, assuming that the SiO_2 interfacial layer does not contain traps (a simplification), the effect of SiO_2 layer thickness was calculated (Fig. 36d). If the SiO_2 layer thickness was higher than 1.5 nm, the direct tunneling through the SiO_2 layer would be weak compared to the tunneling to the donor-originated traps. Within the used parameters, the ionization of donors was the factor which limited the currents.

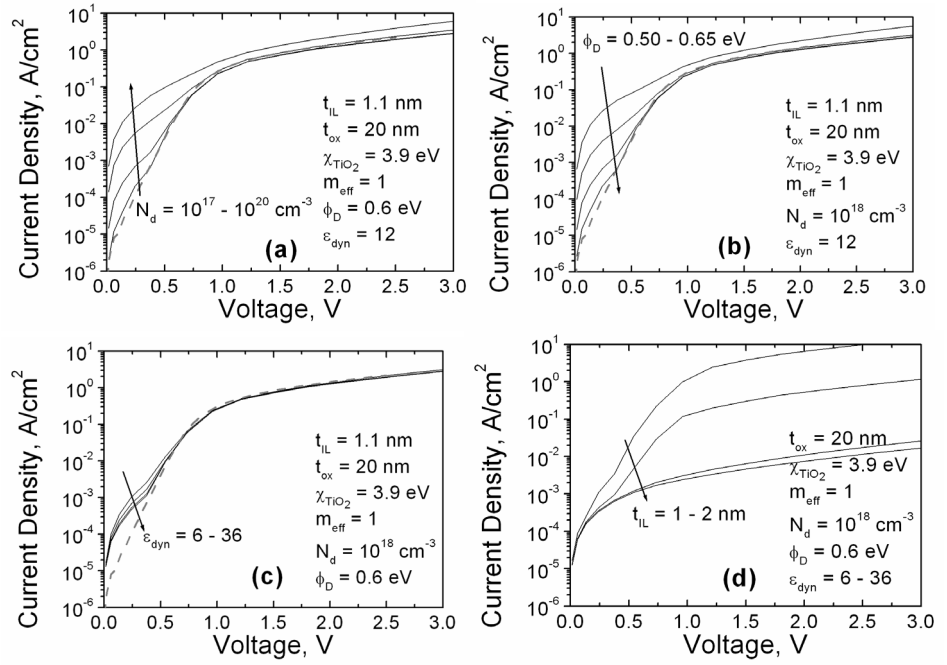

Figure 36. Numerically calculated *J-V* curves of $Si/SiO_2/TiO_2/Al$ stacks considering (a) donor densities of 10^{17}, 10^{18}, 10^{19} and 10^{20} cm^{-3}; (b) donor ionization energies 0.50, 0.55, 0.60 and 0.65 eV; (c) dynamic dielectric constant of TiO_2 layer 6, 12, 25 and 36, and (d) thickness of SiO_2 layer 1, 1.2, 1.5 and 2 nm. Other variables were fixed and are shown in corresponding panels. Dashed lines in panels a, b and c show the results of calculations without traps.

In all cases, the ionization of donors via Poole-Frenkel effect had much higher probability compared to the tunneling to conduction band or to anode. This result was expected because the donor ionization energies used were low (0.6 eV) while the tunneling distance to electrode or to conduction band was rather large (effectively half of the thickness of TiO_2 layer) (see Fig. 34b). However, the multi-step tunneling was not included, although in the case of high defect densities it could have a considerable effect. Nevertheless, two distinct voltage regimes with trap assisted tunneling and direct tunneling would still be apparent. The change from the one mechanism to the other would take

place at the voltages where the work function of Si is at the same energy level with TiO_2 electron affinity and electrons will tunnel only through SiO_2 layer (Fig. 34c).

Comparison of numerical calculation with experimental curves demonstrated that, at higher voltages, the theoretical and experimental *J-V* dependences coincided when the realistic SiO_2 layer thicknesses (1.1–1.2 nm) were used. The effective mass 1 was used in these calculations, whereas the use of effective mass 0.5 required the consideration of approximately 0.5 nm thicker SiO_2 layers (1.6–1.8 nm). The TiO_2 affinity was varied to find the steep current increase at medium voltage range (0.5–1 V). Finally, the region of trap-assisted currents at the lowest voltage range (0–0.5 V) was calculated.

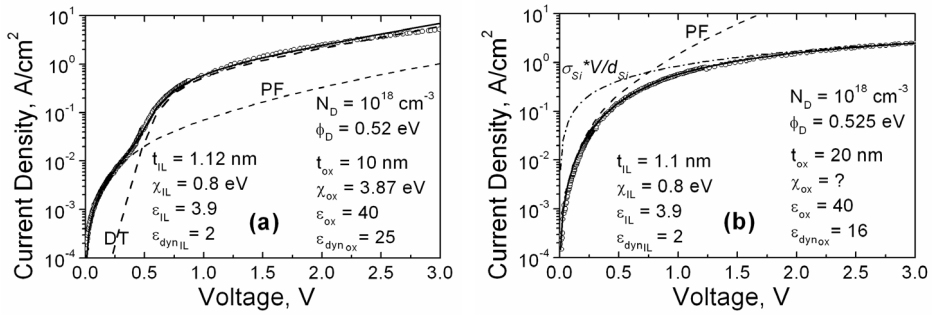

Figure 37. Numerically calculated and experimental curves for (a) as-deposited film grown on HF etched Si from $TiCl_4$ and H_2O at 175°C, and (b) as-deposited film grown on SiO_2/Si from $Ti(OC_2H_5)_4$ and H_2O at 275°C.

The numerically calculated and experimental *J-V* curves coincided when reasonable values of varied parameters were used (Fig. 37). The suitable SiO_2 layer thickness of as-deposited films was approximately 1.1 ± 1 nm for the films grown on HF-etched Si and it had to be somewhat thicker when films were grown on SiO_2/Si. The electron affinity of TiO_2 was approximately 3.9 ± 0.1 eV. The donor density was approximately 10^{18} cm^{-3} with the donor ionization energy of 0.52 eV, but the donor ionization energy should be determined separately by other methods at first. The Poole-Frenkel constant value was the main difference between amorphous TiO_2 films grown at low temperature and polycrystalline TiO_2 films grown at higher temperatures. For amorphous films, the dynamic dielectric permittivity of TiO_2 was rather large ($\varepsilon_{dyn} \geq 25$) even when the compensated Poole-Frenkel effect was assumed. In the case of polycrystalline films the dynamic dielectric permittivity was between 15 and 25 and the normal Poole-Frenkel effect was considered there. Within high current densities of as-deposited films, the space charge due to trapping starts to play considerable role especially in the films with large amount of neutral traps. Because of this charge, the actual voltage drop in the

SiO_2 interfacial layer should be smaller and the electric field in TiO_2 larger than in our calculations and this can account for apparently larger dynamic dielectric permittivity in amorphous films. Another consequence of the field distortions is a larger actual electron affinity of TiO_2 compared to the estimated value. For annealed films, where the SiO_2 layer was thicker than 2 nm, the direct tunneling currents were always too low and the leakage path included the traps. The dynamic dielectric permittivity which resulted in a good fit with experimental curves was unreasonably small and the defect densities were also smaller than 10^{12} cm^{-3}. Thus, the model seemed to be inadequate for the description of the currents in the case of annealed films grown on SiO_2/Si.

Similar calculations can describe also the tendencies observed in other works concerning ALD TiO_2. In a work by Lim *et al*. [42], the *J-E* curves, effective dielectric constants and TEM pictures of TiO_2 containing stacks were substantially different when different oxygen precursors (H_2O, O_2 plasma and O_2/N_2 plasma) were used (TTIP was used as Ti precursor). In the case of conventional, i.e. thermal, ALD the curves were similar to those obtained in our films with thin interface oxide layer and/or high amount of donors (Fig 36a and 36b). With using O_2 plasma [42], the interface layer became probably thicker and the TiO_2 layer contained lower amount of donors resulting in two distinct regions of *J-E* curves. In the case of O_2/N_2 plasma, the interface layer was the thickest and the whole curve became similar to that calculated in the present study (Fig. 36d) with the thickest interface layer. Smallest amount of donors in the film grown using O_2/N_2 plasma can be deduced from the lowest currents [42].

4.3.4. Conclusions

The numerical calculations have demonstrated that the leakage currents in the case of films free of traps depend primarily on the SiO_2 layer thickness and band offset between Si and TiO_2. The leakage at higher voltages is determined either by SiO_2 layer thickness or by the resistance of Si substrate. At lower voltages, the TiO_2 layer influences currents relatively strongly. The voltage where the leakage currents increase abruptly is approximately the sum of flatband voltage and band offset. From experimental evidence, the band offset is smaller than 0.5 V. When low EOT value is targeted, the onset voltage of steep current increase can be controlled only with the flat-band voltage of MIS stack. This trend has been actually observed in experiments where the use of electrodes with high work function resulted in smaller leakage currents [40]. Because the flat band voltage should be close to zero bias voltage, it is hardly possible to achieve leakage currents considerably smaller compared to pure SiO_2 if n-Si is used with targeted EOT values smaller than 2 nm and at voltage 1 V.

4.4. Electrical properties of MIS stacks based on ALD Al_2O_3 and Al_2O_3-TiO_2 mixtures and laminates

The purpose of the investigations on the Al_2O_3 and Al_2O_3-TiO_2 mixtures, was to get some insight of electrical properties and conduction mechanisms in films with high band gap but relatively low permittivity (Al_2O_3), also in the combination with the material of high permittivity (TiO_2). Combination of two different materials in general should also combine their best physical qualities, such as low leakage and high dielectric constant. The electrical properties of mixtures and laminates containing mainstream high-k materials HfO_2 and ZrO_2 are somewhat better established to date, but the comprehensive analysis has not yet been carried out. There have been some theoretical works dealing with conduction mechanisms in films consisting of several layers [254–255]. However, the actual films grown by ALD deviate from the ideal and possess residual impurities as well as phase and composition heterogeneities. Therefore, due to the high amount of different defects the actual mechanisms needed to be verified.

4.4.1. *J-V* characteristics

The comparison of *J-V* characteristics of Al_2O_3 and TiO_2 films and their mixtures or nanolaminates demonstrated that the use of Ti resulted in much higher leakage currents compared to pure Al_2O_3 with similar thicknesses, especially at relatively low voltages (Fig. 38). Similar trends have been observed also in much thicker nanolaminates [256]. In the case of pure Al_2O_3 films, the current densities were higher when the Al top electrode was polarized positively whereas in other as-deposited films containing Ti the dependence on voltage polarity was weak. In the case of Al_2O_3 there appeared also memory effects and because of this, the *J-V* curves from first ramp of fresh capacitors are used in the case of Al_2O_3. After the first ramp, the currents became much higher at higher voltages in Al_2O_3 whereas in other films, the *J-V* curves remained same. Memory effects were not observed when the voltages applied to Al_2O_3 did not exceed the voltages inducing abrupt increments in current density (Fig. 38a).

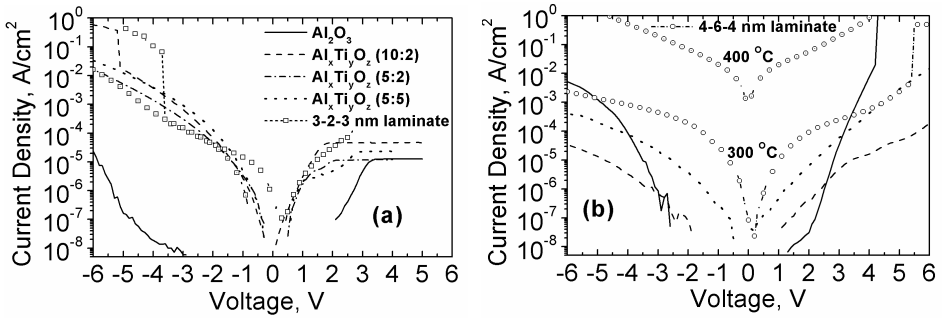

Figure 38. *J-V* characteristics of $Al_xTi_yO_z$ mixtures and Al_2O_3-TiO_2-Al_2O_3 nanolaminates grown on (a) p-Si/SiO_2 and (b) n-Si/SiN_x. Positive voltage polarity is on Al electrode. Lines mark the Al_2O_3 and $Al_xTi_yO_z$ films whereas squares and circles mark the laminates (see subsection 3.1.2. for the notation of films).

In the case of mixtures grown on p-Si substrate, the *J-V* characteristics (Al negatively polarized) were only slightly influenced by the Ti content whereas in the case of n-Si substrate, the current densities were systematically smaller in the films with relatively low Ti content. $Al_xTi_yO_z$ mixtures (5:5) had nearly the same current densities for both types of substrates. The 4-6-4 nm thick laminate (4-6-4 nm denote the thicknesses of subsequentially grown Al_2O_3-TiO_2-Al_2O_3 layers) grown on n-Si possessed much higher leakage currents compared to $Al_xTi_yO_z$ mixtures or the 3-2-3 nm laminate. When a higher substrate temperature (400°C compared to conventional temperature of 300°C) was used for growing the laminate with the configuration similar to 4-6-4 nm, the leakage currents became even higher.

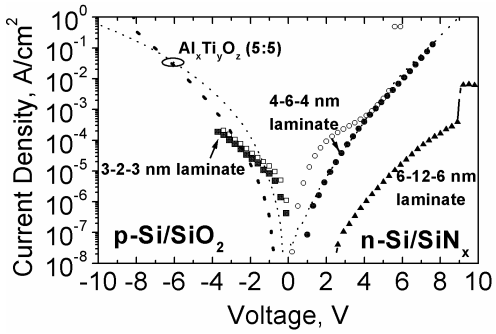

Figure 39. *J-V* characteristics of as-deposited and annealed $Al_xTi_yO_z$ mixtures and Al_2O_3-TiO_2-Al_2O_3 laminates grown on p-Si/SiO_2 (left side) and n-Si/SiN_x (right side). Thicker lines or solid squares and circles mark the annealed films.

In the case of nitrogen annealing the effect of annealing was weak (Fig. 39), whereas the annealing in oxygen resulted in more than one order of magnitude lower currents at low voltages (Fig. 39). The shape of *J-V* curves of oxygen

annealed samples was retained in the case of $Al_xTi_yO_z$ mixture whereas in the case of 4-6-4 nm laminate the shape was different at lower and higher voltages after annealing. Interestingly, the *J-V* curves of 4-6-4 nm annealed laminate coincided with the *J-V* curves of mixture (5:5) (both were grown on n-Si/SiN_x).

4.4.2. Conduction mechanisms

The leakage currents in Al_2O_3 films were comparable to those in earlier works where the TMA-based ALD process was used to grow Al_2O_3 to similar thicknesses [204,228,257]. We did not grow films to variable thicknesses and because of this we could not draw conclusions about the mechanism prevailing in our films. In addition, due to the memory effects and relatively large scatter of *J-V* curves, the temperature measurements were not applicable to Al_2O_3 films. The conductivity depended on the voltage polarity as well as on the substrate type and thence on interface layer. There appeared an abrupt rise of currents at approximately 2 volts (4 V in the case of negative gate voltage of p-Si) and above that voltage the curves could well be described by Fowler-Nordheim tunnelling. Assuming the electron effective mass of 0.2, the effective barrier heights were only 1.7 eV (2.7 eV in other works) in the case of n-Si/SiN_x substrate and in the case of p-Si/SiO_2 with positive gate voltage, but 2.2 eV in the case of negative gate voltage. In the electric field calculations, the work function difference and effective permittivity were taken into account. The Poole-Frenkel mechanism which is a bulk related effect should not depend on the voltage polarity (subsection 2.4.2.). It was possible to achieve polarity-independent *J-E* curves when the voltage curves were shifted to positive voltages by 1.34 V in the case of p-Si and by 0.3 V in the case of n-Si as substrate. The calculated refractive indexes were 1.7 and 1.5 respectively. These values are plausible for Al_2O_3, but the voltage shifts are rather large and the *J-E* curves for different substrates still do not coincide. However, the difference from theoretical flatband voltage shift is by 0.55 V for both substrates which could be due to oxide charge (approximately $4 \cdot 10^{18}$ cm^{-3}).

The temperature dependence and the shape of *J-V* curves of mixtures were consistent with thermally activated mechanisms i.e. Richardson-Schottky emission or Poole-Frenkel effect (subsection 2.4.1.). The *J-V* curves were linear both in Richardson-Schottky and Poole-Frenkel plots and thus the distinction between these mechanisms on the basis of the plots was not possible. The calculated activation energy was approximately 0.4 eV for the $Al_xTi_yO_z$ mixtures (10:2) and (5:2) 0.3 eV in the mixture (5:5). The dynamic dielectric constant derived from the slope of linear region in Richardson-Schottky plot was 5.3 (refractive indice 2.3). The dynamic dielectric constants calculated from Poole-Frenkel coefficient were unrealistically high (from 30 to 100). However, the Poole-Frenkel mechanism can still be plausible if one assumes compensating effect of traps (subsection 2.4.2.2.). Considering the Richardson-

Schottky mechanism, even though the dielectric constants were reasonable, the barrier heights at electrodes should be substantially different.

The laminates had *J-V* characteristics somewhat different from those of mixtures even though the temperature dependence and the magnitude of currents were similar to those in mixtures. However, the Poole-Frenkel or Richardson Schottky plots of the laminates were linear only in a limited range and the derived refractive indices were not realistic. The strong temperature dependence of currents in the $Al_xTi_yO_z$ mixtures and Al_2O_3-TiO_2-Al_2O_3 laminates ruled out the direct tunnelling or Fowler-Nordheim tunnelling as the dominant conduction mechanisms. Some kind of trap assisted tunnelling to the bulk of film and subsequent bulk trap related transport of the carriers is probable, but we were not able to model such mechanisms with satisfying results.

The analysis of experimental curves indicated that although the defects seemingly play a major role determining the leakage, the barrier heights have also some impact to the leakage. It has been found theoretically that, in the case of hydrogen as the source of defect, the energy level is aligned to the oxides valence band edge [258]. Thus we can expect lower ionization energy of donors and, consequently, more intense Poole-Frenkel emission in the films with narrower band gap (higher Ti content).

4.4.3. Modeling of currents injected to stacks based on TiO_2 and Al_2O_3

Numerical calculations of injection currents in the MIS and MIM stacks with different composition were used to compare the leakage currents in the stacks and to predict the behaviour of currents in such stacks with variable constituent layer thicknesses. In some cases, the modeling of injection currents allowed one to confirm the bulk limited nature of experimental currents, as the calculated injection currents were several orders of magnitude higher than the experimentally measured currents.

The injection currents were calculated for both trap-free films and films with discrete donor levels. In a trap-free case, only Richardson-Schottky emission over the barrier according to the formula (3) and tunneling through the barrier by the formula (4) were considered. Two-step tunnelling and tunnelling-assisted Poole-Frenkel currents were also calculated after consideration of donor levels included in the mechanism. In the calculations, the approach described earlier for the $Si/SiO_2/TiO_2/Al$ structures (subsection 4.3.3.) was used. The materials considered in the calculations were TiO_2, Al_2O_3, $Al_xTi_yO_z$ mixtures and Al_2O_3-TiO_2-Al_2O_3 nanolaminates. The band offsets, permittivities and effective masses used in the calculations are given in Table 6. The values are taken from literature and based on experimental works.

22

Table 6. The parameters used to calculate injection currents in films with donor states.

material	affinity	Barrier at Al	ε	ε_∞	donor energy	t_{ox} EOT = 5 nm	t_{ox} EOT = 2 nm
SiO_2	0.8 eV	3.4 eV	3.9	2		1 nm	0 nm
Al_2O_3	2.0 eV	2.2 eV	7	3	1.8 eV	6.5 nm	3.5 nm
$Al_xTi_yO_z$	3.4 eV	0.8 eV	12	4	0.4 eV	12 nm	6 nm
TiO_2	3.9 eV	0.3 eV	40	9	0.2 eV	40 nm	21 nm

At first, the currents were calculated for the case of low work function electrode materials. The electrodes were n-Si with electron affinity of 3.9 eV and Al with work function of 4.18 eV. Relatively low doping density of 10^{15} cm^{-3} was used in these calculations because most of the films characterized in the study were grown on such substrate. Presence of thin interfacial SiO_2layer with thickness of 1 nm was also assumed between the Si substrate and stack (see Fig. 40). In addition, the voltage drop in Si was taken into account.

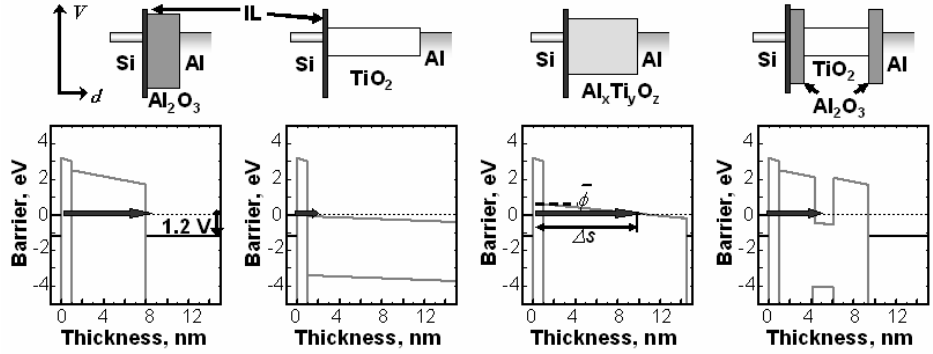

Figure 40. Band diagrams for pure Al_2O_3 and TiO_2 films and for Al_2O_3-TiO_2 mixtures or laminates. Below the schematic band diagrams are the corresponding diagrams quantified for the case of gate voltage of 1.2 V applied to stacks with EOT of 5 nm. In the case of $Al_xTi_yO_z$ mixture, the mean barrier height $\bar{\phi}$ and thickness of the barrier at the cathode Fermi level Δs are also shown.

The results of the calculations are presented in figure 41. As was expected on the basis of literature data, the best results were obtained by using Al_2O_3. In the case of $Al_xTi_yO_x$ and Al_2O_3-TiO_2-Al_2O_3 films, the leakage currents were higher than in the case of pure Al_2O_3. The leakage currents increased with the relative amount of TiO_2. The use of mixtures yielded also higher currents. In the case of TiO_2, the leakage currents were higher than 1 A/cm^2 in the whole voltage range.

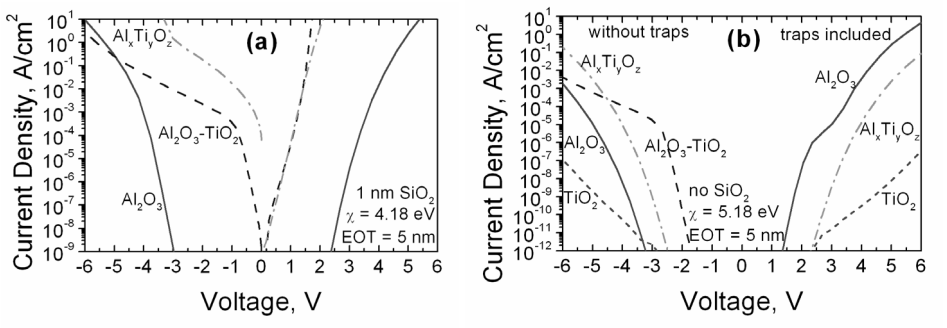

Figure 41. Modeled *J-V* curves for different stacks when (a) the work function of electrodes was 4.18 eV and SiO_2 layer was included and (b) the work function of electrodes was 5.18 eV and without SiO_2 layer. The trap free case is assumed in left side of panel b and donor levels are included on right side of panel b. The *J-V* curves of TiO_2 are not shown for panel (a) because the current densities are several orders of magnitude higher than 1 A/cm^2. The EOT value of 5 nm was used in these calculations.

Electrode work function of 5.18 eV was used to obtain higher barriers at electrode-insulator interfaces. At low voltages, all the films yielded current densities lower than 10^{-12} A/cm^2 (Fig. 41b). The exploitation of pure TiO_2 and Al_2O_3 gave best results in the trap-free case whereas in the case of traps, the leakage currents were the highest in Al_2O_3.

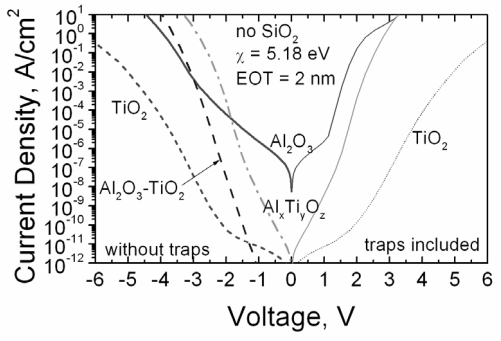

Figure 42. Modeled *J-V* curves of films with different compositions without defects (left side) and with discrete donor levels (right side) with EOT value of 2 nm and electrode work function of 5.2 eV. In all the films modeled, the used donor density was $5 \cdot 10^{18}$ cm^{-3} and electron capture cross section of donors was 10^{-14} cm^2. The energy levels are shown in Table 6.

In the case of films with lower EOT value the permittivity value became even more important (Fig. 42). At low voltages (< 1V), the use of laminate with thin Al_2O_3 layers resulted in the lowest currents because of high barriers at interfaces and high effective permittivity. The currents were the highest in the case of Al_2O_3 at these voltages because the direct tunneling currents were already

prevailing. At higher voltages, where the tunneling currents dominated, the thickest film, TiO_2, possessed the lowest currents. With the inclusion of donor levels, the results remained essentially same. When only shallow donors at 0.2 and 0.4 eV were considered as traps in TiO_2 and $Al_xTi_yO_z$, respectively, then the trap assisted tunneling did not prevail. However, when the trap energy was approximately the same as the electrode Fermi level, the two-step tunneling through the traps became dominant in $Al_xTi_yO_z$ mixture where the distance between electrodes, i.e. the thickness of dielectric layer, was too large for direct tunneling. The TiO_2 film was still too thick for both direct and two-step tunneling. Consequently, the injection and further transport of carrier proceeded mainly through tunneling to traps and the following Poole-Frenkel emission to the conduction band. The importance of large thickness values for TiO_2 increases with the (targeted) decrease in EOT values. In these calculations, the currents through traps distributed in energy scale were neglected. Thus, the actual currents can occur higher in highly disordered films or in films containing trap levels possibly arising from a variety of residual impurities. In the high-k films with thickness higher than the direct tunneling limit, the leakage will dominantly depend on impurities.

4.4.4. Conclusion

Al_2O_3 and TiO_2 mixtures and laminates demonstrated decreased currents in comparison to pure TiO_2 films, although the currents remained much higher compared to pure Al_2O_3. The analysis of conduction mechanisms indicated the importance of defects inducing high leakage currents, when present in considerable amounts. However, low barrier heights at electrode-dielectric interfaces in the case of mixed and laminated films can essentially contribute to the higher leakage compared to pure Al_2O_3. In conclusion, drawn on the basis of modeling studies, the exploitation of a relatively leaky material with enhanced permittivity, such as TiO_2, should become more effective if electrodes with higher work function can be used, in respect with leakage currents taken at constant EOT values. Possibly, the future DRAM technology will exploit alternative electrodes like Ru, RuO_2, or Ir with high work functions. In this case the use of laminates with relatively low band offsets but high permittivity can serve as a viable technique. In the case of real, experimentally grown, films, where the traps play an essential role, the optimization of film growth process aiming at the reduction of trap density becomes even more important.

4.5. Open problems

There were several aspects in this work, which need further studies before it would become possible to successfully implement the TiO_2 based films as reliable insulator materials.

At first, different stacks prepared by the same deposition and electrode evaporation processes occasionally yielded different results. The most likely reason lies in the quality of the top electrode material and its interface with dielectric layer (e.g. Al and Pt). The films were hold in normal conditions with the risk of surface contamination. Proper post-deposition treatment of the films before the deposition of top electrode could help to avoid these problems. In addition, the evaporation process itself can damage the underlying TiO_2 film. Development of the electrode deposition methods, not damaging the insulator film, would be desirable.

Similarly, the use of ALD to grow bottom electrodes (Ru, Ir, Pt) resulted in stacks with many weak spots. For capacitor applications, where the conformal growth is desirable, the ALD of bottom electrode is a necessity and thus the deposition of bottom electrode by ALD has to be optimized.

The post-deposition annealing procedure of the metal-insulator-metal stacks resulted in large scatter of *J-V* curves and thus the annealing procedure needs also further optimization.

The estimation of barrier heights at electrode-TiO_2 interfaces from *J-V* curves yielded reasonable results, but would need complementary verification by methods like XPS, BEES, IPE and VBET. The conductivity of grain boundaries is more successfully studied by C-AFM which could also help to assist in the optimization of post-treatment process.

23

5. SUMMARY

The present study was carried out in order to determine the conduction mechanisms in thin atomic layer deposited TiO_2-containing films. For this purpose, MIM and MIS stacks with thin TiO_2 and Al_2O_3-TiO_2 films were prepared by ALD method. The electrical characteristics of resulting stacks were related to phase, chemical and morphological composition which in turn were influenced by the deposition parameters and electrode materials. The effect of post-deposition annealing on the electrical properties was also studied. The analysis of results was carried out on the basis of a number of samples prepared at the same conditions.

As a rule, in the case of Mo/TiO_2/Al stacks, space charge limited currents were assigned as dominant conduction mechanism and the electrodes had only slight effect on the currents. The current densities were determined by the TiO_2 layer and depended strongly on deposition parameters. At deposition temperatures higher than 200ºC, the films grew polycrystalline and possessed extremely high leakage currents. At lower deposition temperatures the films grew dominantly amorphous and became more insulating. The decrease in temperature increased the amount of defects which further decreased the leakage currents. At the same time, the long term stability also decreased. Besides the growth temperature, the currents depended also on the precursor chemistry. The annealing procedure used in the present study did not improve the insulating properties of TiO_2 films in metal-insulator-stack.

In the case of some Mo/TiO_2/Al stacks the interface layer between aluminum electrode and TiO_2 became insulating. The insulating layer controlled the leakage currents and complicated the analysis of conduction mechanism. Similar insulating layer appeared also in the case of Si substrate. Quality of the Si substrate, i.e. the presence of SiO_2 interfacial layer between TiO_2 and Si substrate had a significant effect on the conductivity of the TiO_2-based capacitor stacks. Numerical calculations were used to account the effect of interface layers on the conduction mechanism. The calculations indicated that at low voltages, trap assisted tunneling through TiO_2 layer was prevailing whereas at higher voltages the tunneling through thin interface layers dominated. The comparison of calculations and experimental results allowed one to evaluate the affinity of our TiO_2 films which was between 3.8–4.0 eV.

Use of electrodes with higher work-function decreased the current through metal-insulator-metal stacks. In the case of Au electrode, Fowler-Nordheim emission through Au/TiO_2 barrier controlled the currents. In the case of Pt electrode, tunneling trough traps apparently reduced the effect of higher barrier at Pt/TiO_2 interface and the conductivity of stacks was controlled by Poole-Frenkel effect. The latter result highlights the influence of electrode preparation technology on the dominant conduction mechanism.

The use of Al_2O_3 together with TiO_2 in mixture and nanolaminate configurations resulted in more insulating films. Both experimental results and numerical calculations demonstrated that the insulating properties of Al_2O_3-TiO_2 mixture and laminate films will still remain inferior to pure Al_2O_3 in MIS structures. Nevertheless, the use of electrodes with higher work function electrodes would make TiO_2 containing films more attractive due to higher permittivity value.

SUMMARY IN ESTONIAN

Juhtivusmehhanismid õhukestes aatomkihtsadestatud TiO_2 sisaldavates kilestruktuurides

Käesolevas töös uuriti õhukesi aatomkihtsadestatud TiO_2 kilesid sisaldavate dielektrikstruktuuride elektrilisi omadusi ja juhtivusmehhanisme. TiO_2 on levinud materjal, mida saab kasutada arvukates rakendustes. Paljude rakenduste korral on aluspind keerulise kujuga ning suure pinnaga ja aatomkihtsadestamis meetod on üks väheseid meetodeid kiletehnoloogias, mis võimaldavad ühtlast kile kasvu sellistele pindadele. Samuti on rakenduste korral sageli olulisel kohal TiO_2 elektrilised omadused, mille optimeerimisel on kasulik teada juhtivusmehhanismi vastavas kilestruktuuris. Samas polnud aatomkihtsadestatud TiO_2 sisaldavate kilestruktuuride juhtivusmehhanisme varem märkimisväärselt uuritud.

TiO_2 sisaldavate kilestruktuuride korral sõltub juhtivusmehhanism tihti parasiitvahekihtidest kile ja elektroodide vahel või lisanditest kile sees. Seetõttu oli töö üheks osaks TiO_2 kilede struktuurse ja keemilise koostise ning kilestruktuuride morfoloogia määramine ning sidumine juhtivusmehhanismiga vastavas kilestruktuuris.

Madala väljumistööga elektroodidega Mo/TiO_2/Al kilestruktuurides oli reeglina domineerivaks mehhanismiks ruumlaengu poolt piiratud vool. Voolutiheduse neis struktuurides olid määratud TiO_2 kihiga ja sõltusid oluliselt kasvatamisparameetritest. Voolud kahanesid madalamate temperatuuride kasutamisel struktuurse korrastatuse vähenemise ja lisandite hulga suurenemise tõttu. Samadel põhjustel vähenes aga ka pikaajaline juhtivuse stabiilsus. Lisaks kasvatamistemperatuurile sõltusid voolud ka lähtematerjalidest. Mõningatel juhtudel toimis TiO_2 kile ja Al elektroodi vahele kasvanud õhuke vahekiht isolaatorina ja raskendas juhtivusmehhanismi määramist. Isoleeriv SiO_2 vahekiht tekkis ka TiO_2 kile kasvatamisel Si alusele ja mõjutas oluliselt vastavate kilestruktuuride elektrilisi omadusi. Selliste vahekihtide mõju arvesse võtmiseks kasutati numbrilisi arvutusi, mis näitasid, et madalatel pingetel domineeris antud kilestruktuurides lõksude poolt assisteeritud tunnelleerumine ja kõrgematel pingetel tunnelleerumine läbi õhukese vahekihi. Pinge, mil toimus üleminek ühelt mehhanismilt teisele, oli eksperimendis selgelt eristatav ja võimaldas määrata uuritud TiO_2 kilede elektronide afiinsuseks 3.8–4. 0 eV.

Suurema väljumistööga elektroodide kasutamisel voolud kilestruktuurides vähenesid. Kulla kasutamisel alumise elektroodina oli domineerivaks mehhanismiks tunnelleerumine läbi Au/TiO_2 barjääri. Plaatina kasutamisel pealmise elektroodina lihtsustas defektne Pt/TiO_2 pind elektronide emissiooni kilesse ja voolu kontrollis Poole-Frenkel'i efekt TiO_2 kihis.

Suurema keelutsooniga Al_2O_3 lisamisel moodustunud $Al_xTi_yO_z$ segude ja Al_2O_3-TiO_2-Al_2O_3 nanolaminaatide isoleerivad omadused olid paremad kui TiO_2 kiledel. Samas aga jäid nende kilede isoleerivad omadused alla Al_2O_3 kiledele. Numbrilised arvutused näitasid, et madala väljumistööga elektroodide korral jäävadki TiO_2 sisaldavate kilestruktuuride lekkevoolud suuremaks kui Al_2O_3 kilestruktuurides, kuna barjäärid elektroodidel on väiksed. Samas aga muudab suurema väljumistööga elektroodide kasutamine TiO_2 atraktiivsemaks, sest siis muutub suurem mahtuvus olulisemaks.

ACKNOWLEDGEMENTS

There are many persons who have contributed to this thesis and who have my greatest gratitude.

At first, I would like to give my special thanks to my supervisors Dr. Kaupo Kukli and Assoc. Prof. Matti Laan for introducing and aiding me in this interesting topic, for the patience in supervising me and for continuous support in numerous other aspects comprising the everyday life of a PhD student.

My co-authors are acknowledged for their contributions in the papers. Dr. Jaan Aarik has provided not only the TiO_2 films but also the knowledge about the growth and properties of these films. Dr. Viktor Bichevin and Dr. Henn Käämbre have helped me at the beginning of the studies with the measurement setup, ideas and in writing the manuscripts. I have my obligations to Dr. A. Aidla for the preparation of films and Dr. Jun Lu, Mr. Martti Pärs, Prof. Väino Sammelselg, Dr. Timo Sajavaara and Dr. Teet Uustare for the characterization of the films studied in this work. Without their contribution, the electrical measurements would have had only little value.

I am grateful to Prof. Mikko Ritala and Prof. Markku Leskelä for providing access to the electrode techniques and to the measurement setup for electrical characterization and XRD. Mr. Marko Vehkamäki is thanked for the evaporation of platinum electrodes. Dr. Ilmar Rammo and Mr. Varpo Redi are acknowledged for the access to the FTIR apparatus. Mr. Aivar Tarre is acknowledged for his assistance in HR-TEM studies

I appreciate the help of my colleagues in Gas Discharge Laboratory and the possibility to perform in numerous seminars of the lab.

I am thankful to my family for the patience during the time I had to spend on my thesis and to my parents for strong support which allowed me to concentrate on the thesis.

REFERENCES

[1] O. Carp, C. L. Huisman, A. Reller, "Photoinduced reactivity of titanium dioxide", Prog. Solid State Chem. 32 (2004) 33.

[2] K. Hashimoto, H. Irie, A. Fujishima, "TiO_2 Photocatalysys: A Historical Overview and Future Prospects", Jpn. J. Appl. Phys. 44 (2005) 8269.

[3] M. Kitano, M. Matsuoka, M. Ueshima, M. Anpo, "Recent developments in titanium oxide-based photocatalysts", Appl. Catal. A: General 325 (2007) 1.

[4] B. S. Richards, "Comparison of TiO_2 and Other Dielectric Coatings for Buried-contact Solar Cells: a Review", Prog. Photovolt: Res. Appl. 12 (2004) 253.

[5] J. W. Fergus, "Doping and defect association in oxides for use in oxygen sensors", J. Mater. Sci. 38 (2003) 4259.

[6] T. Iwanaga, T. Hyodo, Y. Shimizu, M. Egashira, "H_2 sensing properties and mechanism of anodically oxidized TiO_2 film contacted with Pd electrode", Sensors Actuators B 93 (2003) 519.

[7] S. K. Hazra, S. Roy, S. Basu, "Growth of titanium dioxide thin films via metallurgical route and characterizations for chemical gas sensors", Mater. Sci. Eng. B 110 (2004) 195.

[8] B. Huber, H. Gnaser, C. Ziegler, „Electrical properties of nanocrystalline anatase TiO_2 thin films with different crystallite size", Surf. Sci. 566 (2004) 419.

[9] G. Korotcenkov, "Metal oxides for solid-state gas sensors: What determines our choice", Mater. Sci. Engineering B 139 (2007) 1.

[10] T. Suntola, "Performance of ALE-EL devices", Digest of 1981 SID International Symposium (1981) 20.

[11] C. H. L. Goodman, M. V. Pessa, "Atomic layer epitaxy", J. Appl. Phys. 60 (1986) R65.

[12] W.-M. Li, M. Leskelä, R. Lappalainen, J. Jokinen, E. Soininen, B. Hüttl, E. Nykänen, L. Niinistö, "Elemental characterization of electroluminescent SrS:Ce thin films", J. Appl. Phys. 84 (1998) 1029.

[13] T. Yuranova, D. Laub, J. Kiwi, "Synthesis, activity and characterization of textiles showing self-cleaning activity under daylight irradiation", Catal. Today 122 (2007) 109.

[14] J. J. Wang, X. Deng, R. Varghese, A. Nikolov, P. Sciortino, F. Liu, L. Chen, X. Liu, "Filling high aspect-ratio nano-structures by atomic layer deposition and its applications in nano-optic devices and intergrations", J. Vac. Sci. Technol. B 23 (2005) 3209.

[15] R. Matero, M. Ritala, M. Leskelä, T. Salo, J. Aromaa, O. Forsén, "Atomic layer deposited thin films for corrosion protection", J. Phys. IV France 9 (1999) 493.

[16] C. Nistorica, J.-F. Liu, I. Gory, G. D. Skidmore, F. M. Mantiziba, B. E. Gnade, J. Kim, "Tribological and wear studies of coatings fabricated by atomic layer deposition and by successive ionic layer adsorption and reaction for microelectrochemical devices", J. Vac. Sci. Technol. A 23 (2005) 836.

[17] C. R. Stoldt, V. M. Bright, "Ultra-thin film encapsulation processes for micro-electro-mechanical devices and systems", J. Phys. D: Appl. Phys., 39 (2006) R163.

[18] D. F. Bahr, C. L. Woodcock, M. Pang, K. D. Weaver, N. R. Moody, "Indentation induced film fracture in hard film – soft substrate systems", Int. J. Fracture 119/120 (2003) 339.

[19] J. S. King, E. Graugnard, C. J. Summers, "TiO_2 Inverse Opals Fabricated Using Low-Temperature Atomic Layer Deposition", Adv. Mater. 17 (2005) 1010.

[20] E. Graugnard, D. P. Gaillot, S. N. Dunham, C. W. Neff, T. Yamashita, C. J. Summers, "Photonic band tuning in two-dimensional photonic crystal slab waveguides by atomic layer deposition", Appl. Phys. Lett. 89 (2006) 181108.

[21] S. D. Yoon, Y. Chen, A. Yang, T. L. Goodrich, X. Zuo, D. A. Arena, K. Ziemer, C. Vittoria, V. G. Harris, "Oxygen-defect-induced magnetism to 880 K in semiconducting anatase $TiO_{2-\delta}$ films", J. Phys.: Condens. Matter 18 (2006) L355.

[22] J. M. D. Coey, M. Venkatesan, C. B. Fitzgerald, "Donor impurity band exchange in dilute ferromagnetic oxides", Nature Mat. 4 (2005) 173.

[23] G. Glaspell, A. B. Panda, M. S. El-Shall, "Reversible paramagnetism to ferromagnetism in transition metal-doped TiO_2 nanocrystals prepared by microwave irradiation", J. Appl. Phys. 100 (2006) 124307.

[24] M. V. Koudriachova, N. M. Harrison, S. W. Leeuw, "Effect of Diffusion on Lithium Intercalation in Titanium Dioxide", Phys. Rev. Lett. 86 (2001) 1275.

[25] L. J. Hardwick, M. Holzapfel, P. Novák, L. Dupont, E. Baudrin, "Electrochemical lithium insertion into anatase-type TiO_2: An *in situ* Raman microscopy investigation", Electrochim. Acta 52 (2007) 5357.

[26] M. J. Linday, M. G. Blackford, D. J. Attard, V. Luca, M. Skyllas-Kazacos, C. S. Griffith, "Anodic titania films as anode materials for lithium ion batteries", Electrochim. Acta 52 (2007) 6401.

[27] T. Hitosugi, A. Ueda, S. Nakao, N. Yamada, Y. Furubayashi, Y. Hirose, T. Shimada, T. Hasegawa, "Fabrication of highly conductive $Ti_{1-x}Nb_xO_2$ polycrystalline films on glass substrates via crystallization of amorphous phase grown by pulsed laser deposition", Appl. Phys. Lett. 90 (2007) 212106.

[28] Y. Furunayashi, N. Yamada, Y. Hirose, Y. Yamamoto, M. Otani, T. Hitosugi, T. Shimada, T. Hasegawa, "Transport properties of *d*-electron-based transparent conducting oxide: Anatase $Ti_{1-x}Nb_xO_2$", J. Appl. Phys. 101 (2007) 093705.

[29] T. Hitosugi, A. Ueda, Y. Furubayashi, Y. Hirose, S. Konuma, T. Shimada, T. Hasegawa, "Fabrication of TiO_2-Based Transparent Conducting Oxide Films on Glass by Pulsed Laser Deposition", Jpn. J. Appl. Phys. 46 (2007) L86.

[30] J. Domaradzki, A. Borkowska, D. Kaczmarek, E. Prociow, "Transparent oxide semiconductors based on TiO_2 doped with V, Co and Pd elements", J. Non-Crystal. Solids 352 (2006) 2324.

[31] J. Domaradzki, K. Nitsch, "Electrical characterization of semiconducting V and Pd-doped TiO_2 thin films on silicon by impedance spectroscopy", Thin Solid Films 515 (2007) 3745.

[32] J. Exarhos, X.-D. Zhou, "Discovery-based design of transparent conducting oxide films", Thin Solid Films 515 (2007) 7025.

[33] N. S. Xu, S. E. Huq, "Novel cold cathode materials and applications", Mater. Sci. Eng. R 48 (2005) 47.

[34] V. T. Binh, C. Adessi, "New Mechanism for Electron Emission from Planar Cold cathodes: The Solid State Field-Controlled Electron Emitter", Phys. Rev. Lett. 85 (2000) 864.

[35] V. T. Binh, V. Semet, J. P. Dupin, D. Guillot, “Recent progress in the characterization of electron emission from solid-state field-controlled emitters”, J. Vac. Sci. Technol. B 19 (2001) 1044.
[36] V. T. Binh, J. P. Dupin, C. Adessi, V. Semet, “Solid-state field-controlled emitters: a thin-film technology solution for industrial cathodes”, Solid-State Electron. 45 (2001) 1025.
[37] M. Laan, J. Aarik, R. Joosepson, V. Repän, “Low current mode of negative coronas: mechanism of electron emission”, J. Phys. D: Appl. Phys. 36 (2003) 2667.
[38] M. Laan, R. Joosepson, J. Aarik, “UV-initiated current in point-plane gap”, J. Phys. D: Appl. Phys. 40 (2007) 3402.
[39] K. H. Bayliss R. V. Latham, “An analysis of field-induced hot-electron emission from metal-insulator microstructures on broad-area high-voltage electrodes”, Proc. R: Soc. Lond. A 403 (1986) 285.
[40] S. A. Campbell, H.-S. Kim,D. C. Gilmer, B. He, T. Ma, W. L. Gladfelter, “Titanium dioxide (TiO_2)-based gate insulators”, IBM J. Res. Develop. 43 (1999) 383.
[41] J.-J. Park, W.-J. Lee, G.-H. Lee, I.-S. Kim, B.-C. Shin, S.-G. Yoon, “Very Thin TiO_2 Films Prepared by Plasma Enhanced Atomic Layer Deposition (PEALD)”, Integr. Ferroelectr. 68 (2004) 68.
[42] J. W. Lim, S. J. Yun, J. H. Lee, “Characteristics of TiO_2 Films Prepared by ALD With and Without Plasma”, Electrochem. Solid-State Lett. 7 (2004) F73.
[43] S. K. Kim, W.-D. Kim, K.-M. Kim, C. S. Hwang, J. Jeong, “High dielectric constant TiO_2 thin films on a Ru electrode grown at 250 ºC by atomic-layer depositin”, Appl. Phys. Lett. 85 (2004) 4112.
[44] W. D. Kim, G. W. Hwang, O. S. Kwon, S. K. Kim, M. Cho, D. S. Jeon, S. W. Lee, M. H. Seo, C. S. Hwang, Y.-S. Min, Y. J. Cho, “Growth Characteristics of Atomic Layer Deposited TiO_2 Thin Films on Ru and Si Electrodes for Memory Capacitor Applications”, J. Electrochem. Soc. 152 (2005) C552.
[45] S. K. Kim, K.-M. Kim, O. S. Kwon, S. W. Lee, C. B. Jeon, W. Y. Park, C. S. Hwang, J. Jeong, “Transformation of the Crystalline Structure of an ALD TiO_2 Film on a Ru Electrode by O_3 Pretreatment”, Electrochem. Solid-State Lett. 8 (2005) F59.
[46] S. K. Kim, S. Y. Lee, M. Seo, G.-J. Choi, C. S. Hwang, “Impact of O_3 feeding time on TiO_2 films grown by atomic layer deposition for memory capacitor applications”, J. Appl. Phys. 102 (2007) 024109.
[47] G. Wang, D. Moses, A. J. Heeger, H.-M. Zhang, M. Narasimhan, R. E. Demaray, “Poly(3-hexylthiophene) field-effect transistors with high dielectric constant gate insulator”, J. Appl. Phys. 95 (2004) 316.
[48] Z. Q. Li, G. M. Wang, N. Sai, S. Moses, M. C. Martin, M. Di Ventra, A. J. Heeger, D. N. Basov, “Infrared Imaging of the Nanometer-Thick Accumulation Layer in Organic Field-Effect Transistors”, Nano Lett. 6 (2006) 224.
[49] K. Fujimaru, H. Matsumura, “Theoretical Consideration of a New Nanometer Transistor Using Metal/Insulator Tunnel-Junction”, Jpn. J. Appl. Phys. 35 (1996) 2090.
[50] E. S. Snow, P. M. Campbell, R. W. Rendell, F. A. Buot, D. Park, C. R. K. Marrian, R. Mango, “A metal/oxide tunneling transistor”, Semicond. Sci. Technol. 13 (1998) A75.

[51] K. Fujimaru, R. Sasajima, H. Matsumura, “Nanoscale metal transistor control of Fowler-Nordheim tunneling currents through 16 nm insulating channel”, J. Appl. Phys. 85 (1999) 6912.
[52] R. Sadajima, K. Fujimaru, H. Matsumura, “A metal/insulator tunnel transistor with 16 nm channel length”, Appl. Phys. Lett. 74 (1999) 3215.
[53] F.-C. Chiu, S.-K. Fan, K.-C. Tai, J. Y. Lee, Y.-C. Chou, “Electrical characterization of tunnel insulator in metal/insulator tunnel transistor fabricated by atomic force microscope”, Appl. Phys. Lett. 87 (2005) 243506.
[54] F. Wallrapp, P. Fromherz, “TiO_2 and HfO_2 in electrolyte-oxide-silicon configuration for applications in bioelectronics”, J. Appl. Phys. 99 (2006) 114103.
[55] B. J. Choi, D. S. Jeong, S. K. Kim, C. Rohde, S. Choi, J. H. Oh, H. J. Kim, C. S. Hwang, K. Szot, R. Waser, B. Reichenberg, S. Tiedke, “Resistive switching mechanism of TiO_2 thin films grown by atomic-layer deposition”, J. Appl. Phys. 98 (2005) 033715.
[56] K. M. Kim, B. J. Choi, D. S. Jeong, C. S. Hwang, S. Han, “Influence of carrier injection on resistive switching of TiO_2 thin films with Pt electrodes”, Appl. Phys. Lett. 89 (2006) 162912.
[57] B. J. Choi, S. Choi, K. M. Kim, Y. C. Shin, C. S. Hwang, S.-Y. Hwang, S.-S. Cho, S. Park, S.-K. Hong, “Study on the resistive switching time of TiO_2 thin films”, Appl. Phys. Lett. 89 (2006) 012906.
[58] C. Rohde, B. J. Choi, D. S. Jeong, S. Choi, J.-S. Zhao, C. S. Hwang, “Identification of a determining parameter for resistive switching of TiO_2 thin films”, Appl. Phys. Lett. 86 (2005) 262907.
[59] D. S. Jeong, H. Schroeder, R. Waser, “Impedance spectroscopy of TiO_2 thin films showing resistive switching”, Appl. Phys. Lett. 89 (2006) 082909.
[60] K. Tsunoda, Y. Fukuzumi, J. R. Jameson, Z. Wang, P. B. Griffin, Y. Nishi, “Bipolar resistive switching in polycrystalline TiO_2 fims”, Appl. Phys. Lett. 90 (2007) 113501.
[61] H. Schroeder, D. S. Jeong, “Resistive switching in a Pt/TiO_2/Pt thin film stack – a candidate for a non-volatile ReRAM”, Microelectron. Eng. 84 (2007) 1982.
[62] M. Villafuerte, G. Juárez, S. P. Heluani, D. Comedi, “Hysteretic current-voltage characteristics in RF-sputtered nanocrystalline TiO_2 thin films”, Physica B 398 (2007) 321.
[63] H. Wong, H. Iwai, “On the scaling issues and high-κ replacement of ultrathin gate dielectrics for nanoscale MOS transistors”, Microelectron. Eng. 83 (2006) 1867.
[64] J. Nowotny, M. Radecka, M. Rekas, “Semiconducting properties of undoped TiO_2”, J. Phys. Chem. Solids 58 (1997) 927.
[65] B. H. Lee, Y. Jeon, K. Zawadzki, W.-J. Qi, J. Lee, “Effects of interfacial layer growth on the electrical characteristics of thin titanium oxide films on silicon”, Appl. Phys. Lett. 74 (1999) 3143.
[66] M. Kadoshima, M. Hiratani, Y. Shimamoto, K. Torii, H. Miki, S. Kimura, T. Nabatame, “Rutile-type TiO_2 thin films for high-k gate insulator”, Thin Solid Films 424 (2003) 224.
[67] W. P. Chen, Y. Wang, J. Y. Dai, S. G. Lu, X. X. Wang, P. F. Lee, H. L. W. Chan, C. L. Choy, “Spontaneous recovery of hydrogen-degraded TiO_2 ceramic capacitors”, Appl. Phys. Lett. 84 (2004) 103.

[68] Y. Nakano, T. Morikawa, T. Ohwaki, Y. Taga, "Electrical characterization of band gap states in C-doped TiO_2 films", Appl. Phys. Lett. 87 (2005) 052111.
[69] T. Miyagi, M. Kamei, T. Mitsuhashi, A. Yamazaki, "Superior Schottky electrode of RuO_2 for deep level transient spectroscopy on anatase TiO_2", Appl. Phys. Lett. 83 (2003) 1782.
[70] A. B. F. Martinson, J. W. Elam, J. T. Hupp, M. J. Pellin, "ZnO Nanotube Based Dye-Sensitized Solar Cells", Nano Letters, (2007) doi: 10.1021/nl070160.
[71] M. J. Pellin, P. C. Stair, G. Xiong, J. W. Elam, J. Birell, L. Curtiss, S. M. George, C. Y. Han, L. Iton, H. Kung, M. Kung, H.-H. Wang, "Mesoporous catalytic membranes: Synthetic control of pore size and wall composition", Catal. Lett. 102 (2005) 127.
[72] S. J. Park, B. K. Ahn, P. S. Alegaonkar, H. J. Shin, J. B. Yoo, "Fabrication of Porous Al_2O_3 and TiO_2 Thin film hybrid composite using Atomic Layer Deposition and Properties Study", Solid State Phenomena, 124–126 (2007) 1273.
[73] X. D. Wang, E. Graugnard, J. S. King, Z. L. Wang, C. J. Summers, "Large-Scale Fabrication of Ordered Nanobowl Arrays", Nano Letters 4 (2004) 2223.
[74] M. Kemell, M. Ritala, M. Leskelä, E. Ossei-Wusu, J. Carstensen, H. Föll, "Si/Al_2O_3/ZnO:Al capacitor arrays formed in electrochemically etched porous Si by atomic layer deposition", Microelectron. Eng. 84 (2007) 313.
[75] M. Gutsche, H. Seidl, T. Hecht, S. Kudelka, U. Schroeder, "Atomic Layer Deposition for Advanced DRAM Applications", Future Fab Int. 14 (2003) 1009.
[76] "Meet the World's First 45nm Processor", http://www.intel.com/technology/silicon/45nm_technology.htm?iid=.
[77] G. D. Wilk, R. M. Wallace, J. M. Anthony, "High-κ gate dielectrics: Current status and materials properties considerations", J. Appl. Phys. 89 (2001) 5243.
[78] J. Robertson, "High dielectric constant gate oxides for metal oxide Si transistors", Rep. Prog. Phys. 69 (2006) 327.
[79] E. P. Gusev, V. Narayanan, M. M. Frank, "Advanced high-κ dielectric stacks with polySi and metal gates: Recent progress and current challenges", IBM J. Res. Dev. 50 (2006) 387.
[80] M. Ritala, M. Leskelä, E. Nykänen, P. Soininen, L. Niinistö, "Growth of titanium dioxide thin films by atomic layer epitaxy", Thin Solid Films 225 (1993) 288.
[81] J. Aarik, A. Aidla, T. Uustare, V. Sammelselg, "Morphology and structure of TiO_2 thin films grown by atomic layer deposition", J. Cryst. Growth 148 (1995) 268.
[82] J. Aarik, A. Aidla, A.-A. Kiisler, T. Uustare, V. Sammelselg, "Effect of crystal structure on optical properties of TiO_2 films grown by atomic layer deposition", Thin Solid Films 305 (1997) 270.
[83] J. Aarik, A. Aidla, H. Mändar, V. Sammelselg, "Anomalous effect of temperature on atomic layer deposition of titanium dioxide", J. Cryst. Growth 220 (2000) 531.
[84] J. Aarik, A. Aidla, H. Mändar, T. Uustare, "Atomic layer deposition of titanium dioxide from $TiCl_4$ and H_2O: investigation of growth mechanism", Appl. Surf. Sci. 172 (2001) 148.

[85] J. Aarik, A. Aidla, H. Mändar, T. Uustare, M. Schuisky, A. Hårsta, "Atomic layer growth of epitaxial TiO_2 thin films from $TiCl_4$ and H_2O on α-Al_2O_3 substrates", J. Cryst. Growth 242 (2002) 189.

[86] R. Matero, A. Rahtu, M. Ritala, "In Situ Quadrupole Mass Spectrometry and Quartz Crystal Microbalance Studies on the Atomic Layer Deposition of Titanium Dioxide from Titanium Tetrachloride and Water", Chem. Mater. 13 (2001) 4506.

[87] K. Kukli, M. Ritala, M. Schuisky, M. Leskelä, T. Sajavaara, J. Keinonen, T. Uustare. A. Hårsta, "Atomic Layer Deposition of Titanium Oxide from TiI_4 and H_2O_2", Chem. Vap. Deposition 6 (2000) 303.

[88] K. Kukli, A. Aidla, J. Aarik, M. Schuisky, A. Hårsta, M. Ritala, M. Leskelä, "Real-Time Monitoring in Atomic Layer Deposition of TiO_2 from TiI_4 and H_2O-H_2O_2", Langmuir 16 (2000) 8122.

[89] M. Schuisky, J. Aarik, K. Kukli, A. Aidla, A. Hårsta, "Atomic Layer Deposition of Thin Films Using O_2 as Oxygen Source", Langmuir 17 (2001) 5508.

[90] M. Schuisky, K. Kukli, J. Aarik, J. Lu, A. Hårsta, "Epitaxial growth of TiO_2 films in a hydroxyl-free atomic layer deposition process", J. Cryst. Growth 235 (2002) 293.

[91] J. Aarik, A. Aidla, T. Uustare, K. Kukli, V. Sammelselg, M. Ritala, M. Leskelä, "Atomic layer deposition of TiO_2 thin films from TiI_4 and H_2O", Appl. Surf. Sci. 193 (2002) 277.

[92] A. Rahtu, K. Kukli, M. Ritala, "In Situ Mass Spectrometry Study on Atomic Layer Deposition from Metal (Ti, Ta, and Nb) Ethoxides and Water", Chem. Mater. 13 (2001) 817.

[93] A. Rahtu, M. Ritala, "Reaction Mechanism Studies on Titanium Isopropoxide-Water Atomic Layer Deposition Process", Chem. Vap. Deposition, 8 (2002) 21.

[94] J. Aarik, A. Aidla, V. Sammelselg, T. Uustare, M. Ritala, M. Leskelä, "Characterization of titanium dioxide atomic layer growth from titanium ethoxide and water", Thin Solid Films 370 (2000) 163.

[95] J. Aarik, J. Karlis, H. Mändar, T. Uustare, V. Sammelselg, "Influence of structure development on atomic layer deposition of TiO_2 thin films", Appl. Surf. Sci. 181 (2001) 339.

[96] J. Aarik, A. Aidla, T. Uustare, M. Ritala, M. Leskelä, "Titanium isopropoxide as a precursor for atomic layer deposition: characterization of titanium dioxide growth process", Appl. Surf. Sci. 161 (2000) 385.

[97] V. Sammelselg, E. Rauhala, K. Arstila, A. Zakharov, J. Aarik, A. Kikas, J. Karlis, A. Tarre, A. Seppälä, J. Asari, I. Martinson, "Study of Thin Oxide Films by Electron, Ion and Synchrotron Radiation Beams", Microchim. Acta 139 (2002) 165.

[98] M. D. Stamate, "On the non-linear *I-V* characteristics of dc magnetron sputtered TiO_2 thin films", Appl. Surf. Sci. 205 (2003) 353.

[99] A. K. Hassan, N. B. Chaure, A. K. Ray, A. V. Nabok, S. Habesch, J. Phys. D: Appl. Phys. 36 (2003) 1120.

[100] J. Yan, D. C. Gilmer, S. A. Campbell, W. L. Gladfelter, P. G. Scmid, "Structural and electrial characterization of TiO_2 grown from titanium tetrakis-isopropoxide (TTIP) and TTIP/H_2O ambients", J. Vac. Sci. Technol. B 14 (1996) 1706.

[101] H.-S. Kim, D. C. Gilmer, S. A. Campbell, D. L. Polla, "Leakage current and electrical breakdown in metal-organic chamical vapor deposited TiO_2 dielectrics on silicon substrates", Appl. Phys. Lett. 69 (1996) 3860.
[102] S. A. Campbell, D. C. Gilmer, X. Wang, M. Hsieh, H.-S. Kim, W. L. Gladfelter, J. Yan, "MOSFET Transistors Fabricated with High Permittivity TiO_2 Dielectrics", IEEE Trans. Electron. Devices 44 (1997) 104.
[103] H. Fukuda, S. Namioka, M. Miura, Y. Ishikawa, M. Yoshino, S. Nomura, "Structural and Electrica Properties of Crystalline TiO_2 Thin Films Formed by Metalorganic Decomposition", Jpn. J. Appl. Phys. 38 (1999) 6034.
[104] K. Matsuo, K. Nakajima, S. Omoto, S. Nakamura, A. Yagishita, G. Minamihaba, H. Yano, K. Suguro, "Low Leakage TiO_2 Gate Insulator Formed by Ultrathin TiN Deposition and Low-Temperature Oxidation", Jpn. J. Appl. Phys. 39 (2000) 5794.
[105] H.-K. Ha, M. Yoshimoto, H. Koinuma, B.-K. Moon, H. Ishiwara, "Open air plasma chemical vapor deposition of highly dielectric amorphous TiO_2 films", Appl. Phys. Lett. 68 (1996) 2965.
[106] H. Ha, B. K. Moon, T. Horiuchi, T. Inushima, H. Ishiwara, H. Koinuma, "Structure and electric properties of TiO_2 films prepared by cold palsma torch under atmospheric pressure", Mater. Sci. Engineer. B 41 (1996) 143.
[107] V. Mikhelashvili, G. Eisenstein, "Effects of annealing conditions on optical and electrical characteristics of titanium dioxide films deposited by electron beam evaporation", J. Appl. Phys. 89 (2001) 3256.
[108] V. Mikhelashvili, G. Eisenstein, "Composition, surface morphology and electrical characteristics of Al_2O_3-TiO_2 nanolaminates and AlTiO films on silicon", Thin Solid Films 515 (2006) 346.
[109] Z. J. Luo, X. Guo, T. P. Ma, T. Tamagawa, "Temperature dependence of gate currents in thin Ta_2O_5 and TiO_2 films", Appl. Phys. Lett. 79 (2001) 2803.
[110] R. Paily, A. DasGupta, N. DasGupta, T. Ganguli, L. M. Kukreja, "Effect of oxygen pressure and laser fluence during pulsed laser deposition of TiO_2 on MTOS (Metal-TiO_2-SiO_2-Si) capacitor characteristics", Thin Solid Films 462 (2004) 57.
[111] N. B. Chaure, A. K. Ray, R. Capan, "Sol-gel derived nanocrystalline titania thin films on silicon", Semicond. Sci. Technol. 20 (2005) 788.
[112] L.-H. Chong, K. Mallik, C. H. de Groot, "The vertical metal insulator semi-conductor tunnel transistor: A proposed Fowler-Nordheim tunneling device", Microelectron. Eng. 81 (2005) 171.
[113] B. Karunagaran, S. J. Chung, E.-K. Suh, D. Mangalaraj, „Dielectric and transport properties of magnetron sputtered titanium dioxide thin films", Physica B 369 (2005) 129.
[114] M.-K. Lee, J.-J. Huang, T.-S. Wu, „Electrical characteristics improvement of oxygen-annealed MOCVD-TiO_2 films", Semicond. Sci. Technol. 20 (2005) 519.
[115] M.-K. Lee, J.-J. Huang, Y.-H. Hung, „Variation of Electrical Characteristics of Metallorganic Chemical Vapor Deposited TiO_2 Films by Postmetallization Annealing", J. Electrochem. Soc. 152 (2005) F190.
[116] M.-K. Lee, J.-J. Huang, C.-M. Hsu, "High dielectric constant titanium oxide grown on amorphous silicon by metal-organic chemical vapour deposition", Semicond. Sci Technol. 21 (2006) 604.

26

[117] D. V. Gritsenko, S. S. Shaĭmeev, V. V Atucchin, T. I. Grigor'eva, L. D. Pokrovskiĭ, O. P. Pchelyakov, V. A. Gritsenko, A. L. Aseev, V. G. Lifshits, "Two-Band Conduction in TiO_2", Phys. Solid State 48 (2006) 224.

[118] A. P. Huang, P. K. Chu, L. Wang, W. Y. Cheung, J. B. Xu, S. P. Wong, "Fabrication of rutile TiO_2 thin films by low-temperature, bias-assisted cathodic arc deposition and their dielectric properties", J. Mater. Res. 21 (2006) 844.

[119] W. Yang, J. Marino, A. Monson, C. A. Wolden, "An investigation of annealing on the dielectric performance of TiO_2 thin films", Semicond. Sci. Technol. 21 (2006) 1573.

[120] C. K. Maiti, S. K. Samanta, G. K. Dalapati, S. K. Nandi, S. Chatterjee, "Electrical characterization of TiO_2 gate oxides on strained-Si", Microelectron. Eng. 72 (2004) 253.

[121] S. Chakraborty, M. K. Bera, S. Bhattacharya, C. K. Maiti, "Current conduction mechanism in TiO_2 gate dielectrics", Microelectron. Eng. 81 (2005) 188.

[122] M. K. Bera, C. K. Maiti, "Electrical properties of SiO_2/TiO_2 high-k gate dielectric stack", Mater. Sci. Semicond. Process. 9 (2006) 909.

[123] G. K. Dalapati, S. Chatterjee, S. K. Samanta, S. K. Nandi, P. K. Bose, S. Varma, S. Patil, C. K. Maiti, "Electrical properties of ultrathin TiO_2 films on $Si_{1-y}C_y$ heterolayers", Solid-State Electron. 47 (2003) 1793.

[124] R. Mahapatra, A. K. Chakraborty, N. Poolamai, A. Horsfall, S. Chattopadhyay, N. G. Wright, K. S. Coleman, P. G. Coleman, C. P. Burrows, "Leakage current and charge trapping behavior in TiO_2/SiO_2 high-κ gate dielectric stack on 4H-SiC substrate", J. Vac. Sci. Technol. B 25 (2007) 217.

[125] U. Diebold, "The surface science of titanium dioxide", Surf. Sci. Reports 48 (2003) 53.

[126] T. Hori, in Gate Dielectrics and MOS ULSIs. Principles, Technologies, and Applications, I. P. Kaminow, W. Engl, T. Sugano and H. K. V. Lotsch, Editors, Vol. 34, Springer Series in Electronis and Photonics, Springer, Berlin Heidelberg, 1997, pp. 71–74.

[127] D. A. Buchanan, "Scaling the gate dielectric: Materials, integration, and reliability", IBM J. Res. Develop. 43 (1999) 245.

[128] E. Gerritsen, N. Emonet, C. Caillat, N. Jourdan, M. Piazza, D. Fraboulet, B. Boeck, A. Berthelot, S. Smith, P. Mazoyer, "Evolution of materials technology for stacked-capacitors in 65 nm embedded-DRAM", Solid-State Electron. 49 (2005) 1767.

[129] Y. Q. Wu, H. C. Lin, P. D. Ye, G. D. Wilk, "Current transport and maximum dielectric strength of atomic-layer-deposited ultrathin Al_2O_3 on GaAs", Appl. Phys. Lett. 90 (2007) 072105.

[130] P. Kordoš, D. Gregušová, R. Stoklas, K. Čičo, J. Novák, "Improved transport properties of Al_2O_3/AlGaN/GaN metal-oxide-semiconductor heterostructure field-effect transistor", Appl. Phys. Lett. 90 (2007) 123513.

[131] G. Pozzovivo, J. Kuzmik, S. Golka, W. Schrenk, G. Strasser, D. Pogany, K. Čičo, M. Ťapajna, K. Fröhlich, J.-F. Carlin, M. Gonschorek, E. Feltin, N. Grandjean, "Gate insulation and drain current saturation mechanism in InAlN/GaN metal-oxide-semiconductor high-electron-mobility transistors", Appl. Phys. Lett. 91 (2007) 043509.

[132] S. K. Kim, Y. Xuan, P. D. Ye, S. Mohammadi, J. H. Back, M. Shim, "Atomic layerd deposited Al_2O_3 for gate dielectric and passivation layer of single-walled carbon nanotube transistor", Appl. Phys. Lett. 90 (2007) 163108.
[133] J. B. Koo, C. H. Ku, S. C. Lim, S. H. Kim, J. H. Lee, "Hysteresis and treshold voltage shift of pentacene thin-film transistors and inverters with Al_2O_3 gate dielectric", Appl. Phys. Lett. 90 (2007) 133503.
[134] M. Avice, U. Grossner, I. Pintile, B. G. Svensson, O. Nilsen, H. Fjellvag, "Comparison of near-interface traps in Al_2O_3/4*H*-SiC and Al_2O_3/SiO_2/4*H*-SiC structures", Appl. Phys. Lett. 89 (2006) 222103.
[135] Y. C. Chang, H. C. Chiu, Y. J. Lee, M. L. Huang, K. Y. Lee, M. Hong, Y. N. Chiu, J. Kwo, Y. H. Wang, "Structural and electrical characteristics of atomic layer deposited high κ HfO_2 on GaN", Appl. Phys. Lett. 90 (2007) 232904.
[136] H.-S. Kim, I. Ok, M. Zhang, F. Zhu, S. Park, J. Yum, H. Zhao, J. C. Lee, "Gate oxide scaling down in HfO_2-GaAs metal-oxide-semiconductor capacitor using germanium interfacial passivation layer", Appl. Phys. Lett. 91 (2007) 042904.
[137] E. Martinez, O. Renault, L. Fourdrinier, L. Clavelier, C. Le Royer, C. Licitra, T. Veyron, J. M. Hartmann, V. Loup, L. Vandroux, M. J. Guittet, N. Barrett, "Band offsets of HfO_2/GeON/Ge stacks measured by ultraviolet and soft x-ray photoelectron spectroscopies", Appl. Phys. Lett. 90 (2007) 053508.
[138] J. W. Lim, S. J. Yun, J. H. Lee, "Low-Temperature Growth of SiO_2 Films by Plasma-Enhanced Atomic Layer Deposition", ETRI J. 27 (2005) 118.
[139] D. C. Kim, M. J. Lee, S. E. Ahn, S. Seo, J. C. Park, I. K. Yoo, I. G. Baek, H. J. Kim, E. K. Yim, J. E. Lee, S. O. Park, H. S. Kim, U.-I. Chung, J. T. Moon, B. I. Ryu, "Improvement of resistive memory switching in NiO using IrO_2", Appl. Phys. Lett. 88 (2006) 232106.
[140] K. M. Kim, B. J. Choi, B. W. Koo, S. Choi, D. S. Jeong, C. S. Hwang, "Resistive Switching in Pt/Al_2O_3/TiO_2/Ti Stacked Structures", Electrochem. Solid-State Lett. 9 (2006) G343.
[141] C. J. Kim, I.-W. Chen, "Effect of top electrode on resistance switching of (Pr,Ca)MnO_3 thin films", Thin Solid Films (2006) 2726.
[142] R. Dong, D. S. Lee, W. F. Xiang, S. J. Oh, D. J. Seong, S. H. Heo, H. J. Choi, M. J. Kwon, S. N. Seo, M. B. Pyun, M. Hasan, H. Hwang, "Reproducible hysteresis and resistive switching in metal-Cu_xO-metal heterostructures", Appl. Phys. Lett. 90 (2007) 042107.
[143] D. Lee, D.-J. Seong, I. Jo, F. Xiang, R. Dong, S. J. Oh, H. Hwang, "Resistance switching of copper doped MoO_x films for nonvolatile memory applications", Appl. Phys. Lett. 90 (2007) 122104.
[144] A. Rosental, A. Tarre, A. Gerst, J. Sundqvist, A. Hårsta, A. Aidla, J. Aarik, V. Sammelselg, T. Uustare, "Gas sensing properties of epitaxial SnO_2 thin films prepared by atomic layer deposition", Sens. Actuators B 93 (2003) 552.
[145] B. O'Reagan, M. Grätzel, "A low-cost high-efficiency solar cell based on dye-sensitized colloidal TiO_2 films", Nature 353 (1991) 737.
[146] H. Tributsch, "Dye sensitization solar cells: a critical assessment of the learning curve", Coord. Chem. Rev. 248 (2004) 1511.
[147] M. Ritala, M. Leskelä, in Handbook of Thin Film Materials, edited by H. S. Nalwa (Academic, San Diego, 2002), vol. 1, pp. 103–159

[148] M. Leskelä, M. Ritala, "Atomic layer deposition (ALD): from precursors to thin film structures", Thin Solid Films 409 (2002) 138.
[149] L. Niinistö, J. Päiväsaari, J. Niinistö, M. Putkonen, M. Nieminen, "Advanced electronic and optoelectronic materials by Atomic Layer Deposition: An overview with special emphasis on recent progress in processing of high-*k* dielectrics and other oxide materials", Phys. Stat. Sol. A 201 (2004) 1443.
[150] A. Niskanen, K. Arstila, M. Leskelä, M. Ritala, "Radical Enhanced Atomic Layer Deposition of Titanium Dioxide", Chem. Vap. Deposition 13 (2007) 152.
[151] A. Niskanen, K. Arstila, M. Ritala, M. Leskelä, "Low-Temperature Deposition of Aluminium Oxide by Radical Enhanced Atomic Layer Deposition", J. Electrochem. Soc. 152 (2005) F90.
[152] L. Niinistö, M. Leskelä, "Atomic layer epitaxy: chemical opportunities and challenges", Thin Solid Films 225 (1993) 130.
[153] J. W. Lim, S. J. Yun, "Electrical Properties of Alumina Films by Plasma-Enhanced Atomic Layer Deposition", Electrochem. Solid-State Lett. 7 (2004) F45.
[154] S. J. Yun, J. W. Lim, J.-H. Lee, "Low-Temperature Deposition of Aluminum Oxide on Polyethersulfone Substrate Using Plasma-Enhanced Atomic Layer Deposition", Electrochem. Solid-State Lett. 7 (2004) C13.
[155] J. B. Koo, S. J. Yun, J. W. Lim, S. H. Kim, C. H. Ku, S. C. Lim, J. H. Lee, T. Zyung, "Low-voltage and high-gain pentacene inverters with plasma-enhanced atomic-layer-deposited gate dielectrics", Appl. Phys. Lett. 89 (2006) 033511.
[156] V. Pore, M. Ritala, M. Leskelä, S. Areva, M. Järn, J. Järnström, "H_2S modified atomic layer deposition process for photocatalytic TiO_2 thin films", J. Mater. Chem. 14 (2007) 1361.
[157] V. Pore, M. Ritala, M. Leskelä, "Atomic Layer Deposition of Titanium disulfide Thin Films", Chem. Vap. Deposition 13 (2007) 163.
[158] M. Kemell, V. Pore, J. Tupala, M. Ritala, M. Leskelä, "Atomic Layer Deposition of Nanostructured TiO_2 Photocatalysts via Template Approach", Chem. Mater. 19 (2007) 1816.
[159] M. Kemell, V. Pore, M. Ritala, M. Leskelä, "Ir/Oxide/Cellulose Composites for Catalytic Purposes Prepared by Atomic Layer Deposition", Chem Vap. Deposition 12 (2006) 419.
[160] M. Ritala, M. Kemell, M. Lautala, A. Niskanen, M. Leskelä, S. Lindfors, "Rapid Coating of Through-Porous Substrates by Atomic Layer Deposition", Chem. Vap. Deposition 12 (2006) 655.
[161] C. F. Hermann, F. H. Fabrequette, D. S. Finch, R. Geiss, S. M. George, "Multilayer and functional coatings on carbon nanotubes using atomic layer deposition", Appl. Phys. Lett. 87 (2005) 123110.
[162] R. Matero, A. Rahtu, M. Ritala, M. Leskelä, T. Sajavaara, "Effect of water dose on the atomic layer deposition rate of oxide thin films", Thin Solid Films 368 (2000) 1.
[163] A. Rahtu, T. Alaranta, M. Ritala, "In Situ Quartz Crystal Microbalance and Quadrupole Mass Spectrometry Studies of Atomic Layer Deposition of Aluminum Oxide from Trimethylaluminum and Water", Langmuir 17 (2001) 6506.

[164] S.-C. Ha, E. Choi, S.-H. Kim, J. S. Roh, "Influence of oxidant source on the property of atomic layer deposited Al_2O_3 on hydrogen-terminated Si substrate", Thin Solid Films 476 (2005) 252.
[165] A. Heyman, C. B. Musgrave, "A Quantum Chemical Study of the Atomic Layer Deposition of Al_2O_3 Using $AlCl_3$ and H_2O as Precursors", J. Phys. Chem. B 108 (2004) 5718.
[166] S. Dueñas, H. Castán, H. García, A. de Castro, L. Bailón, K. Kukli, A. Aidla, J. Aarik, H. Mändar, T. Uustare, J. Lu, A. Hårsta, "Infuence of single and double deposition temperatures on the interface quality of atomic layer deposited Al_2O_3 dielectric thin films on silicon", J. Appl. Phys. 99 (2006) 054902.
[167] A. Niilisk, M. Moppel, M. Pärs, I. Sildos, T. Jantson, T. Avarmaa, R. Jaaniso, J. Aarik, "Structural study of TiO_2 thin films by micro-Raman spectroscopy", Central Eur. J. Phys. 4 (2006) 105.
[168] A. Niilisk, A. Rosental, A. Gerst, V. Sammelselg, T. Uustare, "Atomic scale optical monitoring of the initial growth of TiO_2 thin films", Proc. SPIE 4318 (2001) 72.
[169] H. Siimon, J. Aarik, "Thickness profiles of thin films caused by secondary reactions in flow-type atomic layer deposition reactors", J. Phys. D: Appl. Phys. 30 (1997) 1725.
[170] M. Ritala, K. Kukli, A. Rahtu, P. I. Räisänen, M. Leskelä, T. Sajavaara, J. Keinonen, "Atomic Layer Deposition of Oxide Thin Films with Metal Alkoxides as Oxygen Sources", Science 288 (2000) 319.
[171] A. K. Jonscher, "Electronic properties of amorphous dielectric films", Thin Solid Films 1 (1967) 213.
[172] A. K. Jonscher, "Electronic Conduction in Amorphous Semiconductors", J. Vac. Sci. Technol. 8 (1971) 135.
[173] J. G. Simmons, "Conduction in thin dielectric films", J. Phys. D: Appl. Phys. 4 (1871) 613.
[174] R. M. Hill, "Poole-Frenkel Conduction in Amorphous Solids", Philos. Mag. 23 (1971) 59.
[175] N. F. Mott, "Conduction in Non-crystalline Systems VII. Non-ohmic Behaviour and Switching", Philos. Mag. 23 (1971) 911.
[176] J. McPherson, J.-Y. Kim, A. Shanware, H. Mogul, "Thermochemical description of dielectric breakdown in high dielectric constant materials", Appl. Phys. Lett. 82 (2003) 2121.
[177] S. Roberts, "Dielectric Constants and Polarizabilities of Ions in Simple Crystals and Barium Titanate", Phys. Rev. 76 (1949) 1215.
[178] Y.-C. Yeo, T.-J. King, C. Hu, "Metal-dielectric band alignment and its implications for metal gate complementary metal-oxide-semiconductor technology", J. Appl. Phys. 92 (2002) 7266.
[179] J. Robertson, "Band offsets of wide-band-gap oxides and implications for future electronic devices", J. Vac. Sci. Technol. B 18 (2000) 1785.
[180] A. A. Demkov, L. R. C. Fonseca, E. Verret, J. Tomfohr, O. F. Sankey, "Complex band structure and the band alignment problem at the Si-high-*k* dielectric interface", Phys. Rev. B 71 (2005) 195306.

27

[181] Y. Lebedinskii, A. Zenkevich, E. P. Gusev, "Measurements of metal gate effective work function by x-ray photoelectron spectroscopy", J. Appl. Phys. 101 (2007) 074504.
[182] K. Ohmori, P. Ahmet, M. Yoshitake, T. Chikyow, K. Shiraishi, K. Yamabe, H. Watanabe, Y. Akasaka, Y. Nara, K.-S. Chang, M. L. Green, "Influences of annealing in reducing and oxidizing ambients on flatband voltage properties of HfO_2 gate stack structures", J. Appl. Phys. 101 (2007) 084118.
[183] Z. Li, T. Schram, L. Pantisano, A. Stesmans, T. Conard, S. Shamuilia, V. V. Afanasiev, A. Akheyar, S. Van Elshocht, D. P. Brunco, W. Deweerd, Y. Naoki, P. Lehnen, S. De Gendt, K. De Meyer, "mechanism of O_2-anneal induced V_{fb} shifts of Ru gated stacks", Microelectron. Rel. 47 (2007) 518.
[184] A. A. Demkov, "Thermodynamic stability and band alignment at a metal-high-k dielectric interface", Phys. Rev. B 74 (2006) 085310.
[185] S.-W. Nam, J.-H. Yoo, S. Nam, D.-H. Ko, J.-H. Ku, C.-W. Yang, "Physical and electrical degradation of ZrO_2 thin films with aluminium electrodes", Mat. Sci. Eng. B 102 (2003) 108.
[186] L. Pantisano, V. Afanas'ev, G. Pourtois, P. J. Chen, "Valence-band electron-tunneling measurement of the gate work function: Application to the high-κ/polycrystalline-silicon interface", J. Appl. Phys. 98 (2005) 053712.
[187] C. W. Pitt, "Contact injection into dielectric films in microelectronic structures", Microelectron. Rel. 9 (1970) 239.
[188] M. Ťapajna, K. Hušeková, D. Machajdík, A. P. Kobzev, T. Schram, R. Lupták, L. Harmatha, K. Fröhlich, "Electrical properties and thermal stability of MOCVD grown Ru gate electrodes for advanced CMOS technology", Micro-electron. Eng. 83 (2006) 2412.
[189] D. Gu, S. K. Dey, P. Majhi, "Effective work function of Pt, Pd, and Re on atomic layer deposited HfO_2", Appl. Phys. Lett. 89 (2006) 082907.
[190] S. Abermann, J. K. Efavi, G. Sjoblom, M. C. Lemme, J. Olsson, E. Bertagnolli, "Processing and evaluation of metal gate/high-κ/Si capacitors incorporating Al, Ni, TiN, and Mo as metal gate, and ZrO_2 and HfO_2 as high-κ dielectric", Microelectron. Eng. 84 (2007) 1635.
[191] F. A. Grant, "Properties of Rutile (Titanium Dioxide)", Rev. Modern Phys. 31 (1959) 646.
[192] H. Tang, K. Prasad, R. Sanjinès, P. E. Scmid, F. Lévy, "Electrical and optical properties of TiO_2 anatase thin films", J. Appl. Phys. 75 (1994) 2042.
[193] R. D. Shannon, J. A. Pask, "Kinetics of the Anatase-Rutile Transformation", J. Amer. Ceram. Soc. 48 (1965) 391.
[194] A. A. Levchenko, G. Li, J. Boerio-Goates, B. F. Woodfield, A. Navrotsky, "TiO_2 Stability Landscape: Polymorphism, Surface Energy, and Bound Water Energetics", Chem. Mater. 18 (2006) 6324.
[195] H. Zhang, J. F. Banfield, "New kinetic model for the nanocrystalline anatase-to-rutile transformation revealing rate dependence on number of particles", Amer. Miner. 84 (1999) 528.
[196] J. M. G. Amores, V. S. Escribano, G. Busca, "Anatase crystal growth and phase transformation to rutile in high-area TiO_2, MoO_3-TiO_2 and other TiO_2-supported oxide catalytic systems", J. Mater. Chem. 5 (1995) 1245.

[197] V. V. Yakovlev, G. Scarel, C. R. Aita, S. Mochizuki, "Short-range order in ultrathin film titanium dioxide studied by Raman spectroscopy", Appl. Phys. Lett. 76 (2000) 1107.
[198] T. Dittrich, V. Zinchuk, V. Skryshevskyy, I. Urban, O. Hilt, "Electrical transport in passivated Pt/TiO_2/Pt Schottky diodes", J. Appl. Phys. 98 (2005) 104501.
[199] R. Könenkamp, I. Rieck, "Electrical properties of Schottky diodes on nano-porous TiO_2 films", Mater. Sci. Eng. B 69–70 (2000) 519.
[200] F. Hossein-Babaei, M. Keshmiri, M. Kakavand, T. Troczynski, "A resistive gas sensor based on undoped p-type anatase", Sens. Actuators B 110 (2005) 28.
[201] Y. S. Cho, J. S. Heo, J. C. Kim, S. H. Moon, "Monitoring of an Interlayer Between Si(100) and TiO_2 Layer Formed During Cyclic CVD", Chem. Vap. Deposition 12 (2006) 659.
[202] G. Zhao, R. P. Joshi, E. Schamiloglu, H. Hjalmarson, "TiO_2 breakdown under pulsed conditions", J. Appl. Phys. 101 (2007) 026110.
[203] D. C. Cronemeyer, "Electrical and Optical Properties of Rutile Single Crystals", Phys. Rev. 87 (1952) 876.
[204] M. D. Groner, J. W. Elam, F. H. Fabreguette, S. M. George, "Electrical characterization of thin Al_2O_3 films grown by atomic layer deposition on silicon and various metal substrates", Thin Solid Films 413 (2002) 186.
[205] A. Paranjpe, S. Gopinath, T. Omstead, R. Bubber, "Atomic Layer Deposition of AlO_x for Thin Film Head Gap Applications", J. Electrochem. Soc. 148 (2001) G465.
[206] M. K. Tripp, C. Stampfer, D. C. Miller, T. Helbling, C. F. Herrmann, C. Hierold, K. Gall, S. T. George, V. M. Bright, "The mechanical properties of atomic layer deposited alumina for use in micro- and nano-eletromechanical systems", Sens. Actuators A 130 (2006) 419.
[207] S. Ferrari, F. Perissinotti, E. Peron, L. Fumagalli, D. Natali, M. Sampietro, "Atomic layer deposited Al_2O_3 as a capping layer for polymer based transistor", Organic Electron. 8 (2007) 407.
[208] P. F. Carcia, R. S. McLean, M. H. Reilly, M. D. Groner, S. M. George, "Ca test of Al_2O_3 gas diffusion barriers grown by atomic layer deposition on polymers", Appl. Phys. Lett. 89 (2006) 031915.
[209] E. Langereis, M. Creatore, S. B. S. Heil, M. C. M. Sanden, W. M. M. Kessels, "Plasma-assisted atomic layer deposition of Al_2O_3 moisture permeation barriers on polymers", Appl. Phys. Lett. 89 (2006) 081915.
[210] K. Kukli, M. Ritala, M. Leskelä, "Properties of $(Nb_{1-x}Ta_x)_2O_5$ solid solutions and $(Nb_{1-x}Ta_x)_2O_5$-ZrO_2 nanolaminates grown by atomic layer epitaxy", NanoStructured Materials 8 (1997) 785.
[211] K. Kukli, M. Ritala, M. Leskelä, T. Sajavaara, J. Keinonen, D. Gilmer, S. Bagchi, L. Prabhu, "Atomic layer deposition of Al_2O_3, ZrO_2, Ta_2O_5, and Nb_2O_5 based nanolayered dielectrics", J. Non-Crystal. Solids 303 (2002) 35.
[212] K. Honda, A. Sakai, M. Sakashita, H. Ikeda, S. Zaima, Y. Yasuda, "Pulsed Laser Deposition and Analysis for Structural and Electrical Properties of HfO_2-TiO_2 Composite Films", Jpn. J. Appl. Phys. 43 (2004) 1571.
[213] S.-H. Kim, S.-W. Rhee, "Cyclic Atomic Layer Deposition of Hafnium Aluminate Thin Films Using Tetrakis(diethylamido)hafnium, Trimethyl Aluminum, and Water", Chem. Vap. Deposition 12 (2006) 125.

[214] M. Li, Z. Zhang, S. A. Campbell, H.-J. Li, J. J. Peterson, “Hafnium titanate as a high permittivity gate insulator: Electrical and physical characteristics and thermodynamic stability”, J. Appl. Phys. 101 (2007) 044509.
[215] H. Jin, S. K. Oh, H. J. Kang, M.-H.Cho, “Band gap and band offsets for ultrathin $(HfO_2)_x(SiO_2)_{1-x}$ dielectric films on Si (100)”, Appl. Phys. Lett. 89 (2006) 122901.
[216] M. Komatsu, R. Yasuhara, H. Takahashi, S. Toyoda, H. Kumigashira, M. Oshima, D. Kukuruznyak, T. Chikyow, “Crystal structures and band offsets of ultrathin HfO_2-Y_2O_3 composite films studied by photoemission and x-ray absorption spectroscopies”, Appl. Phys. Lett. 89 (2006) 172107.
[217] R. Yasuhara, M. Komatsu, H. Takahashi, S. Toyoda, J. Okabayashi, H. Kumigashira, M. Oshima, D. Kukuruznyak, T. Chikyow, “Composition dependence of band offsets for $(LaAlO_3)_{1-x}(Al_2O_3)_x$ gate dielectrics determined by photoelectron spectroscopy and x-ray absorption spectroscopy”, Appl. Phys. Lett. 89 (2006) 122904.
[218] X. F. Wang, Q. Li, R. F. Egerton, P. F. Lee, J. Y. Dai, Z. F. Hou, X. G. Gong, “Effect of Al addition on the microstructure and electronic structure of HfO_2 film”, J. Appl. Phys. 101 (2007) 013514.
[219] A. Laha, E. Bugiel, H. J. Osten, A. Fissel, “Crystalline ternary rare earth oxide with capacitance equivalent thickness below 1 nm for high-*K* application”, Appl. Phys. Lett. 88 (2006) 172107.
[220] N. Lu, H.-J. Li, J. J. Peterson, “HfTiAlO dielectric as an alternative high-*k* gate dielectric for the next generation of complementary metal-oxide-semiconductor devices”, Appl. Phys. Lett. 90 (2007) 082911.
[221] J. G. Simmons, “Generalized Thermal *J-V* Characteristic for the Electric Tunnel Effect”, J. Appl. Phys. 35 (1964) 2655.
[222] K. H. Gundlach, J. G. Simmons, “Range of validity of the WKB tunnel probability, and comparison of experimental data and theory”, Thin Solid Films 4 (1969) 61.
[223] D. L. Pulfrey, A. H. M. Shousha, L. Young, “Electronic Conduction and Space Charge on Amorphous Insulating Films”, J. Appl. Phys. 41 (1970) 2838.
[224] R. Holm, “The Electric Tunnel Effect across Thin Insulator Films in Contacts”, J. Appl. Phys. 22 (1951) 569.
[225] T. W. Hickmott, “Temperature-dependent Fowler-Nordheim tunneling and a compensation effect in anodized Al-Al_2O_3-Au diodes”, J. Appl. Phys. 97 (2005) 104505.
[226] L.-F. Mao, “Temperature dependence of the tunneling current in metal-oxide-semiconductor devices due to the coupling between the longitudinal and transverse components of the electron thermal energy”, Appl. Phys. Lett. 90 (2007) 183511.
[227] E. Suzuki, D. K. Schroder, Y. Hayashi, „Carrier conduction in ultrathin nitrided oxide films“, J. Appl. Phys. 60 (1986) 3616.
[228] O. Blank, H. Reisinger, R. Stengl, M. Gutsche, F. Wiest, V. Capodieci, J. Schulze, I. Eisele, „A model for multistep trap-assisted tunneling in thin high-k dielectrics“, J. Appl. Phys. 97 (2005) 044107
[229] C. Svensson, I. Lundström, „Trap-assisted charge injection in MNOS structures“, J. Appl. Phys. 44 (1973) 4657.

[230] M. Houssa, M. Tuominen, M. Naili, V. Afanas'ev, A. Stesmans, "Trap-assisted tunneling in high permittivity gate dielectric stacks", J. Appl. Phys. 87 (2000) 8615.
[231] V. A. Gritsenko, E. E. Meerson, Y. N. Morokov, "Thermally assisted hole tunneling at the Au-Si_3N_4 interface and the energy-band diagram of metal-nitride-oxide-semiconductor structures", Phys. Rev. B. 57 (1998) 2081.
[232] S. Fleischer, P. T. Lai, Y. C. Cheng, „Simplified closed-form trap-assisted tunneling model applied to nitrided oxide dielectric capacitors", J. Appl. Phys. 73 (1993) 3348.
[233] H. M. Gupta, R. J. Van Overstraeten, „Role of trap states in the insulator region for MIM characteristics", J. Appl. Phys. 46 (1975) 2675.
[234] A. Rose, "Space-Charge-Limited Currents in Solids", Phys. Rev. 97 (1955) 1538.
[235] P. Mark, W. Helfrich, "Space-Charge-Limited Currents in Organic Crystals", J. Appl. Phys. 33 (1962) 205.
[236] S. M. Sze, "Current Transport and Maximum Dielectric Strength of Silicon Nitride Films", J. Appl. Phys. 38 (1967) 2951.
[237] D. S. Jeong, H. B. Park, C. S. Hwang, "Reasons for obtaining an optical dielectric constant from the Poole-Frenkel conduction behavior of atomic-layer-deposited HfO_2 films", Appl. Phys. Lett. 86 (2005) 072903.
[238] P. Bräunlich, P. Kelly, J.-P. Fillard, in Thermally Stimulated Relaxation in Solids, P. Bräunlich, Editors, Vol. 37, Springer Series in Topics in Applied Physics, Springer-Verlag, Berlin Heidelberg, 1979, pp. 49–50.
[239] N. Novkovski, "Limitations in the methods of determination of conduction mechanisms in high-permittivity dielectric nano-layers", Physica B 398 (2007) 28.
[240] J. Aarik, A. Aidla, A. Jaek, M. Leskelä, L. Niinistö, "In situ study of a strontium β-diketonate in vapor phase atomic layer epitaxy", J. Mater. Chem. 4 (1994) 1239.
[241] T. Aaltonen, M. Ritala, K. Arstila, J. Keinonen, M. Leskelä, "Atomic Layer Deposition of Ruthenium Thin Films from $Ru(thd)_3$ and Oxygen", Chem. Vap. Deposition 10 (2004) 215.
[242] T. Aaltonen, M. Ritala, V. Sammelselg, M. Leskelä, "Atomic Layer Deposition of Iridium Thin Films", J. Electrochem. Soc. 151 (2004) G489.
[243] M. Ylilammi, T. Ranta-aho, "Optical determination of the film thicknesses in multilayer thin film structures", Thin Solid Films 232 (1993) 56.
[244] G. L. Snider, I.-H. Tan, E. L. Hu, "Electron states on mesa-etched one-dimensional quantum well wires", J. Appl. Phys. 68 (1990) 2849.
[245] I.-H. Tan, G. L. Snider, E. L. Hu, "A self-consistent solution of Schrödinger-Poisson equations using a nonuniform mesh", J. Appl. Phys. 68 (1990) 4071.
[246] K. Tse, J. Robertson, "Defects and their passivation in high *K* gate oxides", Microelectron. Eng. 84 (2007) 663.
[247] C. D. Valentin, G. Pacchioni, A. Selloni, "Theory of Carbon Doping of Titanium Dioxide", Chem. Mater. 17 (2005) 6656.
[248] V. Cech, "Modeling of the *I–V* characteristics in amorphous silicon n^+-i-n^+ devices", J. Appl. Phys. 88 (2000) 5374.

28

[249] R. B. Wehrspohn, S. C. Deane, I. D. French, M. J. Powell, "Effect of amorphous silicon material properties on the stability of thin film transistors: evidence for a local defect creation model", J. Non-Crystal. Solids 266–269 (2000) 459.
[250] J. C. Shin, J. Park, C. S. Hwang, H. J. Kim, "Dielectric and electrical properties of sputter grown (Ba,Sr)TiO_3 thin films", J. Appl. Phys. 86 (1999) 506.
[251] J. Li, X. Dong, "Simulation of space-charge effects on the leakage currents in (Ba,Sr)TiO_3 thin films", Phys. Lett. A 340 (2005) 303.
[252] E. Atanassova, D. Spassov, A. Paskaleva, "Influence of the metal electrode on the characteristics of thermal Ta_2O_5 capacitors", Microelectron. Eng. 83 (2006) 1918.
[253] J. Lee, M. H. Park, T.-M. Chung, Y. Kim, M. M. Sung, "Atomic Layer Deposition of TiO_2 Thin Films from $Ti(O^iPr)_2(dmae)_2$ and H_2O", Bull. Korean Chem. Soc. 25 (2004) 475.
[254] B. Govoreanu, P. Blomme, M. Rosmeulen, J. Van Houdt, K. De Meyer, "A model for tunneling current in multi-layer tunnel dielectrics", Solid-State. Electron. 47 (2003) 1045.
[255] E. M. Vogel, K. Z. Ahmed, B. Hornung, W. K. Henson, P. K. McLarty, G. Lucovsky, J. R. Hauser, J. J. Wortman, "Modeled Tunnel Currents for High Dielectric Constant Dielectrics", IEEE Trans. Electron Dev. 45 (1998) 1350.
[256] Y. S. Kim, S. J. Yun, "Nanolaminated Al_2O_3-TiO_2 thin films grown by atomic layer deposition", J. Cryst. Growth 274 (2005) 585.
[257] M. Specht, M. Städele, S. Jakschik, U. Schröder, "Transport mechanism in atomic-layer-deposited Al_2O_3 dielectrics", Appl. Phys. Lett. 84 (2004) 3076.
[258] J. Robertson, K. Xiong, S. J. Clark, "Band gaps and defect levels in functional oxides", Thin Solid Films 496 (2006) 1.

PUBLICATIONS

I

J. Aarik, V. Bichevin, I. Jõgi, H. Käämbre, M. Laan, V. Sammelselg,
"Fowler-Nordheim tunnelling in Au-TiO_2-Ag film structures",
Central Eur. J. Phys. 2 (2004) 147.

II

I. Jõgi, J. Aarik, K. Kukli, H. Käämbre, M. Laan, J. Lu, T. Sajavaara, T. Uustare,"The effect of precursors on the structure and conductivity of atomic layer deposited TiO_2 films", Proc. Electrochem. Soc. 2005–09 (2005) 575.

III

I. Jõgi, J. Aarik, M. Laan, J. Lu, K. Kukli, H. Käämbre, T. Sajavaara, T. Uustare, "Effect of preparation conditions on properties of atomic layer deposited TiO_2 films in Mo-TiO_2-Al stacks", Thin Solid Films 510 (2006) 39.

IV

Jõgi, K. Kukli, J. Aarik, A. Aidla, J. Lu,
“Precursor-dependent structural and electrical characteristics
of atomic layer deposited films: Case study on titanium oxide”,
Mat. Sci. Semicond. Process. 9 (2006) 1084.

CURRICULUM VITAE

Name:	Indrek Jõgi
Date and place of birth:	26.05.1980. a. Räpina, Estonia
Citizenship:	Estonia
Current employment:	University of Tartu, Department of Physics and Chemistry, Institute of Experimental Physics and Technology, (researcher, assistant, engineer)
Address:	University of Tartu, Institute of Experimental Physics and Technology, Tähe 4, 51010 Tartu, Estonia
Telephone:	+372 521 1821
E-mail:	indrek.jogi@ut.ee

Education:	Nõo Secondary School, 1998 University of Tartu, Department of Physics and Chemistry, Diploma (in physical information technology), 2001 University of Tartu, Department of Physics and Chemistry, M.Sc. (in applied physics), 2003

Professional employment:

01.10.2005 – ...: University of Tartu, researcher
01.10.2006 – ...: University of Tartu, assistant
01.07.2007 – ...: University of Tartu, engineer

Publications:	5 scientific articles 2 posters and 3 oral presentations in international conferences

ELULUGU

Nimi:	Indrek Jõgi
Sünniaeg ja -koht:	26.05.1980. a. Räpina, Eesti
Kodakondsus:	Eesti
Praegune töökoht:	Tartu Ülikool, Eksperimentaalfüüsika ja tehnoloogia instituut ning Füüsika-Keemia teaduskond (erakorraline teadur, insener ja assistent)
Aadress:	Tartu Ülikool, Eksperimentaalfüüsika ja tehnoloogia instituut, Tähe 4, 51010 Tartu
Telefon:	+372 521 1821
E-post:	indrek.jogi@ut.ee

Haridus:	Nõo Reaalgümnaasium, 1998 Tartu Ülikool, Füüsika-Keemia teaduskond, Diplom (füüsikalise infotehnoloogia erialal), 2001 Tartu Ülikool, Füüsika-Keemia teaduskond, M.Sc. (rakendusfüüsika erialal), 2003
Teenistuskäik:	01.10.2005 – ...: Tartu Ülikool, erakorraline teadur 01.10.2006 – ...: Tartu Ülikool, elektroonika erakorraline assistent 01.07.2007 – ...: Tartu Ülikool, insener
Publikatsioonid:	5 teaduslikku publikatsiooni 2 postrit ja 3 suulist ettekannet rahvusvahelistel konverentsidel

DISSERTATIONES PHYSICAE UNIVERSITATIS TARTUENSIS

1. **Andrus Ausmees.** XUV-induced electron emission and electron-phonon interaction in alkali halides. Tartu, 1991.
2. **Heiki Sõnajalg.** Shaping and recalling of light pulses by optical elements based on spectral hole burning. Tartu, 1991.
3. **Sergei Savihhin.** Ultrafast dynamics of F-centers and bound excitons from picosecond spectroscopy data. Tartu, 1991.
4. **Ergo Nõmmiste.** Leelishalogeniidide röntgenelektronemissioon kiiritamisel footonitega energiaga 70–140 eV. Tartu, 1991.
5. **Margus Rätsep.** Spectral gratings and their relaxation in some low-temperature impurity-doped glasses and chrystals. Tartu, 1991.
6. **Tõnu Pullerits.** Primary energy transfer in photosynthesis. Model calculations. Tartu, 1991.
7. **Olev Saks.** Attoampri diapasoonis voolude mõõtmise füüsikalised alused. Tartu, 1991.
8. **Andres Virro.** AlGaAsSb/GaSb heterostructure injection lasers. Tartu, 1991.
9. **Hans Korge.** Investigation of negative point discharge in pure nitrogen at atmospheric pressure. Tartu, 1992.
10. **Jüri Maksimov.** Nonlinear generation of laser VUV radiation for high-resolution spectroscopy. Tartu, 1992.
11. **Mark Aizengendler.** Photostimulated transformation of aggregate defects and spectral hole burning in a neutron-irradiated sapphire. Tartu, 1992.
12. **Hele Siimon.** Atomic layer molecular beam epitaxy of A^2B^6 compounds described on the basis of kinetic equations model. Tartu, 1992.
13. **Tõnu Reinot.** The kinetics of polariton luminescence, energy transfer and relaxation in anthracene. Tartu, 1992.
14. **Toomas Rõõm.** Paramagnetic H^{2-} and F^+ centers in CaO crystals: spectra, relaxation and recombination luminescence. Tallinn, 1993.
15. **Erko Jalviste.** Laser spectroscopy of some jet-cooled organic molecules. Tartu, 1993.
16. **Alvo Aabloo.** Studies of crystalline celluloses using potential energy calculations. Tartu, 1994.
17. **Peeter Paris.** Initiation of corona pulses. Tartu, 1994.
18. **Павел Рубин.** Локальные дефектные состояния в CuO_2 плоскостях высокотемпературных сверхпроводников. Тарту, 1994.
19. **Olavi Ollikainen.** Applications of persistent spectral hole burning in ultrafast optical neural networks, time-resolved spectroscopy and holographic interferometry. Tartu, 1996.
20. **Ülo Mets.** Methodological aspects of fluorescence correlation spectroscopy. Tartu, 1996.

21. **Mikhail Danilkin.** Interaction of intrinsic and impurity defects in CaS:Eu luminophors. Tartu, 1997.
22. **Ирина Кудрявцева.** Создание и стабилизация дефектов в кристаллах KBr, KCl, RbCl при облучении ВУФ-радиацией. Тарту, 1997.
23. **Andres Osvet.** Photochromic properties of radiation-induced defects in diamond. Tartu, 1998.
24. **Jüri Örd.** Classical and quantum aspects of geodesic multiplication. Tartu, 1998.
25. **Priit Sarv.** High resolution solid-state NMR studies of zeolites. Tartu, 1998.
26. **Сергей Долгов.** Электронные возбуждения и дефектообразование в некоторых оксидах металлов. Тарту, 1998.
27. **Kaupo Kukli.** Atomic layer deposition of artificially structured dielectric materials. Tartu, 1999.
28. **Ivo Heinmaa.** Nuclear resonance studies of local structure in $RBa_2Cu_3O_{6+x}$ compounds. Tartu, 1999.
29. **Aleksander Shelkan.** Hole states in CuO_2 planes of high temperature superconducting materials. Tartu, 1999.
30. **Dmitri Nevedrov.** Nonlinear effects in quantum lattices. Tartu, 1999.
31. **Rein Ruus.** Collapse of 3d (4f) orbitals in 2p (3d) excited configurations and its effect on the x-ray and electron spectra. Tartu, 1999.
32. **Valter Zazubovich.** Local relaxation in incommensurate and glassy solids studied by Spectral Hole Burning. Tartu, 1999.
33. **Indrek Reimand.** Picosecond dynamics of optical excitations in GaAs and other excitonic systems. Tartu, 2000.
34. **Vladimir Babin.** Spectroscopy of exciton states in some halide macro- and nanocrystals. Tartu, 2001.
35. **Toomas Plank.** Positive corona at combined DC and AC voltage. Tartu, 2001.
36. **Kristjan Leiger.** Pressure-induced effects in inhomogeneous spectra of doped solids. Tartu, 2002.
37. **Helle Kaasik.** Nonperturbative theory of multiphonon vibrational relaxation and nonradiative transitions. Tartu, 2002.
38. **Tõnu Laas.** Propagation of waves in curved spacetimes. Tartu, 2002.
39. **Rünno Lõhmus.** Application of novel hybrid methods in SPM studies of nanostructural materials. Tartu, 2002.
40. **Kaido Reivelt.** Optical implementation of propagation-invariant pulsed free-space wave fields. Tartu, 2003.
41. **Heiki Kasemägi.** The effect of nanoparticle additives on lithium-ion mobility in a polymer electrolyte. Tartu, 2003.
42. **Villu Repän.** Low current mode of negative corona. Tartu, 2004.
43. **Алексей Котлов.** Оксианионные диэлектрические кристаллы: зонная структура и электронные возбуждения. Tartu, 2004.

44. **Jaak Talts.** Continuous non-invasive blood pressure measurement: comparative and methodological studies of the differential servo-oscillometric method. Tartu, 2004.
45. **Margus Saal.** Studies of pre-big bang and braneworld cosmology. Tartu, 2004.
46. **Eduard Gerškevitš.** Dose to bone marrow and leukaemia risk in external beam radiotherapy of prostate cancer. Tartu, 2005.
47. **Sergey Shchemelyov.** Sum-frequency generation and multiphoton ionization in xenon under excitation by conical laser beams. Tartu, 2006.
48. **Valter Kiisk.** Optical investigation of metal-oxide thin films. Tartu, 2006.
49. **Jaan Aarik.** Atomic layer deposition of titanium, zirconium and hafnium dioxides: growth mechanisms and properties of thin films. Tartu, 2007.
50. **Astrid Rekker.** Colored-noise-controlled anomalous transport and phase transitions in complex systems. Tartu, 2007.
51. **Andres Punning.** Electromechanical characterization of ionic polymer-metal composite sensing actuators. Tartu, 2007.